

Evaluation, Characterization and Development of Innovative Reactor Systems in Biotechnology

Von der Naturwissenschaftlichen Fakultät
der Gottfried Wilhelm Leibniz Universität Hannover

zur Erlangung des Grades
Doktor der Naturwissenschaften
Dr. rer. nat.

genehmigte Dissertation

von
Dipl.-Chem. Christian Endres
geboren am 2. August 1975 in Hannover

2010

Referent: Prof. Dr. Thomas Scheper

Korreferent: Prof. Dr. Bernd Hitzmann

Tag der Promotion: 15. September 2010

Erklärung

Hiermit versichere ich, dass ich die vorliegende Dissertation selbstständig verfasst habe und die benutzten Hilfsmittel sowie eventuell zu Hilfsleistungen herangezogene Institutionen vollständig angegeben habe. Ferner versichere ich, dass die Dissertation nicht bereits als Diplomarbeit oder andere Prüfungsleistung verwendet worden ist.

Hannover, im September 2010

Kurzbeschreibung

Bioreaktoren sind ein wesentlicher Bestandteil eines jeden biotechnologischen Prozesses. Um mit den individuellen Anforderungen verschiedenster Prozesse zu harmonisieren, existieren Bioreaktoren in verschiedenen Bauformen und Größen. Auch wenn Bioreaktorsysteme bereits weitreichend in der wissenschaftlichen Literatur beschrieben wurden, erfordert der ständige Bedarf an neuen biotechnologischen Produkten die stetige Anpassung bestehender Reaktorsysteme sowie die Entwicklung neuer Reaktortechnologien.

Innerhalb dieser Arbeit werden verschiedene neuartige Reaktorkonzepte für den Einsatz in biotechnologischen Prozessentwicklungen und Produktionsprozessen vorgestellt. Besonders im Bereich der Bioprozessentwicklung muss eine Vielzahl an Experimenten durchgeführt werden, um z.B. den leistungsfähigsten Organismus oder die produktivsten Wachstumsbedingungen zu ermitteln. Diese Entwicklungsschritte werden für gewöhnlich in kleinen Maßstäben durchgeführt, um die kostenintensive Nutzung von Verbrauchsmaterialien und Arbeitszeit zu reduzieren. In diesem Zusammenhang wird ein parallel arbeitendes Rührkessel-Reaktorsystem im Miniaturmaßstab charakterisiert und in Modellprozessen evaluiert.

In einem weiteren Teil dieser Arbeit werden Reaktorsysteme für die Kultivierung von Biofilmen vorgestellt. Die mit diesem Prozess assoziierten Prototypen bestehen aus keramischen Hohlfasern, die sowohl als Matrix für die Ausbildung eines Biofilms, als auch zur Substratzufuhr oder Produktentnahme dienen. Verschiedene Maßstäbe dieser Systeme werden dabei von der Prozessentwicklung bis hin zum Produktionsmaßstab hinsichtlich ihrer Produktivität untersucht. Dabei werden sowohl aerob und fakultativ anaerob wachsende Mikroorganismen, als auch adhärent wachsende Säugerzellen eingesetzt.

Schlagworte: Bioreaktor, optischer Sensor, keramische Membran, Bioprozess, Produktivität

Abstract

Bioreactors are widely used in academic and industrial applications. As bioreactors are an essential part of every biotechnological process, various designs and sizes are necessary to facilitate the individual requirements of each bioprocess. Even though bioreactors have been intensively described in literature, the ongoing demand for biotechnological products requires constant modification of available and development of new technology. Due to the multitude of different microbial and mammalian organisms used for production of valuable products, novel concepts for customized cultivations are necessary.

This thesis presents different novel reactor technologies for the use in biotechnological processes. Especially during bioprocess development an extensive amount of experiments has to be performed to identify the best performing organisms or most productive growth conditions. These developmental stages are usually conducted in small-scale to reduce costs of consumables and in parallel to minimize costs of labor. Independent of the reactor design, small-scale units with physical properties comparable to the ones of large scale production units are necessary to achieve reliable process information. In this context a parallel miniature-scale stirred reactor system equipped with optical sensor units for the determination of process critical variables such as pH and dissolved oxygen is described and evaluated in exemplary processes.

Another bioreactor system for the cultivation of productive biofilms is presented. The reactor prototypes associated with this process are based on ceramic membranes which offer support for biofilm formation, nutrient delivery and product removal. Small-scale reactor units are used for process development and scale-up considerations. Different scaled production units and different process strategies are investigated concerning overall productivity. These processes will include the cultivation of aerobic and facultative anaerobic microorganisms as well as the cultivation of attachment dependent mammalian cell-lines.

Keywords: bioreactor, optical sensor, ceramic membrane, bioprocess, productivity

Danksagung

Die vorliegende Arbeit wurde am Institut für Technische Chemie der Gottfried Wilhelm Leibniz Universität Hannover unter der Leitung von Prof. Dr. Thomas Scheper durchgeführt. Hiermit bedanke ich mich bei Thomas Scheper für die interessante Aufgabenstellung und für die vielen hilfreichen Gespräche zu kleineren und größeren Fragestellungen. Ganz besonders möchte ich ihm aber für die mir eröffneten Möglichkeiten herzlichst danken.

Herrn Prof. Dr. Bernd Hitzmann danke ich für die Übernahme des Koreferats, sowie für seine schnelle und unkomplizierte Hilfe bei der Lösung mathematischer Problemstellungen. Großer Dank geht an Dr. Sascha Beutel, der immer und zu jeder Fragestellung mit Rat und Tat zur Seite stand. Außerdem möchte ich ihm für das tiefgreifende und rasche Korrekturlesen diverser Kurzfassungen, Vorträge und natürlich dieser Arbeit danken.

Besonderer Dank geht an Judi van Heerden und Paul O'Riordan von Synexa Life Sciences für die freundliche Unterstützung und Betreuung während meines Aufenthalts in Südafrika. Herzlichst möchte ich jedoch bei Dr. Sheena Fraser für die endlose Geduld, die unzähligen Gespräche und das Korrekturlesen dieser Arbeit bedanken. Darüber hinaus auch vielen Dank für die freundliche Unterstützung und das Sightseeing während meiner Zeit in Kapstadt.

Janis Dreimann danke ich für die Mitarbeit im Rahmen seiner Diplomarbeit. Ein besonderer Dank gilt auch Sonja Kreß für die prima Mitarbeit an den Reaktorprojekten während ihrer Masterarbeit – und für die vielen netten Gespräche und Extraktsitzungen

Ich danke Christian Benecke, Arne Bluma, Tim Höpfner, Anne Schmidt, Ismet Bice, Michael Bühring und allen anderen Kollegen für die tolle Zeit, die vielen sinnvollen und sinnfreien Gespräche und die geselligen Feierabende.

Des Weiteren möchte ich mich bei den Mitarbeitern der Feinmechanik-Werkstatt des TCI für die schnelle Lösung mechanischer Probleme bedanken. Den Mitarbeitern der Elektronik-Werkstatt danke ich für die geduldige Unterweisung in die Arbeitsweise von Oszilloskopen – und der Funktion des „Chemiker-Knopfes“.

Ewiger Dank gilt meinen Eltern, die mir wie selbstverständlich das Studium ermöglicht und unentwegt an meiner Seite gestanden haben.

Index

1	Introduction and objectives	1
2	Theoretical background	4
2.1	Innovative reactor systems in biotechnology	4
2.1.1	Hollow fibre reactors.....	4
2.1.2	Miniature bioreactors and their application as screening systems	6
2.2	Modern bioprocess analysis and adaption for use in disposable reactor systems.....	10
2.2.1	Overview of disposable sensing systems	10
2.2.2	Optical chemosensors as an example for non-invasive on-line monitoring	13

Part A

3	Miniature-scale bioreactor system for the parallel operation of three stirred tank reactors	19
3.1	Components of the reactor system.....	19
4	Setup and characterization of the hardware environment	21
4.1	Agitation subsystem	22
4.2	Magnetic valve controlled aeration subsystem	23
4.3	Peristaltic pump subsystem.....	23
4.4	Characterization and optimization of the temperature control system.....	24
4.4.1	Optimized temperature control concept	25
4.5	Characterization of the STR units.....	29
4.5.1	$k_L a$ determination and aeration strategies	29
4.5.2	Residence time distributions.....	33
4.6	Characterization of the optical sensor units	35
4.6.1	pH determination based on ratiometric fluorescence intensity measurements.....	35
4.6.2	DO determination based on fluorescence lifetime measurements.....	42
5	Development of a monitoring and control software	49
5.1	Software layout and functionality	49
5.2	Graphical user interface of the monitoring and control software.....	50
6	Example cultivations using the reactor system	52
6.1	<i>E.coli</i> K12 process monitoring and control.....	52
6.2	<i>E.coli</i> JM109 GFP*6His - alternate use of the pH sensor units	54
7	Conclusion part A	57

Part B

8	Ceramic membrane-based bioreactors for microbial biofilm cultivations	61
8.1	Aerobic process for steady-state biofilm cultivations and secreted product recovery	63
8.2	Anaerobic process for submerged biofilm cultivation and secreted product recovery ...	66
8.3	Determination of basic process conditions and scale-up considerations.....	69
8.3.1	Production of xylanase from <i>A.niger</i> D15 as an example for linear scale-up	71
9	Development of a comparative model for efficiency and productivity determination of the ceramic membrane reactors	74
9.1	Production of fungal xylanase from <i>A.niger</i> D15 using the aerobic process	74
9.1.1	Fermentation results	74
9.1.2	Bioreactor efficiency and productivity	78
9.1.3	Modeling of long term operation.....	80
9.1.4	Variation of production time.....	82
9.2	Production of actinorhodin from filamentous <i>S.coelicolor</i> A3(2) using the aerobic process	85
9.2.1	Fermentation results	86
9.2.2	Modeling of long term operation.....	88
9.2.3	Variation of production time.....	90
9.3	Production of β -lactamase from <i>L.lactis</i> as an example for the anaerobic process	92
9.3.1	Fermentation results	93
9.3.2	Modeling of long term operation.....	96
9.3.3	Variation of production time.....	97
9.4	Cost influencing factors in operation	100
9.4.1	Cost distribution for the production of xylanase from <i>A.niger</i> D15	101
9.4.2	Cost distribution for the production of β -lactamase from <i>L.lactis</i> PRA290	102
10	Membrane bioreactor prototype for mammalian cultivations	104
10.1	Reactor and process description	104
10.1.1	Quorus miniCELL and maxiCELL reactors	105
10.1.2	Quorus CELL.....	107
10.2	Example cultivations of CHO-K1 and HEK-293	109
10.3	Effects of variation of membrane setups and aeration strategies.....	109
11	Conclusion part B	114
12	Outlook	119
13	List of abbreviations	121
14	Bibliography	123

15 Appendix.....	127
15.1 Chemicals	127
15.2 Devices	128
15.3 Growth media	128
15.4 Cultivation parameter	130
15.5 Product analysis	132
15.6 Reactor characterization	135
15.7 Wiring diagram of the mini-STR bioreactor hardware environment.....	138
15.8 Calibration parameters	139
Curriculum Vitae.....	140

1 Introduction and objectives

Bioreactors are unquestionably the most important components in every biotechnological production process. These devices provide a controllable environment to host or derive valuable products from biologically active organisms. Bioreactors are therefore of essential use in both academic research and industrial application. They exist in various scales and designs enabling different approaches to facilitate the necessary biological environment.

Selecting a particular bioreactor model for a specific biotechnological process involves considerations concerning the organism to be cultured, its microbiological and biochemical requirements as well as demands arising from marketing and process engineering. All these factors need to be carefully balanced to decide on a bioreactor of optimal design and scale to operate in upmost cost effectiveness and productivity.

Every correlating bioprocess needs to be evaluated and optimized in laboratory scale before scaling up towards the final process to meet the desired production rate. To develop the most efficient process, extensive screening has to be conducted to choose the best performing strain of the desired organism and the most productive growth conditions. The combination and validation of all these variables lead to a fast increase of the number of experiments necessary to be performed. As stirred tank reactors are generally the preferred choice for large scale production, it is perspicuous that such reactor systems should be applied in a much smaller scale in the early process development to determine optimal operation parameters in the shortest time-frame possible. For this reason, these developmental steps are increasingly performed in parallel operated miniature stirred tank reactors with working volumes below 100 mL. To obtain as much process information as possible from a single experiment, the use of multiple sensor systems is necessary. As the narrow space in these systems limits the use of conventional sensor technology, modern non-invasive sensor systems need to be adapted to gain access to the desired information.

In this context, a reactor prototype for the parallel operation of up to three miniature-scale stirred tank reactors is evaluated and optimized. Next to the three reactor units, this prototype is equipped with an optical sensor array for the parallel and non-invasive determination of critical process variables such as pH and dissolved oxygen in each reactor unit. In a first step this prototype is brought into a working state by setting up a computer controllable hardware environment. The essential components of this reactor system are investigated and characterized profoundly. All found characteristics will be implemented into a monitoring and control software module. Finally, the fully controllable reactor system is evaluated in exemplary bioprocesses using different model organisms.

Most industrial bioprocesses facilitate well known microorganisms or robust mammalian cell-lines for production of valuable products. As these organisms are usually optimized towards high productivities and cultivation in stirred tank reactors, stress-sensitive or attachment dependent organisms are less productive using this reactor technology. However, under optimal growth conditions these organisms are capable of producing valuable products, e.g. volatiles, food additives or products of pharmaceutical interest. Therefore new reactor technology for a productive cultivation of such organisms is necessary.

In contrast to conventional stirred tank reactors, membrane-based bioreactors provide a customizable and artificial environment for an increased biomass density and enhanced productivity of such organisms. Especially shear-stress sensitive organisms, which are less productive under the evaluated stress conditions of stirred tank reactors can be cultivated in such systems as productive biofilms.

In this context, the bioprocesses of different novel ceramic membrane based reactor prototypes will be described and characterized in great detail. These systems are customized for the cultivation of either microbial or mammalian organisms.

The reactor prototypes for microbial biofilm cultivations will be investigated by cultivating various aerobic and anaerobic growing organisms. As these prototypes exist in different sizes, a scale-up model from single-fibre reactors towards production-scale units will be introduced. Furthermore a comparative model for the determination of the efficiency of

these systems will be developed. This model will be based on the comparison of the productivity of the investigated prototypes to conventional reactor technology. Based on the calculated productivities, the cost efficiency of these reactor systems will be assessed and suggestions for process optimization will be presented.

As the reactor prototypes for the cultivation of attachment dependent mammalian cell-lines are based on similar membrane technology, the evaluated demands of these organisms onto their environment need to be met by modification of the overall reactor design. Different process strategies to fulfil these requirements will be presented. Results from cultivations of adherent growing mammalian cell-lines utilizing these strategies will be compared to conventional cultivation methods and suggestions for further prototype development will be outlined.

2 Theoretical background

2.1 Innovative reactor systems in biotechnology

2.1.1 Hollow fibre reactors

Compared to conventional stirred tank reactors, an important advantage of membrane-based bioreactors is the provision of an artificial environment for an increased biomass density and enhanced productivity. This artificial environment can further be specified as a platform, which combines biological reactions with membrane separations.

Membrane-based bioreactors are generally comprised of independent feed and removal streams, allowing cell retention and product extraction. Two individual compartments, the extra-capillary (ECS) and intra-capillary space (ICS), are separated by the membranes. Cells are usually grown in the ECS. Additionally, two distinct cycling pathways ensure consistent operation. One is used for medium feed through or from the ICS and the other is used for inoculation or product removal from the ECS. Major advantages of this setup are the possibilities of immediate product removal and adjustment of product concentration through variation of the feed rate. Constant and immediate product removal can additionally be of significant importance when the products are either unstable or lead to product inhibition [1].

Oxygenation or aeration is another crucial factor in membrane reactor operation. Depending on the shear sensitivity of the organism to be cultured, different aeration strategies can be applied. Direct sparging of gas into the cultivation chamber is only permissible for less shear-sensitive organisms like bacteria. However, possible foam formation needs to be considered. Usually, bubble-free gassing strategies are preferred [2]. These strategies include e.g. the direct sparging into a compartment separated from the cultivation chamber or the use of oxygenators to aerate circulated medium. Another possibility is the indirect and bubble-free aeration of the ECS through additional membranes or tubing.

First generation membrane bioreactors relied on diffusion-based mass transfer through the membranes. This operating principle, however, can lead to insufficient aeration,

inhomogeneous production and insufficient removal of e.g. toxic by-products. To circumvent these problems, second generation membrane reactors have been developed [3]. These systems are comprised of additional expansion compartments for each supply and removal pathway. This provides the possibility of selectively varying pressure, thus ensuring a controllable trans-membrane pressure. This advanced control feature leads to a higher mass transfer than the one obtained by solitary diffusion alone. The resulting convective flow additionally enhances mixing effects when the trans-membrane pressure is reversed. In mammalian cell culture the applied perfusion technique supports cell densities above 10^8 cells·mL⁻¹ in a virtually shear stress free environment [3]. However, a disadvantage of such a closed loop operation is the inability to perform sampling for extraction of larger cell amounts for the periodical determination of cell growth and viability. These factors can only be assessed indirectly by measuring metabolic activities such as oxygen and glucose consumption. Cell counts can only be performed in end-point analysis negating online batch to batch comparisons.

A newly developed and disposable membrane bioreactor (ProBioGen AG, Berlin, Germany) not only overcomes scale-up limitations associated with membrane reactors, but additionally inverts the conventional operation principle of cells growing in the ECS [4]. Cells are grown inside horizontally orientated cell culture tubes, which are encased in a rotating reactor compartment. Rotation of the reactor vessel assures alternating exposure of the cells to either oxygen or medium. This system was primarily designed for constant protein production, in order to maintain a continuous and cell-free harvest stream emerging from a high density culture.

The production of secondary metabolites from filamentous microorganisms using membrane-based bioreactors was described by Ntwampe et al. [5]. Here, shear stress sensitive organisms are immobilized on the external surface of the membranes in a fully aerated environment and constantly supplied with substrates enabling a continuous production of valuable secondary metabolites. This membrane gradostat reactor relies on the biofilm formation on the membranes as the support matrix. The theoretical gradostat concept describes the formation of nutrient and oxygen gradients across the biofilm, facilitating steady-state cultivations.

Industrial applications for membrane bioreactors originate from medical applications such as haemodialysis, desalination of seawater or wastewater treatment [6]. Modern biotechnological processes utilize membrane reactors e.g. for the production of ethanol by yeast [7], the continuous production of 1,3-propanediol by *C. butyricum* [8] or for protein synthesis [9]. Membrane based bioreactors are also used in mammalian cultivations and in tissue engineering [10-11]. The wide variety of possible applications demonstrates the potential of membrane bioreactors and the need for further development in this field.

In this context, the profound investigation of three different and novel ceramic membrane based bioreactors was part of this thesis. The results and suggestions for optimization are broadly summarized in chapter 8.

2.1.2 Miniature bioreactors and their application as screening systems

Biotechnological process development and optimization is usually linked with time consuming and expensive screening of different cell lines, culture media optimization and the determination of optimal process conditions. The combination and validation of all these variables leads to a fast increase of the number of experiments necessary to be performed. It is therefore indisputable, that high throughput screenings (HTS) in a small scale are advantageous to significantly increase the number of experiments per time frame [12]. For this reason, bioprocesses are increasingly performed in parallel operated miniature stirred tank reactors (STR) with working volumes below 100 mL [13]. In contrast to laboratory scale bioreactors (working volumes 1–100 L), these systems can considerably decrease medium usage, while the process information attained rises with the degree of parallelization. However, the economical advantages of these systems are controversial. The impact of setup-times on total cost and the savings obtained from increased process information should be determined for each process individually.

Generally, most process information can be obtained from constantly monitored laboratory scale bioprocesses (Fig. 1).

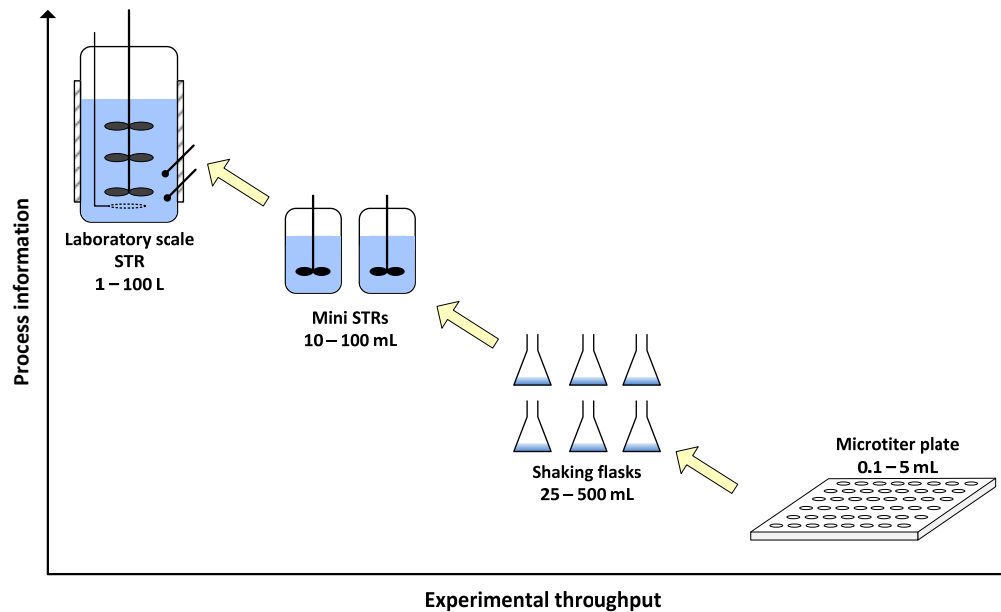


Fig. 1: Experimental throughput and obtainable process information of various bioreactor systems. A scale-up usually coincides with better monitoring options, thus achieving a more detailed process information.

With decreasing scale, the amount of experimental throughput can be increased, but the obtained process information is limited, due to less monitoring options. Considerable effort has therefore been expended on the development of adequate monitoring options for parallel screening systems of various scales [14].

However, not every process development or optimization step requires extensive monitoring. An example for a highly parallel screening with no need for extensive monitoring has been shown by de Jesus *et al.* [15]. They determined the effect of temperature variations on the growth of Chinese hamster ovary cells (CHO). De Jesus *et al.* used a modified version of disposable 50 mL centrifuge tubes with an optimal working volume of 5 mL, in a CO₂ controlled incubator, at agitation rates of 200 rpm. These simple miniature bioreactors have an inner diameter of 28 mm and are equipped with a gas permeable lid to increase mass transfer. They are distributed by TPP (Trasadingen, Switzerland) under the name TubeSpin. Stettler *et al.* [16] e.g. used 1,000 TubeSpins within one week in parallel to analyze the growth pattern of the CHO PPL11 cell line in 29 different media.

Microtiter plates (MTP) are used for e.g. the HTS of expression studies or strain selections in the early process development stages. Due to their small working volumes of 0.1 –

5 mL, MTPs offer a high degree of parallelization [12]. MTP cultivations, especially in the early process stages, are mostly performed under uncontrolled conditions [17]. However, based on their small working volume and the lack of process information, performed end-point analysis of biomass or product titer can lead to inaccurate interpretations. Newly developed systems try to close this gap with the integration of sensor systems for pH, pO_2 and optical density (OD) determination [18-19]. DASGIP AG (Juelich, Germany) has introduced the BioLector system for the MTP cultivation of eukaryotes and prokaryotes [20]. This system can operate and monitor up to four 96-well MTPs. Measurable variables are pO_2 , pH, DO and depending on the filter combination of the attached spectrophotometer e.g. NADH or GFP tagged proteins.

90 % of all cultivation experiments in biotechnology are performed in shaking flasks [21]. Especially because of their low cost of acquisition and easy handling, shaking flasks are the preferred cultivation vessel for a broad range of applications. Shaking flasks can be of reusable or disposable construction and offer volumes between 25 - 500 mL. Since their working volume usually constitutes only 20 % of their total capacity, many experiments performed in these vessels can be considered as miniature scale cultivations. Many systems have been developed in the last years to enable the non-invasive online monitoring of e.g. pH and pO_2 values. Sartorius Stedim Biotech GmbH (Goettingen, Germany) introduced the Sensolux shaker tray, which can measure the pH and pO_2 in up to nine disposable shaking flasks. The respiration activities of prokaryotic and eukaryotic cultures can e.g. be monitored in reusable shaking flasks using the RAMOS system (Hi-Tech Zang GmbH, Herzogenrath, Germany) [22]. Since the degree of parallelization for HTS should be preferably high, these expensive systems are rarely used for HTS purposes. A disadvantage of shaking flask cultivations arises when manual sampling, e.g. for OD determination, is required. The shaking flasks have to be removed from the incubator resulting in a temporal temperature gradient and limited oxygen distribution into the culture broth.

The conventional STR is to date the most important reactor model for biotechnological applications. The constructional differences of MTPs and shaking flasks makes them inappropriate for upscale considerations. Especially in this field of application, the monitoring of process critical parameters like pH and DO concentrations is essential. In

this context, many proposals for the miniaturization of STRs with different degrees of parallelization have been published.

Weuster-Botz *et al.* [23] developed a reactor system for HTS applications based on 48 identical miniature STRs with working volumes of 10 mL and an inner diameter of 15.5 mm. These 48 STRs are arranged in 6 rows, each with 8 STRs. The reactor support station is equipped with a sterile gas distributor and two heat exchangers for incubation and exhaust cooling. An newly developed agitation system is driven magnetically and is additionally used for aeration. This agitator guarantees not only a high oxygen intake, but furthermore a high reproducibility in parallel operation. Fluorescence based optical chemosensors are used for the determination of dissolved oxygen concentrations (DO) in 8 of these STRs. While the sensor units for transmission are located below the reactors, each of the corresponding vessels is equipped with an oxygen sensitive sensor patch. pH values, however, are not monitored constantly in the reactor units. Instead, samples are extracted automatically and aseptically from the STRs, and subsequently pipetted into a commercially available MTP (Hydroplate, PreSens GmbH, Regensburg, Germany). Each well of this MTP is endowed with a pH sensitive sensor spot. An integrated robot moves the MTP into a MTP reader for pH determination. The MTP is afterwards washed and stored in a cooling unit until the next sampling sequence starts. Immediately after pH measurement, the obtained values for each STR are compared with the setpoints and, if necessary, corrected by the individual addition of acid or base. The determination of the optical density is processed in a similar way. Samples are extracted from each STR, pipetted into a MTP, transferred to the MTP reader and diluted by an integrated pump. The optical densities are finally determined at a wavelength of 650 nm. Based on the agitation system and the combination of pipet robots for process monitoring and control, cultivations performed in this system are highly reproducible. A similar reactor system with 24 parallel operated STRs has been presented by Harms *et al.* [24]. The STR working volume constitutes 12 mL. In contrast to the Weuster-Botz approach, non-invasive online monitoring of each STR unit can be performed in parallel. Each STR is equipped with an optical sensor unit to determine the process relevant variables pH and DO. Additionally, the expression of GFP tagged proteins can be monitored with a fluorescence based sensor unit.

Another approach for a miniature STR system was published by Ge *et al.* [25]. This system possesses a lower degree of parallelization. It is comprised of 12 identical STR units with working volumes up to 30 mL. Like in the approach presented by Harms *et al.* all reactor vessels are arranged in a circle around a single supply station. To reduce overall cost of the technical equipment, this reactor system is equipped with only one optical sensor unit for pH and pO₂ measurement. Process information of each STR unit is recorded after positioning the reactor vessel above the sensor unit via an automated rotation mechanism. This system has been commercialized by Fluorometrix Corp. (Baltimore, USA) under the name Cellstation [26] and has been slightly modified to additionally measure the optical density of the cultivation broth of each reactor unit.

2.2 Modern bioprocess analysis and adaption for use in disposable reactor systems

The constant monitoring of biotechnological processes is of significant importance to ensure or optimize process productivity and product quality. Especially pharmaceutical and food related processes are often strictly regulated by authorities. For this reason, the United States Food and Drug Administration (FDA) has started the process analytical technology (PAT) initiative for designing, controlling and analyzing such processes [27]. The rising interest in disposable bioreactors and the transition to applying disposable technology in bioprocesses, results in a growing need for disposable and reliable sensor systems, consistent with the PAT initiative [28].

2.2.1 Overview of disposable sensing systems

Biotechnological process analysis can generally be divided into three categories: measurement of physical variables (e.g. temperature, conductivity), chemical variables (e.g. pH, dissolved oxygen) and biological variables (e.g. biomass, viability).

Monitoring and analysis of bioprocesses is often carried out offline by complex analytical techniques. For offline analysis, representative samples are usually extracted from the process via adequate sampling systems and are analyzed outside of the process unit's proximity. Such procedures normally provide precise information for a multitude of process variables. These offline procedures, however, are usually time consuming and valuable information for process control can therefore only be applied with a large delay.

In contrast, online sensors provide necessary information instantly and directly out of the process environment [29].

Depending on the analyte to be measured, the options for technical process implementation of disposable sensors are limited. Basically, two scenarios are possible: disposable in-situ sensors in direct contact with the analyte or (non-invasive) ex-situ sensors that are in contact with the analyte either optically or via a sterile sampling system [30] (Fig. 2).

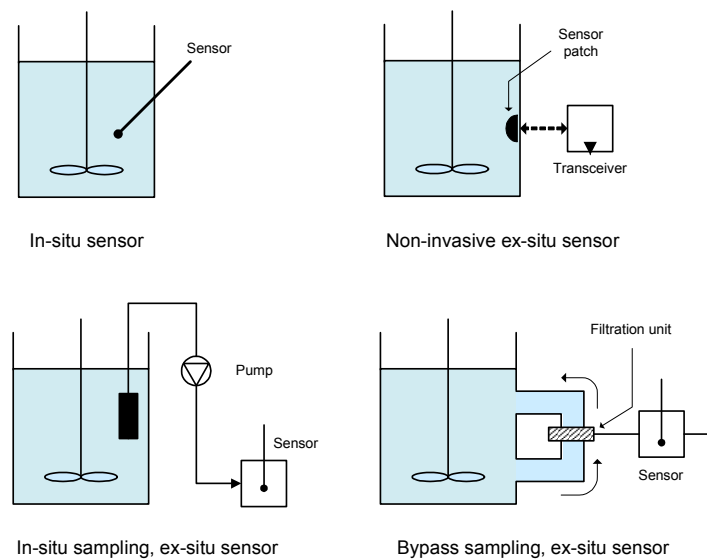


Fig. 2: Possible implementations of disposable sensor systems into bioprocesses. In-situ sensors are directly integrated into the bioprocess, whereas ex-situ sensors can be coupled to the process via optical windows, in-situ or bypass sampling.

Disposable sensor systems must fulfill certain requirements. Sensors in direct contact with the culture medium must be physically or chemically sterilizable. Additionally, these sensors must provide reliable information for a certain time frame and should be cost effective on a per use basis. Especially in-situ sensors or parts thereof must be disposable, rendering conventional and expensive electrodes unusable for disposable applications. However, an alternate approach to integrate an invasive pH probe into a disposable reactor system has been described by Bernard *et al.* [31]. Here a disposable, gamma irradiable and short bodied pH electrode is welded to a disposable bioreactor via a locking mechanism. The pH electrode is encased within a housing, which can be filled aseptically with buffer solutions for sensor calibration. After calibration or validation, the pH electrode can be inserted manually and aseptically into the bioreactor using the locking

mechanism. Other approaches divide the invasive sensors into two parts: inexpensive and disposable sensing elements are placed inside and expensive, reusable measuring equipment is placed outside of the disposable reactor system.

Inexpensive and disposable sensors can be based on semiconductor devices, e.g. pH-ISFETs [32] or conductivity cells [33], which are placed into the gas or liquid phase.

Table 1: Relevant bioprocess variables and possible disposable sensor concepts. The status of the concepts is marked as C (commercially available), R (in research) and N (not yet available).

Process variable	Sensor concept	Disposable system
Temperature	Thermistor	C
	Optical	R
Conductivity	Thick film electrodes	R
	Semiconductor	N
pH	Optical	C
	Optical	C
pO ₂	Optical (fluorescence)	R, C
pCO ₂	Optical (IR)	R
	Optical (ATR-IR)	N
Glucose, lactate	Optical (in-situ microscopy)	N

Optical sensor systems can be used alternatively. These systems allow non-invasive, ex-situ monitoring through a transparent observation window for a wide variety of process variables (Table 1). The term “optical sensor” is not clearly defined, but two areas of application can basically be recognized: direct optical sensing and optical chemosensors. For direct optical sensing nearly all forms of spectroscopy, e.g. ATR-MIR [34] can be applied. Especially fluorescence based sensing is widely used in research and industrial processes. Based on one pair of excitation and emission wavelengths e.g. nicotinamide adenine dinucleotide (phosphate) (NAD(P)H) sensing has been used for biomass estimation [35]. 2D-fluorimeters, e.g. Bioview (DELTA Light and Optics, Hørsholm, Denmark), are used for the detection of multiple components such as proteins, vitamins or metabolites [36].

Because of the increasing application of optical chemosensors for the monitoring of important process variables (e.g. pH and pO₂), the most common measurement principles are described in the following chapter.

2.2.2 Optical chemosensors as an example for non-invasive on-line monitoring

Optical chemosensors rely on indicators with optical properties which are affected by the target analyte. These optical properties comprise e.g. absorption, reflection or luminescence. Optical chemosensors have already been adapted for use in a wide range of disposable technology [14, 37]. The transceiver, the optoelectronic used for fluorescence excitation and emission detection, and analyte sensitive component (e.g. sensor patches) can be interfaced via optical fibers. While the disposable sensor spot is placed inside the reactor vessel, the reusable measurement equipment is positioned outside. Coupling of both components is generally realized by transparent observation windows [38].

Numerous varieties of disposable optical chemosensors for the detection of process critical variables such as pH, pO_2 or pCO_2 have been developed and rely mostly on fluorescence measurements [39]. The applied measurement technique, however, can influence overall sensor precision and long-term stability. Fluorometric sensing is often based on the specific fluorescence properties of ions, molecules or the use of fluorescent labels and indicators. Measured parameters are e.g. intensity, polarization, lifetime, decay time, polarization or quenching efficiency.

2.2.2.1 Intensity based measurements

Quantitative, intensity based fluorometry is widely used in (bio)chemical analysis due to the linear relationship between fluorescence intensity and analyte concentration. However, fluorescence intensity is strongly affected by a wide range of factors including e.g. sample turbidity, external quenchers or drifts of the optoelectronics. Such adverse effects can partly be overcome by applying ratiometric measurements. One way of applying ratiometric measurements is by rationing the intensities of two excitations or emissions at different wavelengths, resulting in an intrinsically referenced parameter. Kermis *et al.* used this approach for the development of a non-invasive pH sensor based on the immobilized fluorescence dye HPTS (8-hydroxy-1,3,6-pyrene trisulfonic acid) [40]. HPTS possesses two excitation maxima and shows a pH-dependent shift of its excitation maximum at pK_a 7.3. The ratio of the luminescence intensities at both excitation wavelengths can be correlated to the pH value of a monitored medium. A practical implementation of such a measurement is shown in chapter 4.6.1.

2.2.2.2 *Life-time based measurements*

Another, meanwhile widely used approach is based on the conversion of analyte induced changes in fluorescence lifetime into a phase shift. Phase shifts are usually not affected by the above mentioned interferences. The most common phase based measurements are phase fluorometric oxygen sensors. For these measurements, an excitation source is modulated at a particular frequency. The fluorescence emission is modulated at a similar frequency f , but phase shifted relative to the excitation signal. Electronic systems, such as lock-in amplifiers compare the excitation and emission signals, granting direct access to the phase shift ϕ , which is directly related to the lifetime τ of the indicator dye (Eq. 1).

$$\tan\phi = 2\pi f\tau \quad \text{Eq. 1}$$

ϕ = phase shift; f = modulation frequency; τ = lifetime of the indicator complex

The indicator dye needs to be sufficiently long lived to be accessible by the applied modulation frequency of the used sensor electronics. Phase fluorometric oxygen sensors utilize in this context Ruthenium based indicators with lifetimes in the microsecond range. A practical implementation of this measurement technique for the determination of dissolved oxygen is described in chapter 4.6.2.

However, indicator dyes used for pH or CO₂ detection have generally shorter life-times and require a modified measurement technique. Following a ratiometric approach, two fluorophores with different decay times are excited by one modulated light source. The ratio of the fluorophores intensities can be converted into a single phase shift. One of these fluorophores acts as a fluorescence indicator and the other one as an inert reference dye with a longer decay time than the indicator [41]. This measurement principle is called dual lifetime referencing (DLR) [42]. The ratio of both intensities can either be calculated in the frequency-domain (FD) or the time-domain (TD).

2.2.2.3 *Life-time based measurements in the frequency-domain*

Frequency domain measurements are widely used for the determination of fluorescence decay times. By exciting a luminophore with sinusoidal modulated light (at a single frequency), the phase angle of the luminescent signal correlates with its decay time. If two luminophores with comparable spectral properties, but differing decay times are

excited, the luminescence signal measured will be a combination of both responses. The phase angle of this signal correlates with the intensity ratio and therefore to the ratio of the decay times of both signals. The measured signal is basically a superposition of the sine functions of both luminophores (Fig. 3).

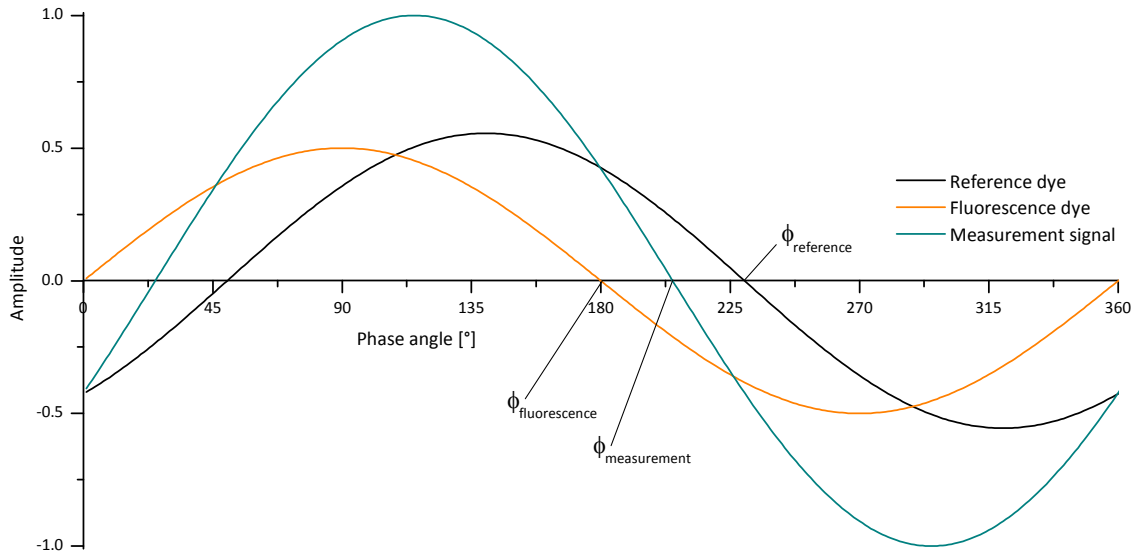


Fig. 3: Frequency domain DLR. The measurement signal is a superposition of the sin functions of the short lived fluorescence indicator and the long lived phosphorescence reference. The determined phase angle $\phi_{\text{measurement}}$ correlates to the ratio of the amplitudes of both luminophores.

Assuming that the reference dye possesses a constant decay time and luminescence intensity, and that the fluorescence dye has a variable emission intensity, the resulting signals can be described by Eq. 2 and Eq. 3.

$$A_{\text{measurement}} \cdot \cos \phi_{\text{measurement}} = A_{\text{reference}} \cdot \cos \phi_{\text{reference}} + A_{\text{fluorescence}} \cdot \sin \phi_{\text{fluorescence}} \quad \text{Eq. 2}$$

$$A_{\text{measurement}} \cdot \sin \phi_{\text{measurement}} = A_{\text{reference}} \cdot \sin \phi_{\text{reference}} + A_{\text{fluorescence}} \cdot \cos \phi_{\text{fluorescence}} \quad \text{Eq. 3}$$

A_x = amplitude measurement signal / reference dye / fluorescence indicator

ϕ_x = phase shift measurement signal / phase angle reference dye / fluorescence indicator

For practical applications the reference dye is usually a phosphorescence dye, e.g. Ruthenium (polypyridil) complexes [43], with much longer decay times than the fluorescence indicator. Additionally, no phase shift from the fluorescence indicator will be obtained when modulation frequencies are in the lower kHz range ($\phi_{\text{fluorescence}}=0$). Based on these assumptions, Eq. 2 can be divided by Eq. 3 resulting in the correlation of the

measured phase shift and the intensity ratio of the reference dye and fluorescence indicator (Eq. 4) [42].

$$\frac{A_{\text{measurement}} \cdot \cos \phi_{\text{measurement}}}{A_{\text{measurement}} \cdot \sin \phi_{\text{measurement}}} = \cot \phi_{\text{measurement}} = \cot \phi_{\text{reference}} + \frac{A_{\text{fluorescence}}}{A_{\text{reference}} \cdot \sin \phi_{\text{reference}}} \quad \text{Eq. 4}$$

The cotangent of the measured phase shift ($\phi_{\text{measurement}}$) describes the referenced intensity of the fluorescence indicator. If the reference phase angle is known, $\cot \phi_{\text{measurement}}$ relates linearly to the intensity ratio of both luminophores.

2.2.2.4 Life time based measurements in the time-domain

By contrast, measurements in the time-domain do not rely on frequency modulated light, but on squared pulses of light for luminescence excitation. The excitation light source, usually a light emitting diode (LED), is periodically switched on and off, thus opening two measurement windows: excitation (LED on) and emission (LED off). The period of these pulses is of the same magnitude as the decay time of the reference dye (Fig. 4).

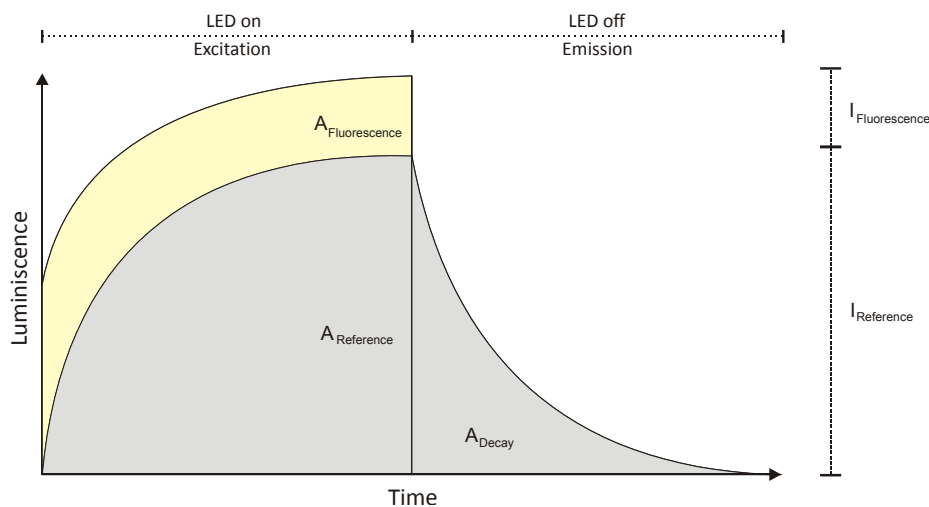


Fig. 4: Time domain DLR. A mixture of fluorescence indicator and phosphorescence reference dye is excited by a square wave pulse train of light. In the excitation window the cumulative intensities of both dyes is measured, while in the emission window only the decay of the long-lived reference dye is detected.

The signal measured in the excitation window derives from the intensity accumulation of the fluorescence indicator (yellow) and the reference dye (grey). In the emission window only the phosphorescence of the reference dye is detected. Both obtained signals are separated due to the considerably longer decay time of the reference dye. Assuming the

reference possesses a mono exponential decay, the following mathematical relation can be formed:

$$\frac{A_{\text{fluorescence}} + A_{\text{reference}}}{A_{\text{decay}}} = R = k_1 \cdot \frac{I_{\text{fluorescence}}}{I_{\text{reference}}} + (k_2 - 1) \quad \text{Eq. 5}$$

While $A_{\text{fluorescence}}$ and $A_{\text{reference}}$ describe the signal intensities of the fluorescence indicator and reference dye in the excitation window, A_{decay} describes the signal intensity from the reference obtained in the emission window. k_1 and k_2 are system specific constants. From Eq. 5 it can be seen, that the ratio R between excitation and emission correlates linearly with the ratio of the signal intensities of the fluorescence indicator ($I_{\text{fluorescence}}$) and the reference dye ($I_{\text{reference}}$).

Both measurements methods, FD-DLR and TD-DLR, are similar in precision and interference elimination. However, practical applications for sensor systems is dominated by frequency domain measurements, because the overall technical setup is cheaper and easier to realize. Particularly the use of dual phase lock-in amplifiers having phase resolutions of a hundredth of a degree, significantly increases measurement precision.

2.2.2.5 Examples of optical chemosensors

The measurement principle of optical oxygen sensors is based on the dynamic quenching of a fluorescence indicator dye by molecular oxygen. For detection a fluorescence dye is immobilized in a polymer matrix and attached either to the tip of an optical fiber or is encased in a disposable sensor patch. LEDs are typically used for excitation. The indicator fluorescence lifetime is directly related to the oxygen partial pressure (pO_2) in the proximity to the sensor. In contrast to established electrochemical sensors like the Clark electrode, optical oxygen sensors offer various advantages. These sensors can be arbitrary scaled down, they operate non-invasively, possess a high spacial resolution and through applying DLR measurements an excellent long term stability. Such sensor systems are already commercially available (e.g. neFOX, Ocean Optics Inc., Dunedin, USA).

The optical detection of pH values can either be accomplished by fluorescence or absorption based pH indicators. The measurement principle is closely related to the one of optical oxygen sensors. The optical properties of the immobilized dye are changed by the proton concentration of the medium in contact. As described above, optical pH

determination can be performed with an intensity based ratiometric measurement or by addition of a reference dye by DLR measurements. Disadvantages of optical based pH measurements are the limited operation range of 3 – 4 pH units and sensitivity towards ionic strength variations of the analyte. Optical pH sensors are e.g. commercially available by Fluorometrix (Cellphase, Baltimore, USA) or Presens (pH mini, Regensburg, Germany).

Fibre-optic pCO₂ sensors are mostly based on the Severinghaus principle. This electrode is encased in a CO₂ permeable membrane and is composed of a pH and reference electrode in contact with a carbonate buffer. The sensor detects the pH value of the carbonate buffer, which is in equilibrium with the CO₂ outside the membrane. By a variation of the CO₂ concentration in the medium, CO₂ diffuses through the membrane and subsequently changes the pH value by interfering with the proton-carbonate-equilibrium. This change can be detected electrochemically. Optical CO₂ sensors function accordingly and often utilize the same fluorescence indicators as optical pH sensors. Instead of a carbonate buffer solution, the membranes of newer pCO₂ chemosensors contain quaternary ammonium hydroxide cations and pH indicator dye anions. Interference eliminating DLR type sensors are based on the pH indicator HPTS dissolved in an ethylcellulose matrix with poly(acrylonitrile) encapsulated Ru(dpp) as reference dye [44].

PART A

3 Miniature-scale bioreactor system for the parallel operation of three stirred tank reactors

Bioprocess development and optimization is a broad and intensive field of academic and especially industrial research. Intensive strain selection, culture media optimization and determination of critical process parameters are crucial steps towards highly productive bioprocesses. Due to the high number of experiments necessary in the early stages of process development, established cultivation techniques are constantly adapted to achieve as many results as possible within the shortest time frame. The parallelization of cultivations is one possibility to significantly reduce this expenditure of time.

In this context, a reactor system for the parallel operation of up to three mini-scale stirred tank reactors will be evaluated and optimized in this part of the thesis. Miniature-scale stirred tank reactors are commonly defined as reactor systems with working volumes below 100 mL [45]. This reactor prototype will further be referenced to as Tristation and was originally constructed by Fluorometrix Corp. (Baltimore, USA). It was provided by Sartorius Stedim Biotech GmbH (Goettingen, Germany) for the duration of this work. The aim of this project was not only to evaluate, but also to characterize and optimize this prototype. The essential components of the Tristation will be profoundly investigated and all characteristics will be implemented into a monitoring and control software module. Finally, the reactor system will be evaluated in exemplary bioprocesses.

3.1 Components of the reactor system

The Tristation is composed of three support stations for the parallel operation of up to three mini-STRs (Fig. 5). Each of these support stations is equipped with a metal-block (A) attached to a peltier element (B) (Qualitykits QK66, Kingston, Canada) to temper the reactor units (Fig. 6). These metal blocks possess a circular gap with an inner diameter matching the outer diameter of the reactor modules, in order to ensure maximum heat transfer. Optical sensor units (Fluorometrix, Baltimore, USA) for the determination of pH and DO values are centered below each reactor station (C). Furthermore, each station is

equipped with an individually controllable stepping motor (Lin Engineering, Santa Clara, USA) to power the STR agitators (D). Six peristaltic pumps (Instech Laboratories Inc. P625, Plymouth, USA) are located on the upper side of the reactor system (E). Two pumps are allocated to each of the three reactor stations. These pumps can be used e.g. for pH-correction or nutrient feed.

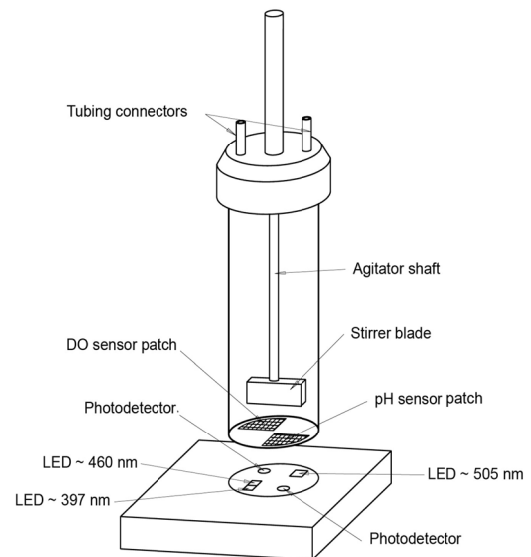
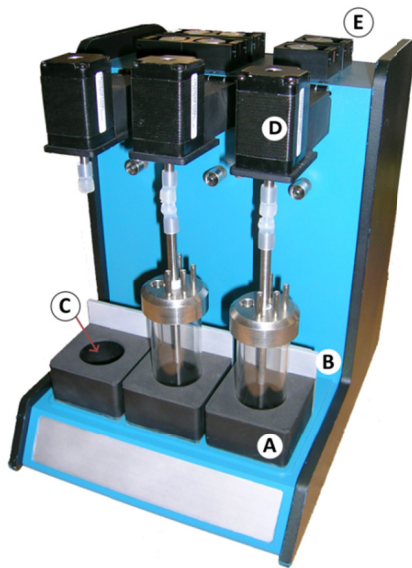


Fig. 5: Tristation prototype: metal heating blocks (A), peltier elements (B), location of the optical sensor units (C), stepping motors (D) and peristaltic pumps (E).

Fig. 6: Illustration of the STR units and the optical sensor systems of the Tristation.

Two additional supports for storage vessels are located on the back of the reactor system. One of these supports is equipped with an air-cooled peltier element e.g. to cool induction solutions or nutrient additives. The reactor system can be connected to four different gas sources, which can be individually dispersed to each reactor station via a magnetic valve array (SMC, Hallbergmoos, Germany).

The reactor modules are composed of a cylindrical glass vessel with a total volume of 40 mL and a stainless steel reactor-cap (Fig. 6). This cap offers various tube connectors, a sealable port for inoculation or sampling and a gap for the agitator shaft. The agitators are currently equipped with a straight paddle type impeller. pH and DO sensitive sensor patches can be attached adhesively to the vessel bottom at a defined orientation, thus being located exactly above the sensor units.

4 Setup and characterization of the hardware environment

For the characterization of the Tristation and the subsequent development of a monitoring and control software, the reactor unit has been divided into five subsystems: agitation, feeding, aeration, monitoring and temperature control. Each of these subsystems is driven by an (electro)mechanical or electronic device with an individual control concept (Fig. 7). While agitation is realized through stepping motors driving the agitators, solution delivery for feeding or pH control is based on the use of peristaltic pumps. Incubation of the reactor chambers is accomplished by peltier elements and gas supply can be controlled through magnetic valves. Online monitoring of pH and DO values is based on the use of non-invasive optical sensor technology.

In the following chapters, these subsystems will be evaluated and optimized, if necessary. The control concept will be based on multi-I/O controllers (Plug-In Electronic GmbH, Eichenau, Germany) operated by software modules designed in Labview 8.2 (National Instruments, Austin, USA).

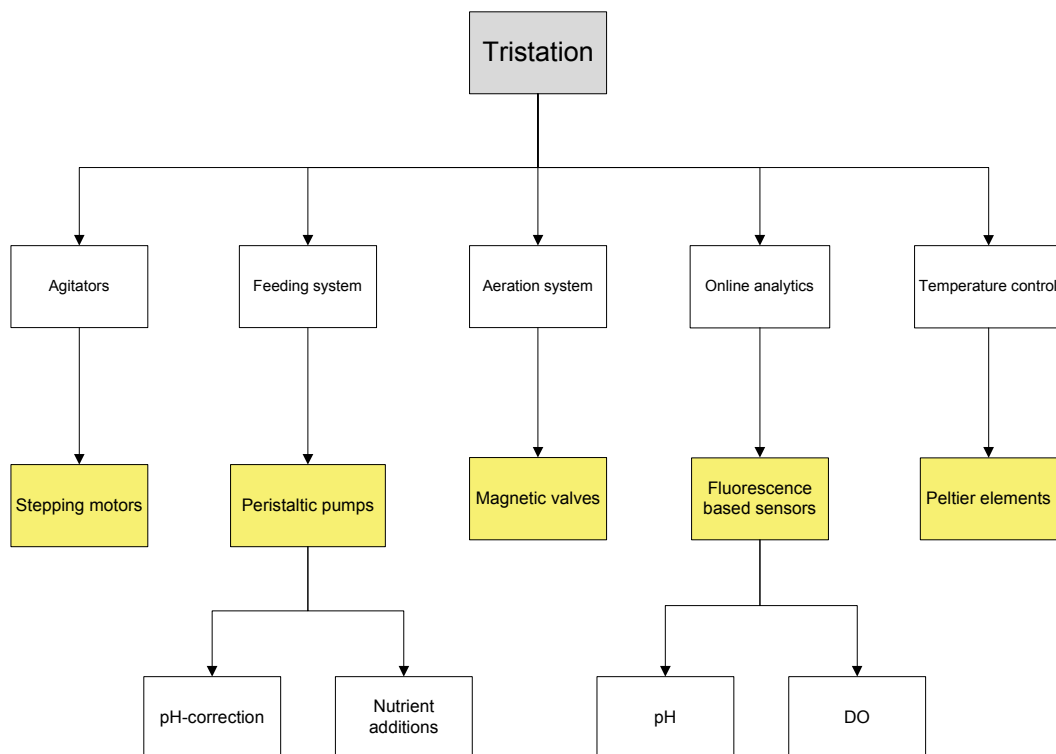


Fig. 7: Flow chart of the controllable devices (yellow) of the Tristation to influence or monitor the environmental conditions agitation, feeding, aeration, temperature, pH and dissolved oxygen.

4.1 Agitation subsystem

Each reactor station is equipped with a stepping motor to drive a STR's agitator. To individually control the stirring rates of each motor, a command sequence (Fig. 8) needs to be transmitted to a proprietary motor driver (Fluorometrix, Baltimore, USA), which subsequently translates this sequence into a command which changes the motor steps.



Fig. 8: Software sequence to individually change the stirring rates of the Tristation's agitation units.

This sequence is comprised of a command to select the desired motor, a TTL pulses train (transistor-transistor-logic) to change the stirring rate, a deselecting command and information to increase or decrease rotation speed. The TTL pulse train has a 50 % duty cycle with a duration of 50 ms. The proprietary motor driver is enabling 128 pulses to control stirring rates from 10 – 1,000 rpm in a non-linear relation (Fig. 9).

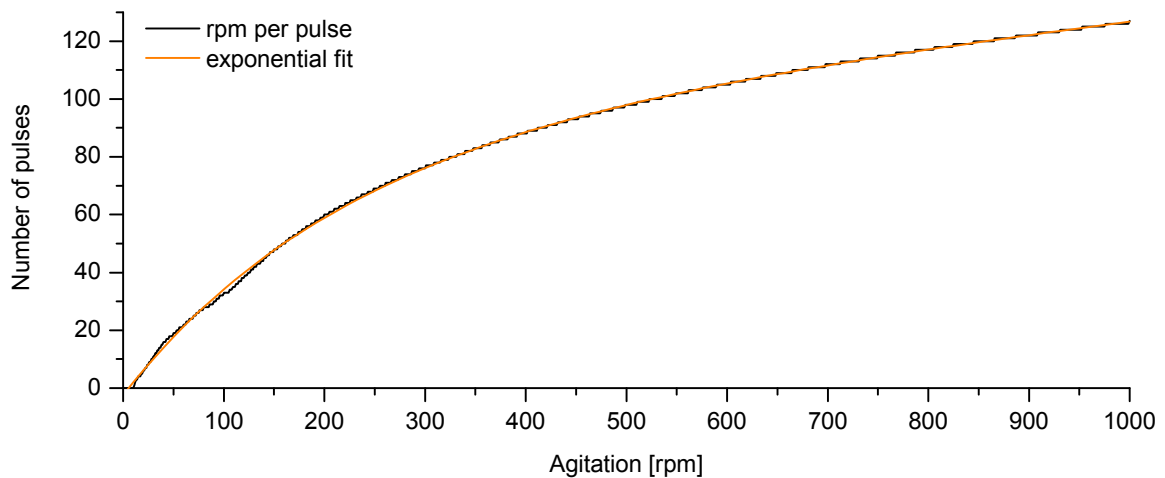


Fig. 9: Correlation of rotations per minute and necessary number of TTL-pulses. The 7 bit motor driver board is allowing 128 pulses to control stirring rates from 10 – 1,000 rpm. The most precise control ranges from 10 – 2,000 rpm with an error ± 2 rpm.

The most precise agitation control is achieved from 10 – 200 rpm. The necessary pulses to change agitation to a desired rotational speed can be calculated using Eq. 6 with subsequent rounding to the nearest whole number.

$$P \in \mathbb{N} = -89.93 \cdot e^{\frac{rpm}{-221.72}} - 7.27 \cdot 10^5 \cdot e^{\frac{rpm}{-1.7 \cdot 10^7}} - 7.27 \cdot 10^5 \quad \text{Eq. 6}$$

4.2 Magnetic valve controlled aeration subsystem

The Tristation is equipped with four connectors for the separate supply of four different gases. These four gas lanes are connected to three magnetic valve arrays (SS3Y1, SMC, Hallbergmoos, Germany) allowing independent dispersion to each reactor station (Fig. 10). Since this system is not equipped with a mass flow based blending station, desired volumetric flow rates have to be adjusted by interconnected mass flow controllers (MFC). For all subsequent experiments Bronkhorst F-201C MFCs have been used. Gas mixtures can alternatively be provided by pulsing additional components, e.g. oxygen or carbon dioxide, into the carrier stream. Opening and shutting of the magnetic valves is achieved by sending high or low TTL signals.

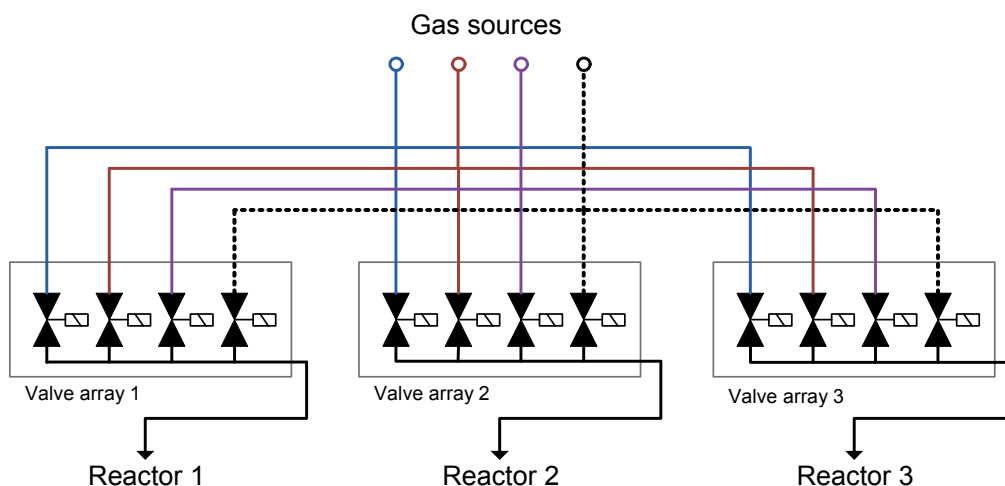


Fig. 10: Magnetic valve setup of the reactor system. Each reactor station can be individually connected to four gas sources.

In the course of this work, the magnetic valves proved to be working properly from an electronically perspective. But upon application of pressures above 50 mbar, the valves did not close completely, allowing undesired blending. If necessary, gas mixing was realized instead using an external gas mixing station (Bronkhorst E-7110, Bronkhorst Maettig GmbH, Kamen, Germany) connected directly to the reactor modules.

4.3 Peristaltic pump subsystem

Each reactor station is equipped with two peristaltic pumps which can be used for pH control or medium supplement delivery. These pumps can only be operated at a fixed

rotational speed as they lack the technical capability of step control or supply voltage variation. Instead, a defined feed rate can only be achieved by switching the pump on or off using high or low TTL signals. For the implementation of a pH-control module into the control software to develop, the individual rotational speeds and feed rates of each pump have been determined.

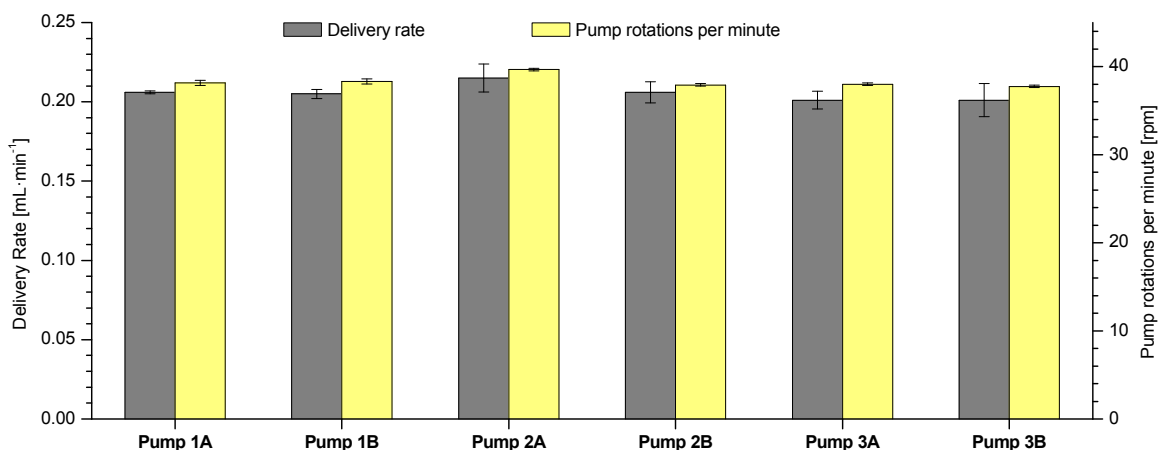


Fig. 11: Determination of the delivery rates and pump rotations of the peristaltic pumps used in the Tristation.

All calibrations have been performed in triplicate using pump specific peristaltic tubing (P625/TS015S, Instech, Plymouth, USA). Even though all pumps were operated with the same supply voltage of 13 V, slight variations in feed rate and rotational speed have been observed (Fig. 11). As the pump heads rotational speed ranges from 38 rpm (Pump 3B) to 40 rpm (Pump 2A), the delivery rates are varying accordingly from 0.201 mL·min⁻¹ (Pump 3A) to 0.216 mL·min⁻¹ (Pump 2A). Overall mean delivery rate is $206 \pm 5 \mu\text{L}\cdot\text{min}^{-1}$. For a precise recording of supplied solutions, the final control and monitoring software was equipped with a subroutine to store individual calibration constants for all peristaltic pumps.

4.4 Characterization and optimization of the temperature control system

A precise temperature control in ongoing cultivations is of significant importance in order to avoid high deviations from the optimal temperature. Such deviations can lead to possible variations in cell growth or productivity. Each reactor station of the Tristation is therefore equipped with a metal-block attached to a peltier element. A circular gap in

the middle of each metal-block is used to support and temper the reactor unit in contact. The heat transfer is thereby realized from the peltier element onto the metal-block, possibly through an air layer and finally from the vessel wall into the growth medium. As temperature is only monitored by a K-type thermocouple located between the peltier element and the metal-block, a temperature gradient to the reactors interior is apparent.

A temperature profile of reactor station 1 equipped with a STR unit filled with 25 mL water at an agitation rate of 200 rpm was recorded for further evaluation. The peltier element was operated with its specified supply voltage of 5 V and a current of 1.5 A. A maximum temperature of 40.9 °C of the reactor station was reached after 56 min. Internal reactor temperature was monitored using an invasive PT-100 temperature sensor (Modig 008V2, Megatron, Munich, Germany). Maximum temperature of the bulk solution contained in the reactor reached 40.1 °C within the same time frame. The disconnection of the power supply resulted in cooling of both the reactor station and the bulk medium. Since the control system is technically not designed to support active cooling, cooling will be determined mainly by the ambient temperature. For the duration of the above described experiment, the internal reactor temperature did not match the set temperature of the heating system at any time.

4.4.1 Optimized temperature control concept

Since the mechanical setup of the Tristation is not designed to support monitoring of the internal reactor temperature, a customized control concept was established. This concept is based on the use of a correction function taking the difference between the temperature of the heating system and the internal reactor temperature into account. Various step profiles using different working volumes and temperature setpoints have been recorded to calculate a mean correction function for each reactor station.

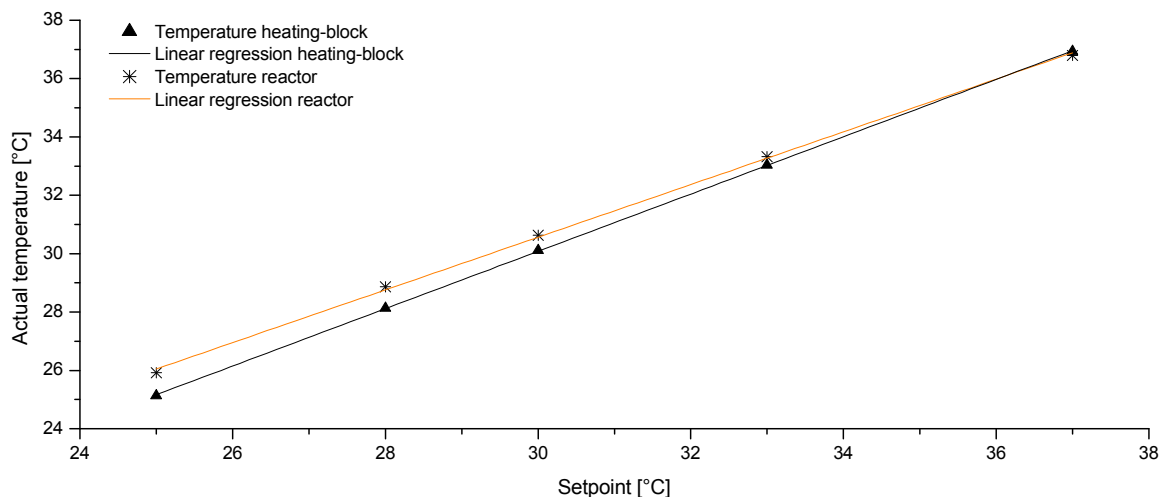


Fig. 12: Linear regression of the mean values of internal reactor temperature and temperature of the heating system as a basis for the calculation of a correction function. Displayed data was recorded on reactor station 1 using a STR unit with a working volume of 25 mL and an agitation rate 200 rpm.

For these step profiles a series of increasing temperature setpoints was defined (25 °C, 28 °C, 30 °C, 33 °C and 37 °C). Since a non-variable power supply was used, the peltier elements were operated with an on-off control routine, which powered the peltier element until a predefined setpoint was reached. The peltier element was subsequently powered off until the station temperature dropped below the setpoint. The on/off duration was defined as 5 s. Standard deviations from the setpoint using this control routine were not exceeding 0.18 K. When a setpoint was reached, the mean temperatures for the reactor station and the internal reactor temperature were calculated from 100 data samples. Plotting these results followed by a linear regression, the individual profiles for internal reactor temperature and reactor station temperature can be obtained. A profile, describing the tempering of a STR unit with 25 mL, at an agitation rate of 200 rpm in reactor station 1 is exemplary shown in Fig. 12. By calculation of the difference of both linear functions, the necessary correction function to estimate internal reactor temperature can be assessed. The mean correction functions for each reactor station are listed in Table 2 – they are applicable for working volumes ranging from 10 - 35 mL.

All resulting correction functions were referenced to a Megatron Modig 008V2 PT-100 sensor (MEGATRON Elektronik AG & Co., Munich, Germany) used for measuring internal reactor temperature.

Table 2: Correction functions to optimize internal reactor temperatures based on the readings of the reactor station temperatures. y^{corr} represents the internal reactor temperature, whereas x is the temperature determined by the K-type thermocouple positioned between peltier element and metal-block.

	Reactor station 1	Reactor station 2	Reactor station 3
Correction function	$y^{corr} = x + 0.082 \cdot x - 2.903$	$y^{corr} = x + 0.101 \cdot x - 3.105$	$y^{corr} = x + 0.079 \cdot x - 2.615$

These correction functions were implemented into a software module to validate the effectiveness of the optimized control. Two sets of experiments were performed. For each set five temperature setpoints ranging from 25 – 37 °C were defined. Using a STR unit with a 25 mL working volume and an agitation rate of 200 rpm, step profiles based on a non-optimized and optimized control scheme were recorded. Temperatures in the reactor chambers were recorded using the above mentioned Modig 008V2 sensor. Measured deviations of the internal reactor temperature from the defined setpoints are displayed in Fig. 13.

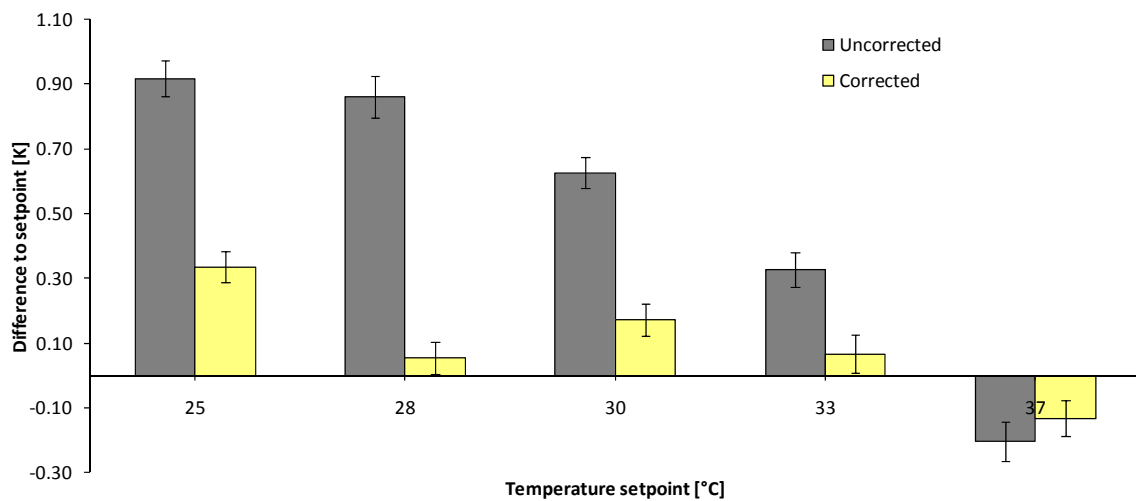


Fig. 13: Mean deviations of the internal reactor temperature from the setpoint: non-optimized temperature control (grey) and optimized control (yellow).

Deviations from the predefined setpoints could be improved considerably by using the optimized control. Especially in the temperature range below 30 °C deviations of up to 0.9 K could be reduced by the factor of three. The most significant improvement was observed for the setpoint of 28 °C. While non-optimized control led to a 0.86 ± 0.06 K deviation, the use of the optimized control could reduce this difference to 0.06 ± 0.05 K.

The influence of agitation on the internal reactor temperature has been investigated using the optimized control, a working volume of 25 mL, a temperature setpoint of 37 °C and stirring rates varying from 20 - 700 rpm.

Agitation rates of as low as 20 rpm lead to actual-temperature-setpoint deviations of - 0.5 °C. Increasing stirring rates resulted in decreasing deviations from the temperature setpoint. Stirring rates above 150 rpm were found to be of low deviation from the setpoint. For cultivations with stirring rates below 150 rpm should be considered that the predefined setpoint might eventually not be reached.

Based on the above described optimizations, a software routine for the final control software was established (Fig. 14). This software routine will read the reactor station temperature and estimate the internal reactor temperature using the correction functions (see Table 2). The on-off controller will determine if the corrected temperature is higher or lower than the setpoint and will accordingly switch the peltier element on or off. The sequence loop will restart after a definable iteration delay.

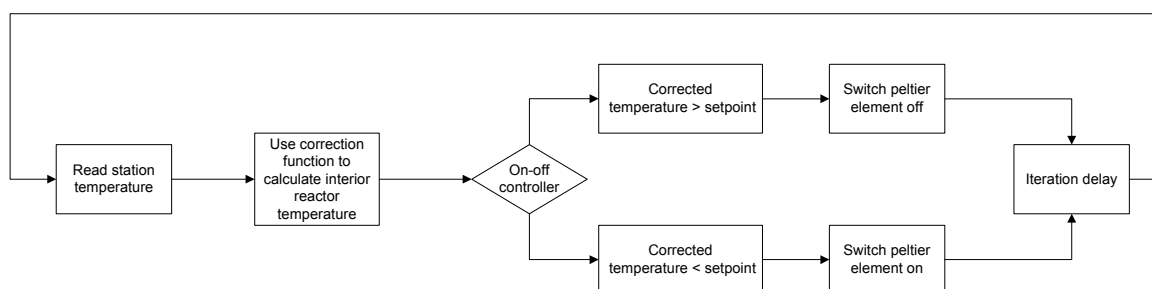


Fig. 14: Schematic representation of the Labview software routine to control the internal reactor temperature of a STR unit positioned in the Tristation.

The cooling mechanism located at the backside of the Tristation is operated by an air-cooled, inversely operated peltier element. No control routine was applied to this unit, since the cooling capability is dependent on the ambient temperature. Operating the peltier element within its specifications resulted in a cooling performance of approximately 4 K below ambient temperature.

Further optimization of the temperature control could be achieved by replacing the K-type thermocouple by a PT-100 sensor and subsequent repositioning towards the vessel wall of the STR unit. Additionally, the use of a variable power source could not only

lower heating times by applying higher voltages, but could additionally reduce hysteresis around the setpoint when based on a PID-controller.

4.5 Characterization of the STR units

For a further characterization of the reactor system and especially of the STR units, the determination of characteristic reactor numbers is required. In this chapter k_La values, characteristic for oxygen intake efficiency and residence time distributions as an index for mixing quality, will be presented.

4.5.1 k_La determination and aeration strategies

Oxygen is often a limiting factor in aerobic cultivations with a significant influence on biological growth and product formation. It is therefore of interest to determine the efficiency of oxygen intake into the bioreactor, to outline the performance of the aeration system or to optimize this system to suit the needs of specific biological conditions. The k_La value is generally a measure for the quantity of oxygen being transferred into a volume element within a certain time frame.

All following k_La determinations are based on the sulfite-method (chapter 15.6.1). In this method a sodium sulfite solution with a defined concentration is allocated in the STR unit. Aeration and dissolved oxygen monitoring is started upon injection of a catalytic amount of a divalent copper salt. In the presence of divalent copper ions, sulfite ions are oxidized to sulfate ions. As long as sulfite ions are present, dissolved oxygen (DO) remains 0 %. The time frame required, until DO [%] starts to rise, can be mathematically correlated to the k_La value. All determinations were carried out at 23 °C. DO monitoring in the reactor vessels was accomplished using a non-invasive optical chemosensor (Oxy 4, Presens, Regensburg, Germany).

Since the STR units in their original design only support surface aeration, k_La values for working volumes from 13 – 35 mL at 1 vvm surface aeration (pressurized air) have been determined (23 °C, 100 rpm) (Fig. 15).

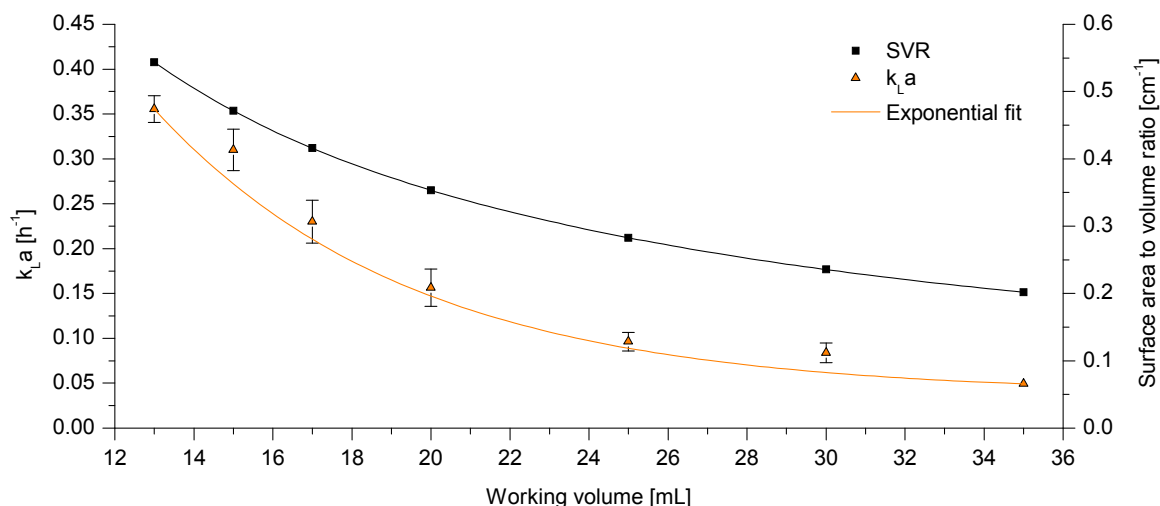


Fig. 15: Determination of $k_{L,a}$ values for different working volumes at surface aeration rates of 1 vvm (23 °C, 100 rpm). Additionally, the corresponding surface area to volume ratios (SVR) are plotted.

$k_{L,a}$ values are decreasing with increasing working volumes. With a working volume of 35 mL and surface aeration at 1 vvm a $k_{L,a}$ value of 0.05 h^{-1} was obtained. Reduction of the working volume to 13 mL at 1 vvm aeration rate resulted in six fold higher $k_{L,a}$ values (0.35 h^{-1}). Working volume and corresponding $k_{L,a}$ values are not related linearly, but can instead be described by an exponential fit - just like the correlating SVRs. Depending on the organism to be cultured, such small $k_{L,a}$ values, mostly dependent on the small SVRs, will most likely lead to an oxygen intake limitation affecting the overall biological growth. Especially if using the Tristation for scale-up considerations, alternative aeration strategies are necessary.

In this context, different components to increase the overall oxygen transmission rate have been evaluated: silicon tubing, perforated silicon tubing, eluent frit (A-303A 10 μm), hydrophilic hollow fibre (UltraPES 0.7, Membrana, Wuppertal, Germany) and a self-constructed aerating agitator (Fig. 16).

All aeration elements, except the aerating agitator, were attached to the internal aeration connection of the reactor cap. The UltraPES hollow fiber were operated dead-end. The immersion depth of these components was chosen to be as deep as possible, as to avoid mechanical interference with the stirrer blade. The aerating agitator was developed to reduce overall space consumption of the aeration unit. This agitator is comprised of a hollow shaft and a static aeration ring equipped with a gas source

connector. Inbound gas is transferred from the aeration ring via a perforated section of the hollow shaft into its inner cavity. To avoid leakage, the transmission section of the aeration ring is sealed on both sides by silicon gaskets. Introduced gas emerges into the culture medium through an open shaft section directly below the stirrer blade. Gas dispersion into the bulk medium is enhanced by reduction of bubble size through the stirrer blade.

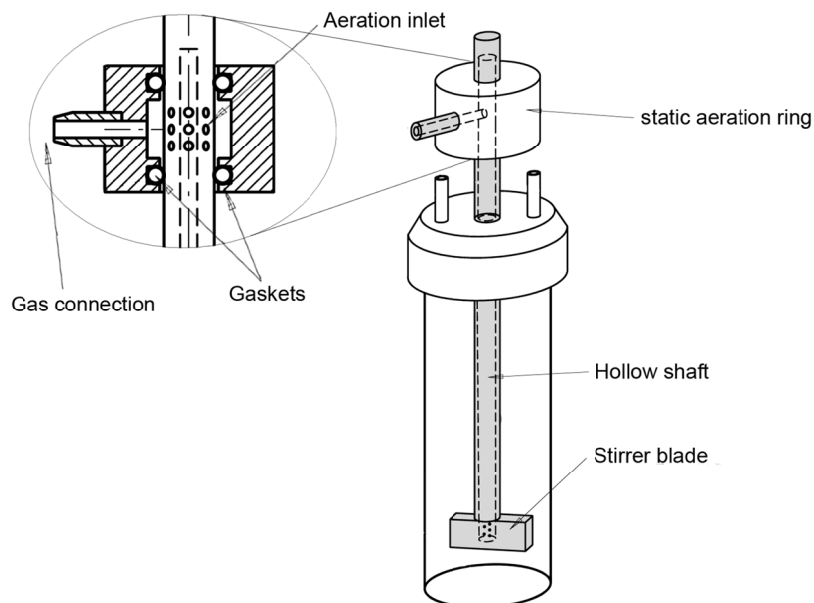


Fig. 16: Construction sketch of the aerating agitator. Gas can be connected to the static aeration ring via a hose connection. Within this ring the hollow shaft is perforated so that inbound gas can be transferred to the inner cavity. The lower end of the hollow shaft is open to release the gas directly underneath the stirrer blade into the culture medium.

For all evaluated aeration elements, $k_L a$ values were determined in triplicate using the sulfite-method and working volumes of 20 mL (1 vvm pressurized air, 23 °C, 100 rpm).

In contrast to surface aeration, $k_L a$ values could be increased at least fivefold to $0.8 \pm 0.1 \text{ h}^{-1}$ using silicon tubing or the aerating agitator (Table 3). Higher $k_L a$ values using these aeration elements are most likely not possible, since emerging air bubbles are rather large and are insufficiently crushed by the stirrer blade to increase their SVR. Ten times higher $k_L a$ values compared to surface aeration were observed when using perforated silicon tubing ($1.5 \pm 0.1 \text{ h}^{-1}$). Highest $k_L a$ values were reached using an eluent frit ($3.1 \pm 0.1 \text{ h}^{-1}$) or UltraPES hollow fiber ($4.3 \pm 0.3 \text{ h}^{-1}$). These values can be explained by

the fine distribution – the hollow fiber aeration was non-diffusive – of air bubbles with a high SVR enhancing oxygen diffusion into the culture broth.

Table 3: Mean k_La values and standard deviations from triplicate measurement using different aeration elements. All determinations were carried out with a working volume of 20 mL, 1 vvm pressurized air, 23 °C and a stirring rate of 100 rpm.

	Surface aeration	Aerating agitator	Silicon tubing	Silicon tubing perforated	Eluent frit	UltraPES hollow fibre
k_La [h^{-1}]	0.16 ± 0.1	0.75 ± 0.1	0.81 ± 0.1	1.54 ± 0.1	3.09 ± 0.2	4.28 ± 0.3

All five aeration elements can be used for invasive aeration. Since k_La values with these devices range from $0.8 h^{-1}$ – $4.3 h^{-1}$, the demands of the organism to be cultured need to be determined previously. Even though the oxygen intake performance of the eluent frit was lower than the one of the UltraPES hollow fiber, it was used for all subsequently performed cultivations. It was preferred because it is autoclavable and easier in overall handling.

The aerating agitator is an interesting option for cultivations where oxygen intake via surface aeration is not sufficient enough or the use of invasive aeration elements is unfeasible due to mechanical or process restrictions. With further modification of this agitator, e.g. by decreasing bubble sizes through smaller exit pores, its efficiency can be increased.

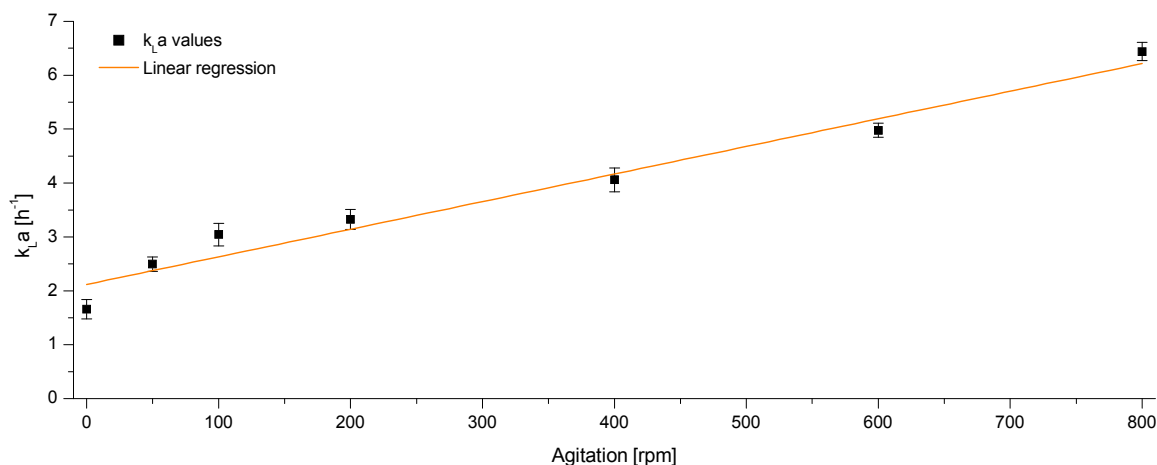


Fig. 17: Linear relationship of k_La values and agitation rate using an eluent frit as aeration element, an aeration rate of 1 vvm pressurized air at 23 °C in a 20 mL working volume.

In addition, the influence of increased gas dispersion by accelerated agitation on oxygen intake efficiency was determined using the eluent frit, a 20 mL working volume and 1 vvm pressurized air at 23 °C. Agitation rates were varied from 0 – 800 rpm (Fig. 17). Oxygen transmission into the medium increases in linear relation with mixing performance and accordingly with gas dispersion. Without agitation k_{La} values of $1.7 \pm 0.2 \text{ h}^{-1}$ were reached and nearly quadrupled to $6.4 \pm 0.2 \text{ h}^{-1}$ when stirring rate was increased to 800 rpm.

4.5.2 Residence time distributions

The formation of mass transfer limiting aggregates in bioreactors is often a drawback concerning optimal nutrient delivery or representative broth sampling. These aggregates or volume elements can be understood as individual STRs. To avoid the formation of such aggregates a preferably ideal homogenous mixing is favored. The mixing capability of STRs is usually characterized by determination of the residence time distribution (RTD), a probability distribution function which describes the amount of time a volume element remains inside a bioreactor.

An optical measuring method based on the use of methylenblue as tracer component was used for the RTD determination of the STR units (chapter 15.6.2). Stirring rates were varied from 20 - 800 rpm and the working volume was 25 mL. The STR units were operated as CSTRs by coupling them with a multichannel pump (IPC4, Instech, Glattbrugg, Switzerland) at a feed rate of $0.7 \text{ mL} \cdot \text{min}^{-1}$. The relative change of the tracer concentration after injection (pulse experiment) was recorded using a photometer (Cary 50, Varian Inc., Palo Alto, USA). The resulting concentration profile correlates directly with the exit age distribution $E(\theta)$. The corresponding cumulative RTD function $F(\theta)$ can be calculated from Eq. 7.

$$F(\theta) = \int_0^{\infty} E(\theta) d\theta \quad \text{Eq. 7}$$

$F(\theta)$ = cumulative residence time distribution function; $E(\theta)$ = exit age distribution; θ = dimensionless time

The courses of the $E(\theta)$ and $F(\theta)$ functions are comparable for all stirring rates within the range of 20 – 800 rpm and are similar to the ones of an ideal CSTR (chapter 15.6.2). After

exchanging the working volume approximately seven times ($\theta = 7$), all tracer molecules have been removed completely from the reactors ($E(\theta) = 0$ and $F(\theta) = 1$).

The mean residence time t' is another term to describe the mixing performance of a bioreactor. t' describes the amount of time a volume element resides inside a reactor. In contrast to the hydrodynamic residence time (τ_h) the mean residence time t' considers that different amounts of tracer elements emerge from the reactor at different points in time. While τ_h for all stirring rates is 36.9 min, t' needs to be calculated from Eq. 8 for each agitation rate (Table 4)

$$t' = \int_0^{\infty} E(t) \cdot t \cdot dt \quad \text{Eq. 8}$$

t' = mean residence time; $E(t)$ = exit age distribution; t = time

Table 4: Mean residence time t' [min] of the STR units for agitation rates from 20 – 800 rpm

Rpm	20	50	100	150	200	400	600	800
t' [min]	55.9	56.1	57.8	55.1	56.0	54.7	55.7	53.2

As all mean residence times t' are similar and average at 55.6 ± 1 min, it can be assumed that the mixing performance of the STR units with the blade impeller is comparable for all agitation rates.

The Bodenstein number Bo is a dimensionless number characterizing the backmixing within a reactor system and is defined as the ratio of convective to diffusive flow. A Bo tending to zero describes a reactor system behaving as a CSTR with ideal mixing conditions. In case Bo is tending to be infinite, the observed reactor system most likely represents a plug flow reactor (PFR). The Bo numbers for the studied STR units and agitation rates can be calculated with Eq. 9 from the exit age distributions.

$$Bo = \frac{\sqrt{1 + (8 \cdot \sigma_{\theta}^2)}}{\sigma_{\theta}^2} \quad \text{with} \quad \sigma_{\theta}^2 = \frac{t^2 \cdot E(t)}{\tau_h^2} \quad \text{Eq. 9}$$

σ_{θ}^2 = mean quadratic variance of the hydrodynamic residence time;
 $E(t)$ = exit age distribution; t = time; τ_h = hydrodynamic residence time

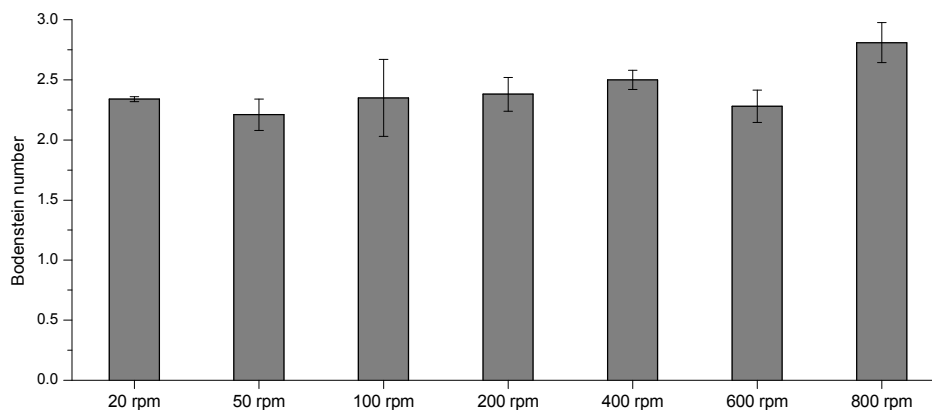


Fig. 18: Mean Bodenstein numbers and standard deviations at various agitation rates in the STR units with a working volume of 25 mL.

The determined Bodenstein numbers, just like the mean residence times show just a slight variation for all monitored agitation rates. The overall mean Bo is 2.4 ± 0.2 and can therefore be considered to tend to zero (Fig. 18). The backmixing in the reactor for all monitored agitation rates can be considered to be nearly ideal. Based on the accomplished determinations of RTDs and Bodenstein numbers it can be concluded, that the STR units show at all applicable stirring speeds nearly ideal mixing capability.

4.6 Characterization of the optical sensor units

4.6.1 pH determination based on ratiometric fluorescence intensity measurements

To maintain the pH of a cultivation within an optimal range, it is of significant importance to achieve high cell densities and cell viabilities, as well as good productivities. During the course of a cultivation, organisms start to produce metabolites affecting the overall pH of the culture broth. It is therefore necessary to not only constantly monitor, but also to control the pH of the cultivation. Optical chemosensors provide in this context a non-invasive and non-toxic possibility for pH regulation. However, in contrast to conventional pH-electrodes, their measuring range is limited and needs to be adapted to suit the required needs.

The Tristation is equipped with fluorescence intensity based sensor units to determine the pH of the culture broth in each of the three STR units. This sensor system is comprised of two parts: an optoelectronic and an analyte sensitive sensor spot. The

optoelectronics is placed outside of the cultivation environment and is composed of two light emitting diodes (LEDs) for excitation and a photodiode to detect fluorescence emission. A pH-sensitive and fluorescence active sensor patch was attached to the inner reactor wall (Fig. 19). The sensor patches used for all following experiments were provided by Sartorius Stedim Biotech GmbH (SSB, Goettingen, Germany) and originated from the same production lot (recipe # 43-0207). These patches are comprised of the polymerized fluorescence dye 8-hydroxy-1,3,6-pyrene-trisulfonic-acid-trisodium salt (HPTS) immobilized in a polyethylene glycol matrix. This hydrogel matrix is sandwiched between a microfiltration membrane pointing towards the culture medium and a transparent adhesive for attachment to the vessel wall. The microfiltration membrane is suited for proton diffusion and acts additionally as an optical barrier to avoid fluorescence interference from the culture broth.

Because of its chemical composition of a pyrene core, three sulfonic acid groups and a hydroxyl group, HPTS possesses pH sensitivity around its pK_a of 7.3. HPTS has two excitation wavelengths of 405 nm (UV) and 457 nm (blue) corresponding to its acidic and conjugated base forms [46]. Due to a pH-dependent shift of its excitation maximum (isosbestic point) at pK_a 7.3, HPTS enables ratiometric dual excitation, single emission pH detection within the physiological range of pH 6.0 – 9.0 (Fig. 20).

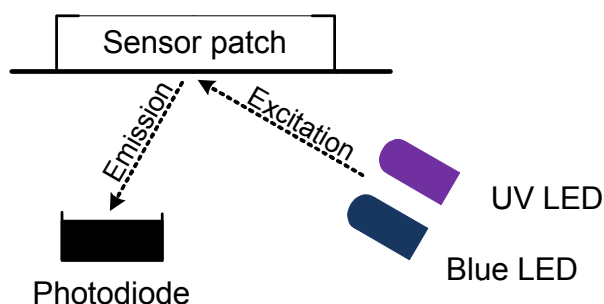


Fig. 19: Setup of the pH sensor unit. Two LEDs are used for excitation of a fluorescence dye embodied in a sensor patch. Fluorescence emission is detected with a photodiode.

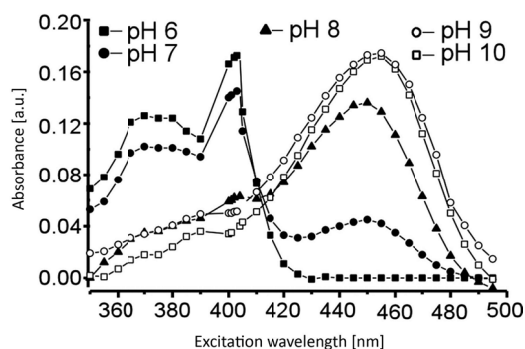


Fig. 20: Absorption spectra of HPTS. The loss of its hydroxylic proton leads to a large change in the absorption spectrum. Graphics modified after Dela Cruz *et al.* [47].

For pH measurement in the Tristation, the STR units are equipped with a pH-sensor-patch and are placed into the support station with the transceiver unit located below. The sensor patch needs to be positioned directly above the corresponding excitation

sources and photo detector. Two LEDs are used for dual excitation and are further referenced to as UV LED (emission maximum at 400 nm) and blue LED (emission maximum at 460 nm).

4.6.1.1 Development of a calibration routine for the optical pH sensors

Prior to the setup of a software based measurement, a proper calibration routine was established. The prefabricated pH sensor units (Fluorometrix Corp., Baltimore, USA) were connected to a 12 bit multi I/O measurement box (USB 1208-LS, Plug-In Electronic GmbH, Eichenau, Germany) comprised of differential analog inputs for photodiode voltage determination and digital outputs for sensor control. For a physical baseline correction in the final measurements, the offset voltages for each sensor unit with both excitation light sources were determined. This offset determination was performed prior to each cultivation. The corresponding software routine is illustrated in Fig. 21.

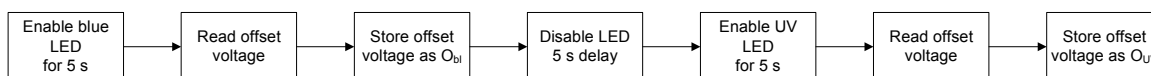


Fig. 21: Schematic flow-chart of the software routine to determine offset voltages of the sensor units to compensate for system variances.

All reactor vessels are removed from the support station, the LEDs of the sensor units are illuminated for 5 s, offset voltages are read and finally stored in a calibration file.

Since fluorescence intensities are comparably low, the intensities detected and subsequently transformed by the photodiode need to be amplified and filtered to remain within a measurable range. The electronic circuit necessary will have a certain response time for signal amplification and transmission. To avoid measurements on the shoulder of the transmitted signal, the maximum gain time for the signal to reach 100 % of its intensity (t_{100}^{rise}) was determined in a series of experiments for each excitation source (Fig. 22).

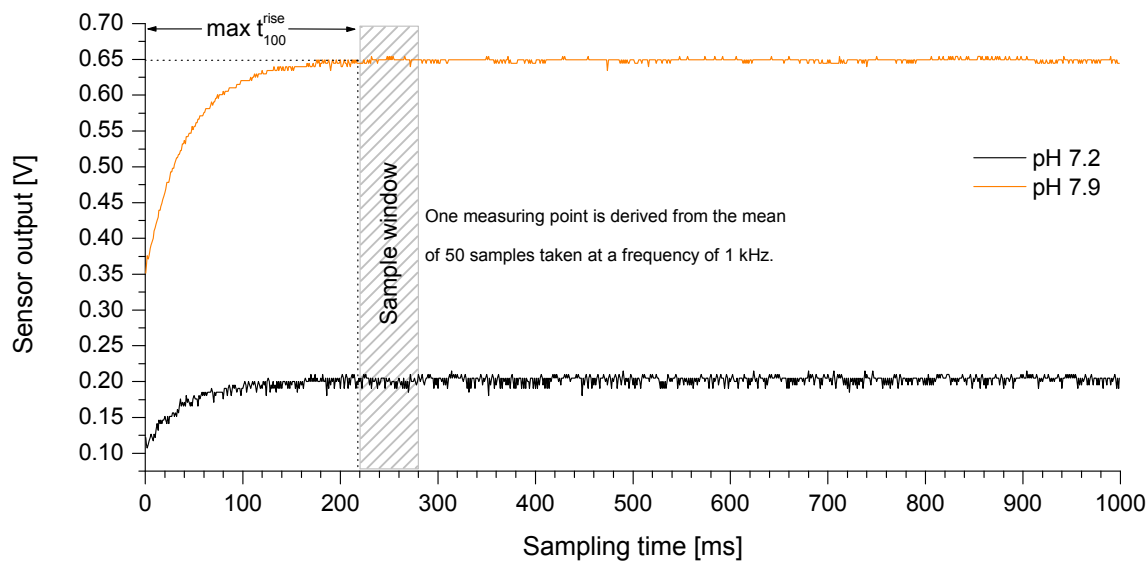


Fig. 22: Sensor response time to reach maximum signal intensity when measuring different emission intensities resulting from different pH values. Maximum response time t_{100}^{rise} was determined to be 220 ms.

A STR unit equipped with a pH sensor patch and solutions of various pH values was placed above the sensor units. The sensor patch was illuminated with both excitation light sources and the sensor output was monitored with a 1 kHz sample frequency. Depending on the solution pH relative to the intensity shift of HPTS at pK_a 7.3, the sensor signal output will increase with more basic solutions (457 nm) or with acidic solutions (405 nm), respectively. Increasing sensor output will affect t_{100}^{rise} to increase as well. In all cases t_{100}^{rise} never exceeded 220 ms, therefore this time frame was defined as the minimum illumination length before detection of fluorescence emission and was subsequently integrated into the monitoring software. One measuring point is thereby derived from the mean of 50 samples taken at a frequency of 1 kHz.

As stated above, the measurement principle to determine pH values with this sensor unit relies upon the calculation of the signal intensity ratio of the fluorescence emission of HPTS excited at 405 nm and 457 nm. To correlate these ratios to a certain pH value a calibration routine was established. STR units were equipped with pH sensor patches and placed in the Tristation. Multiple 0.1 M buffer solutions (chapter 15.3.5) with an overall ionic strength of 150 mM were used to access a pH range from 5.0 - 10.0 with a step width of approximately 0.5 pH units. Measurements were carried out at 37 °C for 15 min per step to achieve most stable intensity outputs. The signal intensities were

recorded using an adapted Labview program and referenced against a conventional pH electrode (Metrohm 605, Metrohm AG, Herisau, Germany). The Labview program automatically calculated the offset corrected signal intensity ratio R using Eq. 10.

$$R = \frac{V_{bl} - O_{bl}}{V_{UV} - O_{UV}} \quad \text{Eq. 10}$$

R = intensity ratio; V_{bl} = sample voltage blue LED; O_{bl} = offset voltage blue LED; V_{UV} = sample voltage UV LED; O_{UV} = offset voltage UV LED

Plotting the measured pH against R results in a sigmoidal relation, which can be described best using a Boltzmann fit. Fig. 23 displays the results of six calibrations using sensor patches from the same production lot. The grey marked area represents the maximum deviations of single calibrations from the mean Boltzmann fit (black line).

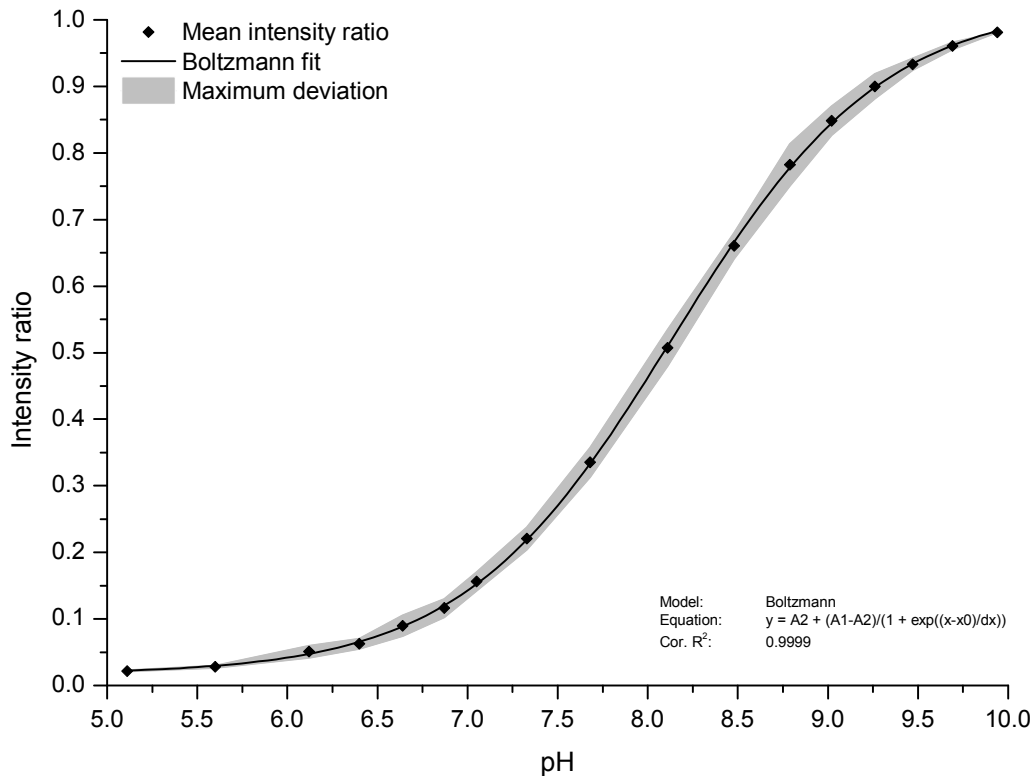


Fig. 23: Sigmoid relation between the measured intensity ratio using a Tristation sensor unit and the pH of the monitored solution. The grey shaded area represents the maximum deviation from the Boltzmann fit calculated from the mean ratios. Regression parameters obtained from the Boltzmann fitting can be used for software based online pH calculation.

The used sensor patches showed a sensitive measurement range between pH 6.0 and pH 9.5. Largest deviations from the mean Boltzmann fit reside within the pH range 7.5 – 8.5, but do not exceed ± 0.1 pH units. For an automated and software-based monitoring

of the pH during a cultivation, the obtained regression parameters A_1 , A_2 , dx and x_0 need to be stored previously into a calibration file to be accessible for online computation. Typical regression parameters are listed in the appendix (chapter 15.8). The pH can finally be calculated from the determined intensity ratio R using the inverted Boltzmann regression function (Eq. 11).

$$pH = \ln \left(\frac{A_2 - A_1}{A_2 - R} - 1 \right) \cdot dx + x_0 \quad \text{Eq. 11}$$

A_1, A_2, dx, x_0 = regression parameters; R = calculated intensity ratio

4.6.1.2 Validation of the calibration routine and adaption for software based pH monitoring

Validation of the previously described calibration routine was performed using a new sensor patch from the same production lot. Freshly prepared Britton-Robinson buffer (0.1 M, 37 °C, initial pH = 5.5) (chapter 15.3.5.1) was titrated with 1 M NaOH. Emission intensities were determined with the defined Tristation hardware setup and the pH was automatically calculated using the programmed software module based on the above listed specifications. Additionally, the pH was monitored using the Metrohm 605 reference electrode (Table 5). As observed during the calibration routine, the newly calculated pH values show only a minor deviation from the reference electrode and are not exceeding ± 0.1 pH units.

Table 5: Deviation of the pH measured with the Tristation based on the established calibration routine from the Metrohm 605 reference pH electrode.

	pH							
Metrohm 605	5.67	6.21	6.60	7.20	7.68	8.35	8.86	9.21
Tristation	5.62	6.13	6.53	7.25	7.74	8.43	8.93	9.27
Deviation	0.05	0.08	0.07	-0.05	-0.06	-0.08	-0.07	-0.06

Photobleaching of the fluorescence dye embodied in a sensor patch is generally a critical factor in long term operation of a single patch when based on intensity measurements. Dual excitation ratiometric measurements, as used with the optical pH sensor units in

the Tristation, are less sensitive to bleaching, since the intensity ratio will only be insignificantly influenced by degrading excitation maxima. To validate the effect of intense illumination onto the used sensor patches, a long term operation of a single patch was simulated. A pH sensor patch was illuminated twelve times per minute with the blue and UV LED resulting in an illumination period of 2.5 s per LED. Variation of the intensity ratio with 1 M KPP buffer (pH 7.5) as bulk medium was monitored over a period of 150 h. The intensity ratio decreased linearly from initially 0.25 to 0.21, which correlates with a reduction of the pH value from 7.5 to 7.35 (Fig. 24). Considering that the simulated long term operation corresponds to $2.4 \cdot 10^6$ measurements based on the above specified 220 ms illumination periods, an excellent long term stability can be confirmed. Accordingly, a software based drift compensation was not applied.

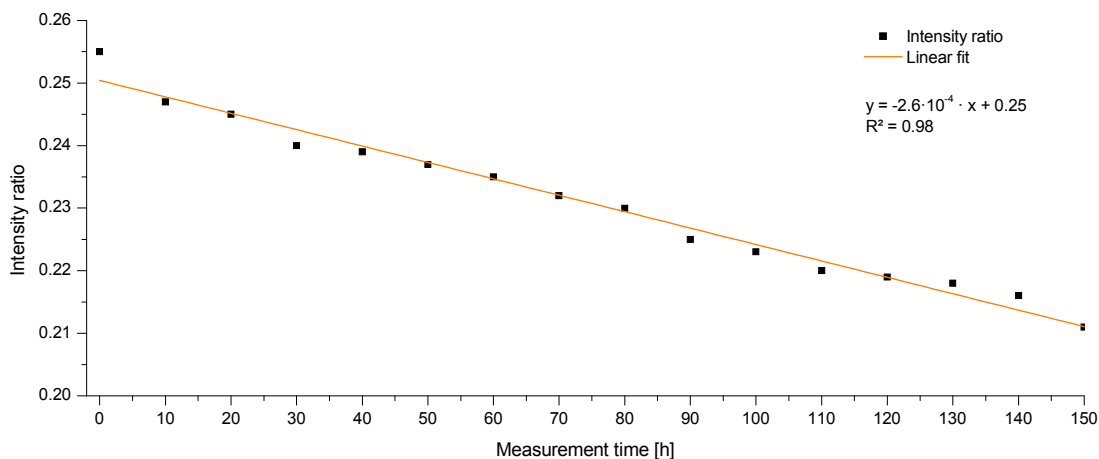


Fig. 24: Linear reduction of the signal intensity ratios of a 1 M KPP buffer solution during constant illumination of the pH sensor patch with both excitation sources.

The optical chemosensors used with the Tristation are based on a ratiometric dual excitation single emission principle with HPTS as a pH sensitive fluorescence dye. The established calibration routine compensates for electronic variances in the single sensor units. A software based measurement routine calculating the pH values from the measured emission intensities and predetermined calibration parameters was compiled and showed a high precision and reproducibility. The command sequence of this software routine is illustrated in Fig. 25 and was integrated into the final monitor and control software.

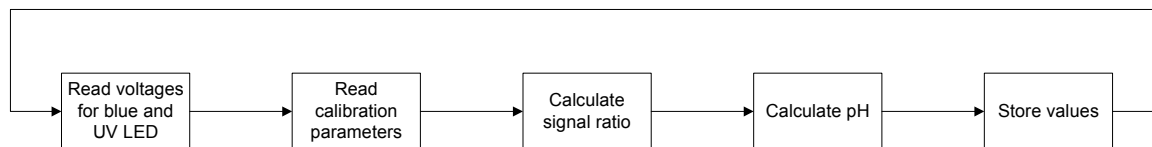


Fig. 25: Command sequence to be integrated into the monitor and control software for measuring fluorescence intensities with the Tristation sensor units and calculating the pH value of the monitored solution.

After measurement of the fluorescence emission intensities as voltages with a photodiode, stored calibration parameters are being used for pH calculation. Resulting values are finally stored in a data file.

4.6.2 DO determination based on fluorescence lifetime measurements

Due to its low solubility in aqueous solutions, oxygen is often a limiting factor in aerobic cultivations. To avoid low concentrations of oxygen impacting on cell growth or productivity during the course of a cultivation, dissolved oxygen (DO) is usually not only being monitored constantly, but moreover controlled by agitation, aeration or both in order to reside within a certain range of concentration.

Each reactor station of the Tristation is equipped with a fluorescence based sensor unit (Fluorometrix Inc, Baltimore, USA) to non-invasively determine the amounts of dissolved oxygen. Like the pH sensor unit, this sensor system is comprised of a transceiver and a sensor patch. The transceiver system is positioned outside and below the culture vessel. It is composed of a single LED for excitation and a filtered photo detector for emission readings. The sensor patch is comprised of an immobilized fluorescence dye, which is quenchable by oxygen. The sensor patches used for all following experiments were provided by SSB and originated from the same production lot (charge date 30.07.08). They are chemically comprised of the oxygen sensitive fluorescence dye [1,2-bis(diphenyl-phosphino)ethane Pt[S₂C₂(CH₂-CH₂-N-2-pyrimidine)](BPh₄) embedded in a silicone matrix and are adhesively attached to a vessel wall.

The measurement principle of this oxygen sensor is based on the frequency domain lifetime measurements as described in chapter 2.2.2. Briefly, a fluorescence dye is excited and quenched in the presence of oxygen resulting in a lifetime reduction of its

excited state. The period of the excited state correlates to the oxygen concentration in the proximity of the fluorescence dye. Since the excitation source is sinusoidal modulated in intensity, the fluorescence emission of the excited state will create a time lag expressed as a shifted phase and decreased modulation. This phase shift, if compared to its reference phase, correlates with the excited state lifetime and therefore with the dissolved oxygen concentration. High oxygen concentrations reduce the lifetime of the excited state resulting in a reduced phase shift and vice versa.

The transceiver of the Fluorometrix DO sensor is comprised of a blue LED used as the excitation light source and a photodiode detecting the emission at a wavelength of 580 nm (Fig. 26). The LED emits sinusoidal modulated light at a wavelength of 505 nm. Since every sinusoid can be expressed as a sum of a sine and a cosine function, two excitations at the same frequency but shifted by the lock-in amplifier by $\pi/2$ or 90° lead to two fluorescence emissions, from which the phase shift and therefore the fluorescence lifetime can be calculated – briefly a modification of the quadrature amplitude modulation. For the following discussion the sine part represents the in-phase and the cosine part the quadrature component.

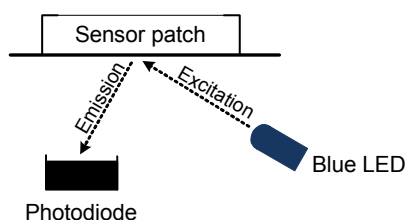


Fig. 26: Setup of the DO sensor unit. One LED is used for excitation of a fluorescence dye embodied in a sensor patch with two sinusoidal modulations. Fluorescence emission is detected using a photodiode.

4.6.2.1 Development of a calibration routine for the optical DO sensors

Prior to a defined calculation of the percentage of oxygen dissolved in a culture broth, a calibration routine for the sensor patches needs to be established. The DO sensor units were wired to the same multi I/O measurement box as the pH sensor units. Its analog inputs were used for determination of the voltage output of the photo detectors and the

digital ports were used for sensor control. A baseline correction was firstly applied to measure the offset voltages of each excitation source. Hereby, the reactor vessels need to be removed from the reactor stations and then the voltage output of the photo diode is measured after a 5 s illumination of the LED at each modulation. The obtained values are stored, just as the in-phase (O_{ip}) and quadrature offset voltages (O_{qd}). To compensate for phase delays introduced by the electronics, a red reflector disc is placed above each sensor unit and a second set of offset voltages is recorded from both modulations (V_{ips} and V_{qds}). The reflector disc mimics a short lived fluorophore with a zero decay rate. The calculation of the phase offset for each reactor station is subsequently performed using Eq. 12.

$$O_{ps} = \arctan\left(\frac{V_{ips} - O_{ip}}{V_{qds} - O_{qd}}\right) \quad \text{Eq. 12}$$

O_{ps} = phase offset; O_{ip} = in-phase offset voltage; O_{qd} = quadrature offset voltage;

V_{ips} = in-phase offset voltage short lived fluorophore; V_{qds} = quadrature offset voltage short lived fluorophore

These offset determinations have been integrated into a software routine as shown in Fig. 27.

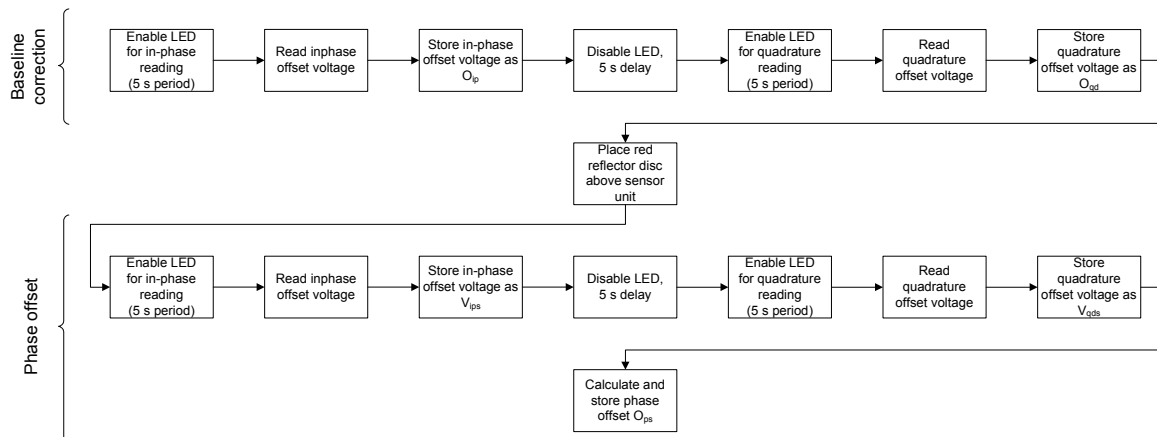


Fig. 27: Software sequence to determine sensor and phase offsets introduced by the electronic circuits.

After measurement of the sensor offsets for baseline correction, a red reflector disc acting as a short lived fluorophore is manually placed above the sensor unit to calculate the phase offset introduced by the electronic circuit. All measured and calculated values are stored in a configuration file for further use in the final monitor and control

software. This procedure needs to be performed for each rector station to guarantee reliable measurement results. Obtained calibration data is exemplary shown in the appendix (chapter 15.8).

As already observed for the transceiver component of the pH sensor unit (chapter 4.6.1.1), the maximum response time of the amplified photo detector signal to gain maximum intensity is of crucial importance for reliable measurements. Since the same circuits are used for signal amplification, t_{100}^{rise} showed in accordingly modified experiments (gassing in - gassing out using nitrogen and pressurized air, data not shown) a comparable illumination period of above 210 ms to reach maximum intensity. Intensity measurement is therefore started after 220 ms of illumination and one measuring point is thereby derived from the mean of 50 samples taken at a frequency of 1 kHz.

For a calibration of the sensor patches, the obtained phase shifts resulting from the variation of the fluorescence dyes lifetime need to be correlated to the corresponding dissolved oxygen concentrations. For that purpose STR vessels have been equipped with DO sensor patches from the same production lot as described above. 25 mL deionized water (d-H₂O) (Arium, Sartorius Stedim Biotech GmbH, Goettingen, Germany) were used as the bulk medium and tempered in the Tristation at 37 °C using the introduced temperature control program. Pressurized air and nitrogen were mixed at certain ratios using a blending station (Bronkhorst Hi-Tech GmbH, Kamen, Germany) and fed into the bulk medium via an eluent frit at a flow rate of 25 mL·min⁻¹. The maximum solubility of oxygen in water at 37 °C is 6.7 mg·L⁻¹ (100 % DO). The corresponding offset corrected phase shift ϕ was calculated from Eq. 13.

$$\phi = \left| \arctan \left(\frac{V_{ip} - O_{ip}}{V_{qd} - O_{qd}} \right) - O_{ps} \right| \quad \text{Eq. 13}$$

ϕ = phase shift; O_{ip} = in-phase offset voltage; O_{qd} = quadrature offset voltage;

V_{ip} = sample in-phase voltage; V_{qd} = sample quadrature voltage

Gas blending was undertaken with a step width of approximately 10 % ranging from 0 - 100 % pressurized air and a step period of 20 min. The in-phase and quadrature emission intensities were recorded using a Labview program. 20 samples in a stable

phase shift zone were averaged and referenced against a properly calibrated optical oxygen chemosensor (OXY-4, Presens GmbH, Regensburg, Germany).

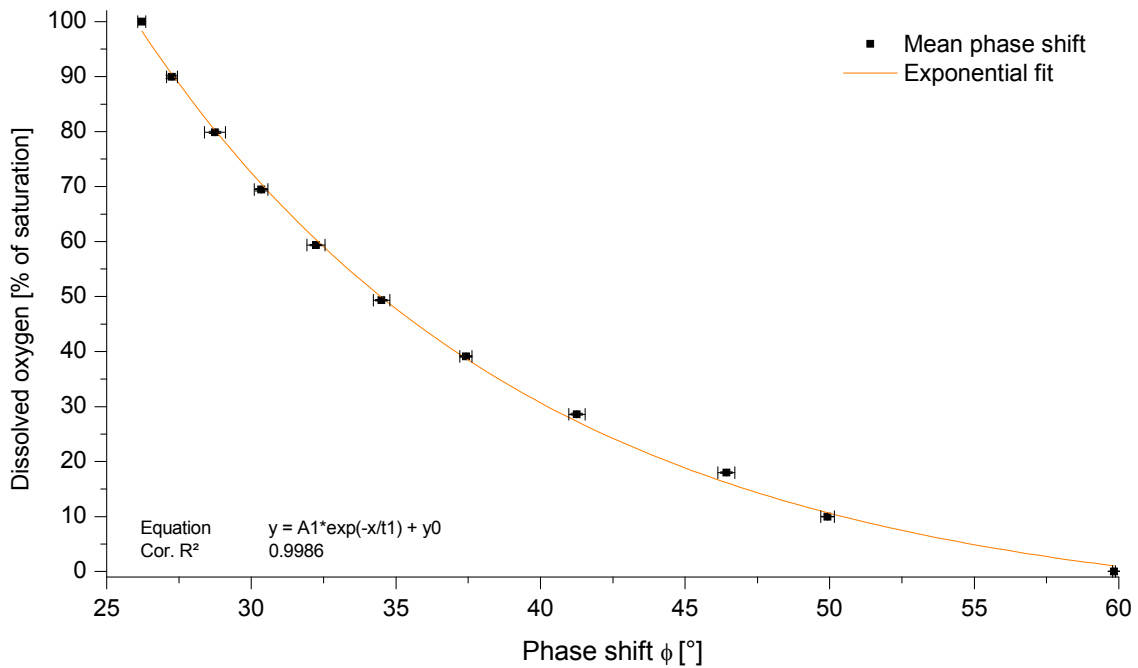


Fig. 28: Exponential fit of measured phase shifts to the corresponding dissolved oxygen in % of saturation. Highest sensor patch sensitivity resides within the DO range of 0 – 50 %.

Fig. 28 displays the correlation of phase shift to DO as percent of saturation. The depicted phase shifts represent the mean values from five calibrations including their standard deviations. With decreasing oxygen concentration the phase shift increases as expected. The sensitivity of the sensor patch increases with dissolved oxygen below 50 % of saturation. Exponential regression of the plotted data showed high accuracy and enables direct calculation of the DO from the measured phase shift using Eq. 14. Typical regression parameters for all the reactor stations are listed in the appendix (chapter 15.8).

$$DO = A_1 \cdot e^{\frac{-\phi}{t_1}} + y_0 \quad \text{Eq. 14}$$

A_1, t_1, y_0 = regression parameters; ϕ = calculated phase shift

Alternatively a relationship of DO and phase shift can be assessed using the Stern Volmer equation (Eq. 15). Since the tangent of a phase shift is proportional to the fluorescence dyes lifetime, the ratio of the phase shift at 0 % DO and current % DO can be plotted against the measured oxygen concentration (Fig. 29).

$$\frac{\tau_0}{\tau} = \frac{\tan\phi_0}{\tan\phi} = 1 + k_{sv} [O_2] \quad \text{Eq. 15}$$

τ_0 = decay rate at 0 % oxygen; τ = current decay rate; ϕ_0 = phase shift at 0 % oxygen; ϕ = current phase shift;

k_{sv} = Stern Volmer constant; $[O_2]$ = oxygen concentration

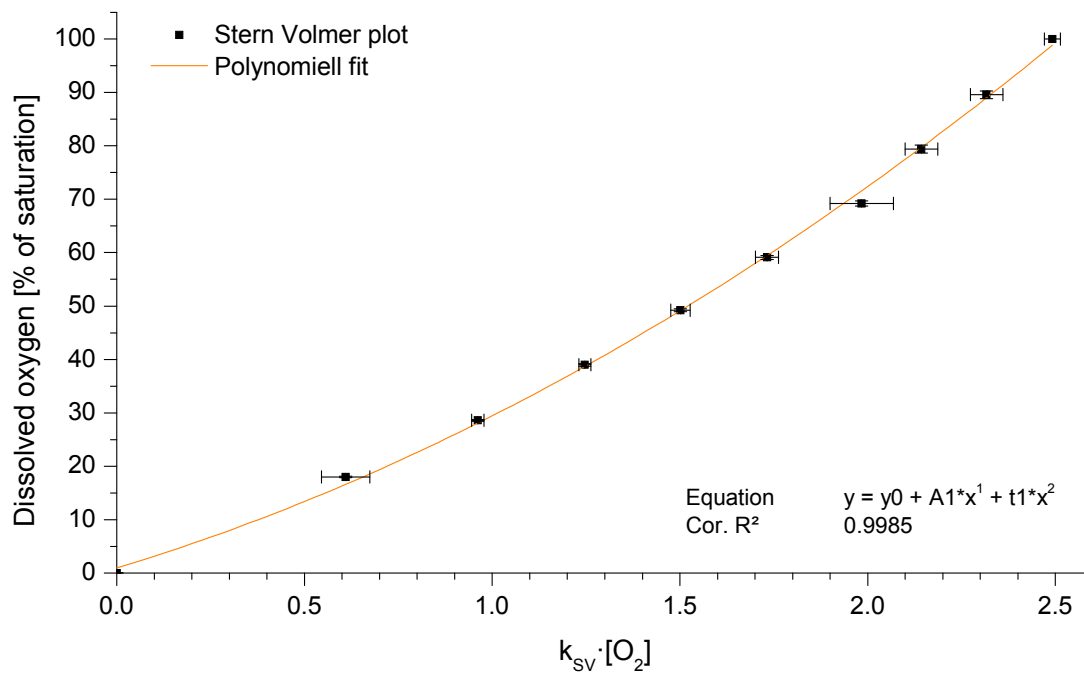


Fig. 29: Stern Volmer plot of the measured phase shifts as a ratio of current phase to zero phase against the corresponding dissolved oxygen concentration. The model could be best fitted with a second degree polynomial.

The Stern Volmer plot could be best fitted using a second degree polynomial. The deviation from a linear plot is not uncommon for polymer based sensor patches [48]. Next to a lesser sensitivity of the sensor patches above DO saturations of 50 %, the accuracy of this model decreases within the same range, as shown by the increasing standard deviations.

4.6.2.2 Validation of the calibration routine and adaption for software based DO monitoring

A comparison of both fitting models using new sensor patches and the calibration data shown above, reveals that the Stern Volmer model has a slightly higher accuracy for DO saturations below 40 % (Fig. 30). However, for dissolved oxygen saturations of 50 - 80 %

lower deviations from the reference system could be achieved using the exponential fitting model.

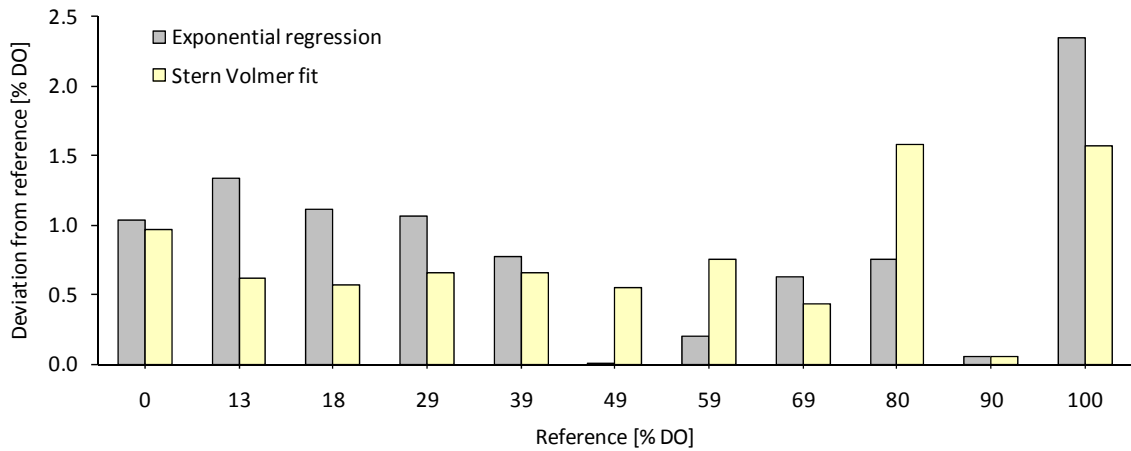


Fig. 30: Deviations in % DO of the exponential fit and the Stern Volmer model from the reference sensor. Both models have a mean deviation of about 0.8 % DO.

Both models show a mean deviation of approximately 0.8 % DO from the reference system over the whole measurement range. Because of its higher precision in the mean and upper % DO saturation range, the exponential fit model was chosen for integration into the final measurement and control software. The resulting software sequence is illustrated in Fig. 31.

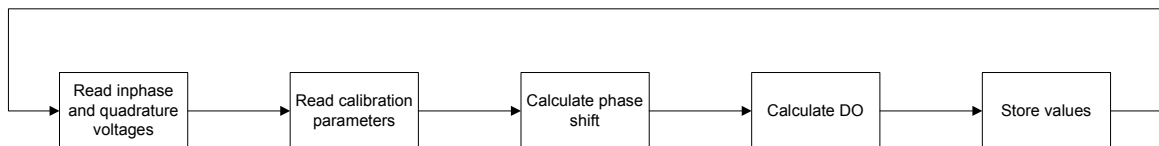


Fig. 31: Software routine to calculate the dissolved oxygen in % of saturation of a culture broth using the sensor systems integrated into the Tristation.

After determination of the in-phase and quadrature voltages, offset and exponential fit calibration constants are loaded and used for DO calculation. Final values are stored in a data file for each reactor station.

5 Development of a monitoring and control software

For a further use of the Tristation, an appropriate monitoring and control software was developed to guarantee a reproducible functionality and handling. Cultivations often require constant monitoring and the possibility to control specific process functions such as aeration or agitation rates. For this reason the measurement and control routines of the individual Tristation components described in the previous chapters have been implemented into a single and self-programmed software to monitor and control all three reactor stations in parallel. This software module will be further referenced to as *Tricontrol* and was designed using the Labview Professional Development Edition 8.2 (National Instruments, Austin, USA).

5.1 Software layout and functionality

Based on the previously established software sequences, e.g. to control temperature or monitor dissolved oxygen, the interdependencies of these individual components are of importance in bridging between simple monitoring and advanced controlling. The schematic layout of the programmed software is illustrated in Fig. 32.

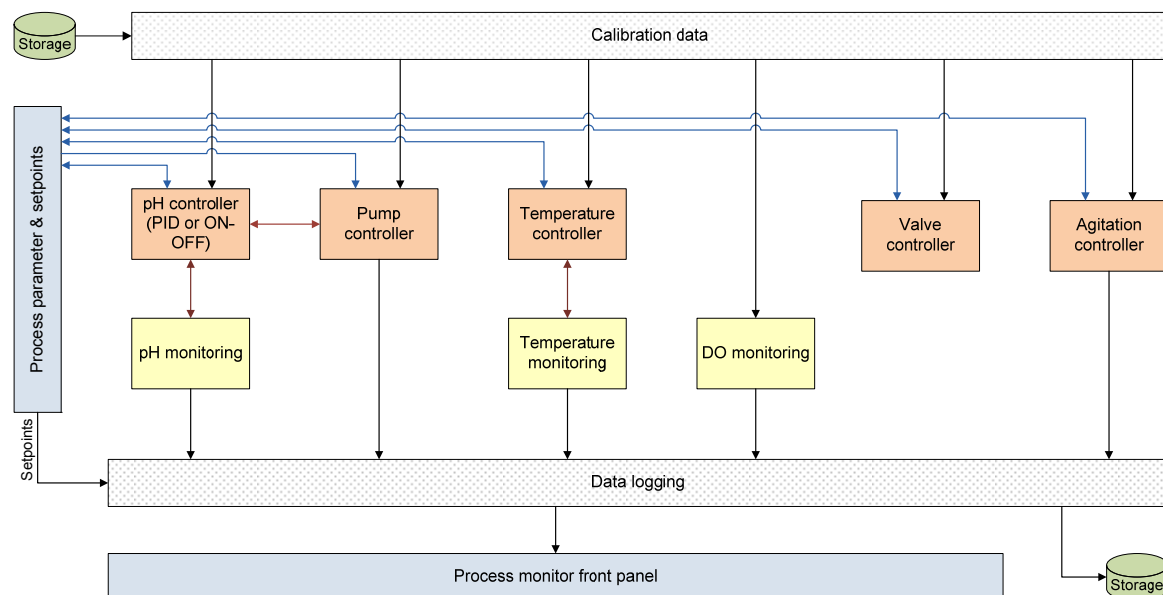


Fig. 32: Schematic layout of the Tricontrol software. Interdependencies of the subcomponents are marked by the connecting lines.

The software is basically comprised of five layers with different functions. Blue marked components require user interaction or are used for graphical display. Data operations

such as reading or writing variables are marked in grey, storage operations (e.g. log files) in green. Yellow components represent monitoring functions and orange colored components are used for process control. The interdependencies of the single components are described by the corresponding arrows.

In a first step, a preconfigured calibration file containing all constants and parameters for the individual components is loaded into the computer's memory. These values comprise e.g. of calibration constants for the pumps and the regression parameters of the sensor patches. Process parameters, such as pH or temperature setpoints, need to be entered manually using a graphical user interface. They are transferred directly to the individual control components and therefore allow online variation of process parameters. Information obtained from the pH or temperature sensors are not only stored in a log-file, but are additionally transferred to the correlating control components. Monitored pH values are compared with the defined setpoint and the corresponding control component decides on pump interaction. Three pH controls can be applied: none, on-off (2 way controller) or PI control. Individual pumps can additionally be disconnected from the controller, e.g. to only maintain a lower or upper pH thresholds. DO control through variation of agitation rate has not yet been implemented and should be subject to further optimization. Static values such as agitation rates or setpoints, as well as variable information (pH and DO [% of saturation]) are also stored in the process log file. All relevant process information is furthermore displayed at the process monitor front panel, which is part of the graphical user interface (GUI) described in the following chapter.

5.2 Graphical user interface of the monitoring and control software

The graphical user interface of the Tricontrol software is comprised of five tabs: process monitor, process parameter, data logging, calibration data and program information. The process monitor displays relevant process information for each reactor station (Fig. 33A). Next to the numerical display of current process variables (1), e.g. temperature, pH or DO concentration, the accumulated amounts of supplied acid and base are shown (2).

One diagram per reactor station is used to illustrate the time course of temperature, pH and DO concentration.

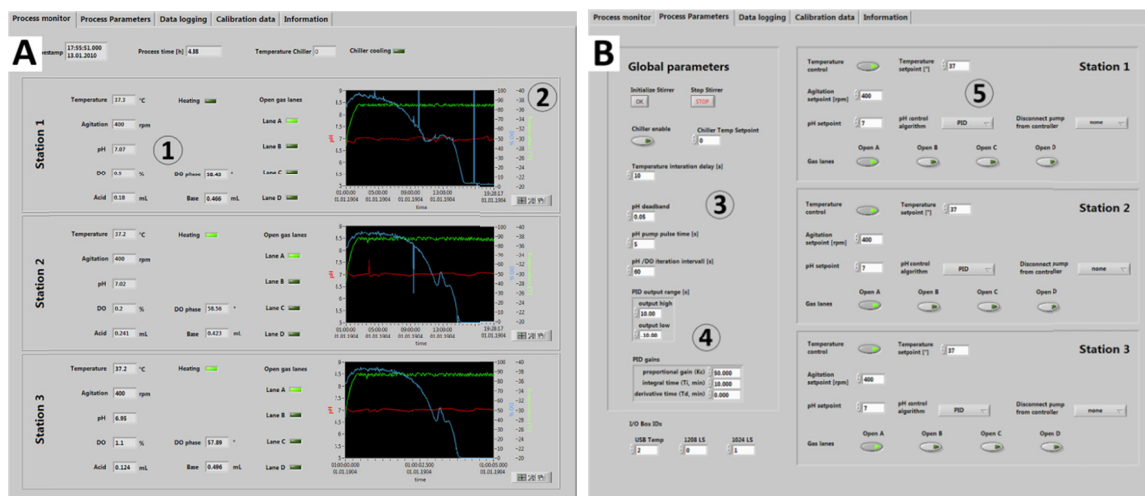


Fig. 33: **A:** Process monitor tab of the Tricontrol software to display relevant process information of each reactor station. 1: current process variables, 2: process chart. **B:** Process parameter tab of the Tricontrol software to define setpoints and controller options. 3: global control parameter, 4: PID parameter, 5: setpoints for the individual reactor stations.

The process parameter tab provides all necessary options to define process conditions and global control parameters. The global parameters comprise of stirrer initialization, iteration intervals and pH controller parameters (Fig. 33B). Temperature and pH/DO iteration intervals define the time lag between measurements and pump pulse time defines the time of pump rotation when pH control is set to on-off mode (3). PID controller constants can be altered in the appropriate input boxes (4). Additionally, the addresses of the multi I/O boxes used for hardware control can be modified.

Process parameters such as agitation rate, temperature, pH setpoints and control modes can be defined individually for each reactor station (5).

The remaining tabs are merely used for data logging options, loading of the calibration file or display of program revision information (not shown).

6 Example cultivations using the reactor system

Finally, to evaluate the performed optimizations on the Tristation, as well as the final monitoring and control software, two exemplary cultivations were conducted. In a first process, *E.coli* K12 was cultivated under pH controlled conditions (chapter 6.1). The second process utilized *E.coli* JM109 pGFP*6His to demonstrate further fields of application for the Tristation, by the alternate use of the pH-sensor units to detect green fluorescent protein (GFP) (chapter 6.2). GFP is widely used as a reporter for protein expression or localization (Philips 2001).

6.1 *E.coli* K12 process monitoring and control

Based on the previously implemented pH control routine into the monitoring and control software Tricontrol, the adaptability of this controller for bioprocesses was evaluated in three parallel and pH controlled cultivations of *E.coli* K12.

Three STR units were operated with a working volume of 25 mL LB-medium (pH 7.0) (chapter 15.3.5). Cultivation temperature was set to 37 °C and agitation rate was defined as 400 rpm. Pressurized air was used for aeration at a rate of 1 vvm and controlled through an external mass flow controller attached to gas inlet A of the Tristation. Eluent frits were used as aeration elements. pH setpoint was defined as 7.0 and 1 M HCl and 1 M NaOH were used for pH correction. All three reactors were inoculated with 1 % v/v of an *E.coli* K12 stock culture ($7 \cdot 10^8$ cells·mL⁻¹).

Dissolved oxygen and pH were detected using sensor patches from the same production lot as described in chapter 4.6.1 and 4.6.2. The three parallel cultivations were monitored over a period of 10 h. Optical density (OD) was measured manually by aseptically extracting 0.2 mL of culture broth and determining absorbance at 600 nm (UVIKON 922, Kontron Instruments, Munich, Germany).

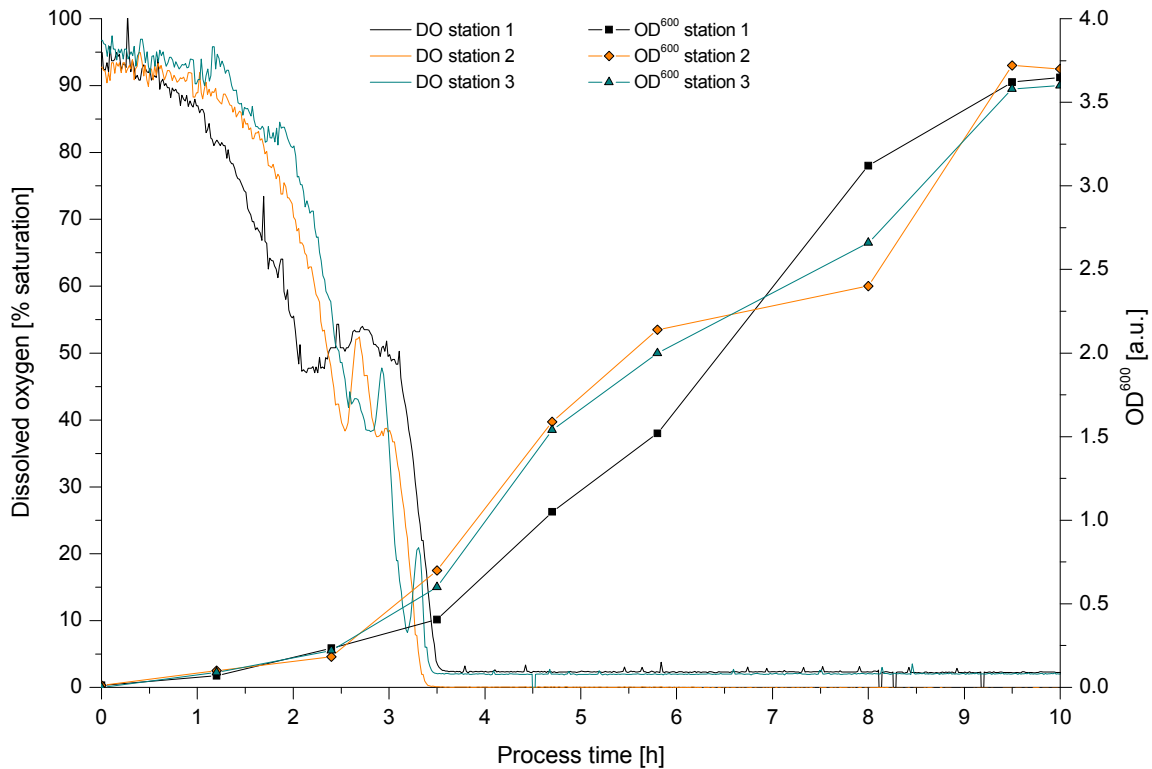


Fig. 34: Growth curves and dissolved oxygen time course studies of three *E.coli* K12 cultivations in the Tristation at 37 °C, 400 rpm and an aeration rate of 1 vvm.

Dissolved oxygen consumption and bacterial growth are comparable for all three cultivations (Fig. 34). After a short lag-phase of approximately 1 h, dissolved oxygen concentration decreases rapidly and reaches 0 % after 3.5 h. The exponential phase of bacterial growth lasts for another 6 h to descent into a stationary phase towards the end of the monitored period. 0 % DO for station 1 and 3 show a slight offset of 2 %, which results from the chosen calibration routine as described in chapter 4.6.2.

All three cultivations were pH-controlled with a setpoint of 7.0. The control was based on a PID algorithm implemented in the Tricontrol software. Since the equipped pumps lack the ability of dividing their rotation into steps, the pump control scheme used time of rotation as a basis for PID control. The deadband for the controller not responding was set to ± 0.5 pH units around the setpoint (Fig. 35).

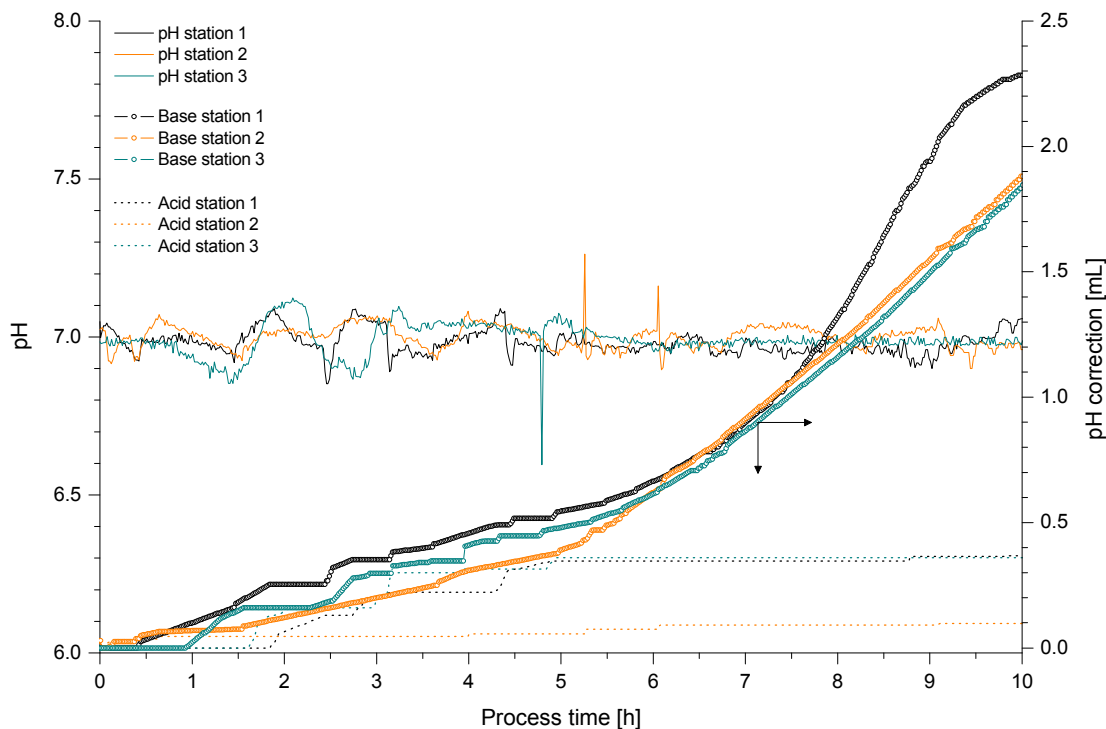


Fig. 35: pH course of three pH controlled *E.coli* K12 cultivations in the Tristation. Additionally plotted: usage of acid (1 M HCl) and base (1 M NaOH) to maintain the pH at a setpoint of 7.0.

In the beginning of the fermentation the pH remained within the defined deadband. With bacterial growth entering the adaption phase (1.0 – 2.0 h of process time) pH drops below the lower threshold, resulting in the controller responding with base addition. Subsequent transient oscillation of the controller lasts for approximately 1.5 h, which can be reduced by additional PID tuning. After about 4 h of process time culture pH is mainly influenced by acidic metabolites resulting in the increasing feed of base. The pH value remained within the defined pH deadband for the rest of all three cultivations. Usage of acid and base was calculated from the rotational time of the calibrated pumps. Occasional spikes in the pH readings, as seen in Fig. 35 for station 2 and 3, are of random and unreproducible nature. They result from misreadings of single sensor intensities which are most likely introduced by surges or bursts of improperly grounded exterior electronics.

6.2 *E.coli* JM109 GFP*6His - alternate use of the pH sensor units

Green fluorescent protein is often used in biotechnological applications as a fusion protein to monitor the concentration of a labeled protein during the course of a cultivation. Wild type GFP possesses two excitation maxima at 395 nm and 475 nm. Its

corresponding fluorescence emission wavelength is located at 509 nm. As the pH sensor units of the Tristation utilize two LEDs (397 nm and 465 nm) for dye excitation and a photodiode for emission detection at 515 nm, they can be alternatively used for GFP monitoring.

To demonstrate this application three cultivations of *E.coli* JM109 GFP*6His have been performed in the Tristation in parallel. This strain of *E.coli* produces GFP after induction with L-arabinose. Each STR unit was equipped with 25 mL LB-medium and 50 μ L chloramphenicol. Fermentation temperature was set to 37 °C, agitation to 400 rpm and aeration rate to 1 vvm using pressurized air. Dissolved oxygen was detected using the provided sensor patches. The pH sensor unit was used for direct GFP detection in the culture broth. All reactors were inoculated with 1 % v/v of *E.coli* JM109 GFP*6His stock culture ($6.0 \cdot 10^8$ cells·mL⁻¹). GFP production in the reactors positioned in station 1 and 2 was induced after 5.2 h with 0.2 mL L-arabinose. The reactor in station 3 was operated as a negative control. The Tricontrol software was slightly modified to additionally log emission intensities.

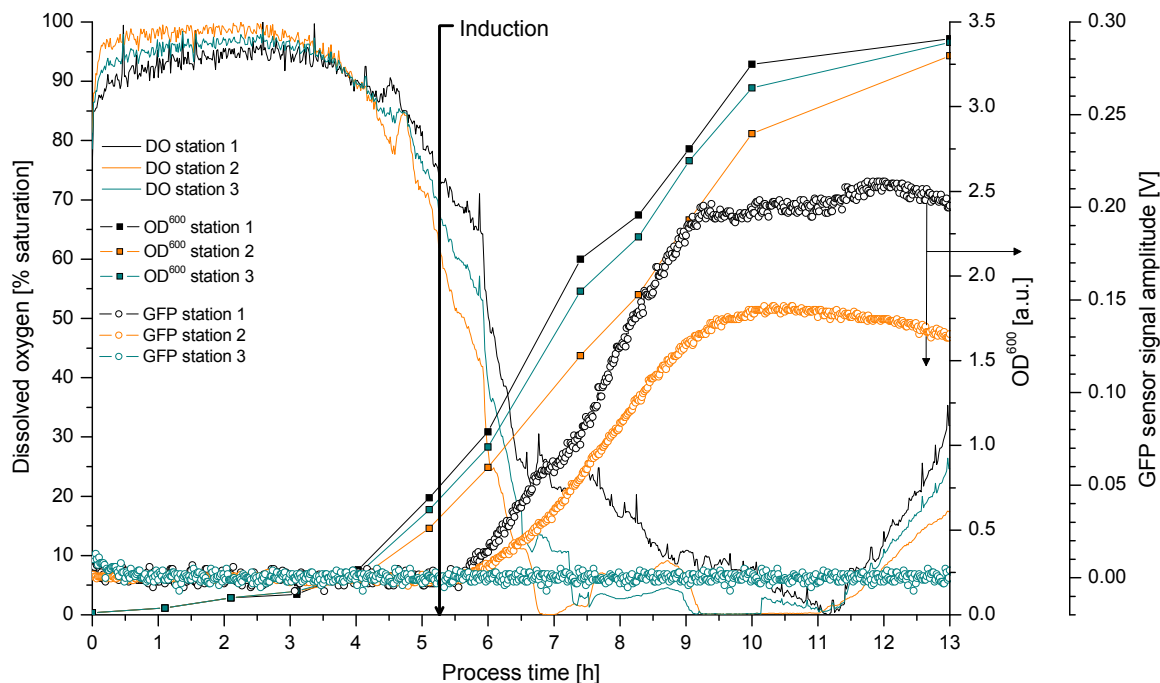


Fig. 36: Growth curves and dissolved oxygen time course studies of three JM109 GFP*6His cultivations in the Tristation at 37 °C, 400 rpm and an aeration rate of 1 vvm. GFP production in station 1 and 2 was induced with L-arabinose, station 3 acted as a negative control. GFP expression was monitored using the pH sensor array.

All three cultivations show similar growth curves and dissolved oxygen consumptions (Fig. 36). Exponential bacterial growth starts after approximately 4 h, coinciding with an increased dissolved oxygen consumption. DO saturation minimizes after 7–8 h of process time and starts to rise again when bacterial growth enters the stationary phase after 11.5 h. GFP production in station 1 and 2 starts after induction, as the sensor intensity output starts to increase rapidly with a profile comparable to the bacterial growth curves. The non induced cultivation in station 3 shows no change in emission intensity. GFP curves in Fig. 36 originate from the fluorescence emission intensities after excitation at 465 nm. Emissions after excitation at 397 nm possess a similar profile (data not shown), but with a lower intensity. Since both excitation sources of the sensor units were used, this difference results from the photoisomerization effect in wild type GFP. Here excitation at 395 nm leads to increased quenching resulting in an increase in absorbance at 475 nm [49]. The depicted GFP curves were manually offset corrected for better visualization. Original offsets were 0.04 V (station1), 0.09 V (station 2) and 0.11 V (station 3).

It can be concluded that the pH sensor units of the Tristation can additionally be used for the monitoring of relative GFP concentrations.

7 Conclusion part A

The Tristation prototype is a bioreactor system for the parallel operation of up to three mini-STRs with working volumes of up to 35 mL. This system was originally constructed by Fluorometrix Corp. (Baltimore, USA) and was provided by Sartorius Stedim Biotech GmbH (Goettingen, Germany) for the duration of this work. The aim of this project was to not only evaluate this system, but furthermore to characterize and optimize this prototype. For this reason the essential components of the Tristation have been profoundly investigated and all found characteristics have been implemented into a monitoring and control software module. The whole system was finally evaluated in two microbial cultivation processes.

Agitation of culture solutions is realized by the use of stepping motors to drive the stirring units of the individual mini-STRs. These stepping motors rely on a pulse train to increase or decrease stirring speed. 128 pulses are used to control stirring rates of up to 1,000 rpm. The resulting non linear correlation allows a precise agitation control of ± 2 rpm only between 0 – 200 rpm (chapter 4.1).

The Tristation is equipped with an array of twelve magnetic valves to individually disperse four different inbound gas supplies into the three reactor stations (chapter 4.2). A flow controlled gas supply or blending on the basis of this array is not possible. External mass flow controllers were instead connected to the gas inlets and the valves were merely used for on-off switching. The valves could be used, however, for gas pulsing, e.g. to control pH in mammalian cultivations by the supply of CO₂.

Two peristaltic pumps with an average delivery rate of 0.2 mL·min⁻¹ per reactor station can be used for pH control or nutrient delivery (chapter 4.3). As the pumps are not operated with a stepping control, they can only be turned on or off. To circumvent this limitation the pumps were instead calibrated by numerous routines, with time of rotation as the control basis.

Temperature control of the STR units is achieved by peltier elements attached to circular recessed metal blocks for STR support. Temperature sensing is performed by K-type thermocouples positioned between the peltier element and the metal blocks (chapter

4.4). Since the heat transfer from the peltier elements into the reactors is restrained by different materials with different heat conductivities, a temperature gradient was apparent. A series of correction functions were established to predict the temperatures of the bulk media in the reactor vessels from the readings of the external thermocouples. Through the use of these functions, deviations of the internal reactor temperature from the setpoints could be decreased from max. 0.9 K to 0.3 K. As the electronic setup of the Tristation only supports on and off switching of the peltier elements, a precise control is limited by the switching speed of the peltier elements – which, however, impacts the lifetime of these devices. Temperature control should be therefore optimized by the use of variable power supplies allowing the implementation of a PID control. By replacing the K-type thermocouples with PT100 resistors and subsequent repositioning towards the reactor vessel, temperature reading precision could be significantly increased.

The STR units were characterized further with regard to aeration and mixing capabilities. In their original setup the STR units are designed for surface aeration, which generally leads to low k_La values. To increase the k_La values, e.g. to suit higher dissolved oxygen demands, various other invasive aeration elements have been reviewed. Highest k_La values were obtained by the use of hollow fibers (chapter 4.5.1). Eluents frits, however, showed a slightly lower k_La value, but proved to be autoclavable and easier in overall handling. In addition, an agitator with aeration capability was developed. Even though the k_La values achieved with this unit were fairly low, the aerating agitator concept is an interesting option when available space in the reactor vessel is limited by mechanical or process technical restrictions. Through further diminution of the discharged bubble sizes, the k_La value could be increased significantly. A determination of residence time distributions revealed that mixing capability was nearly ideal at all agitation rates (chapter 4.5.2).

Each reactor station is equipped with two optical sensor units for non-invasive pH and DO detection placed below the STR units. Necessary sensor patches were supplied by SSB and are positioned on the bottom of the reactor vessels, directly above the corresponding sensor unit. Both sensor systems rely on fluorescence dyes encased in the patches, which show an analyte concentration dependent fluorescence emission. These

sensors, however, utilize different measurement methods. The pH sensor is based on a dual excitation, single emission ratiometric measurement (chapter 4.6.1). The HPTS based fluorescence dye shows a pH dependent shift in its excitation maxima. With forgone calibrations, the pH value of the culture broth can be calculated from the ratio of the corresponding emission intensities. A proper calibration routine was established and the subsequently determined pH values showed a good accuracy of ± 0.1 pH units.

In contrast, the DO sensor unit does not apply an intensity based, but a fluorescence lifetime based measurement. Here a fluorescence dye is excited twice by sinusoidal modulated light and subsequently quenched in the presence of oxygen. The lifetime of the excited state creates a time lag in the fluorescence emission, which can be translated into a phase shift. This phase shift correlates to a certain dissolved oxygen saturation. For further process monitoring, a dedicated calibration routine was established to calculate the DO from the measured phase shift (chapter 4.6.2). Two models were applied: exponential regression of phase shift to DO saturation and a non-linear Stern Volmer fit. The exponential regression model was preferred because of its higher precision in the middle and upper DO saturation range. Overall accuracy of this model proved to be around $\pm 1\%$ DO. Further optimization and accuracy of the calibration routine could be achieved by the use of high precision gas blending units and an improved mathematical fitting model.

Software-based control routines for all described components were developed in parallel. With the integration of these routines into a single software module, a fully operational monitoring and control software was designed. This software was written using the Labview graphical programming interface (chapter 5). It incorporates various functions to operate all three STR units of the Tristation in parallel. Process parameters or control mechanisms can be manipulated online and important process variables are graphically displayed and stored in a log file. The functionality of the program could additionally be increased by the direct implementation of the calibration routines or additional control options, such as an agitation based DO control.

The Tristation and the control software were finally evaluated in two exemplary bioprocesses. Three parallel and pH controlled *E.coli* K12 cultivations showed similar growth and pH control precision (chapter 6.1). *E.coli* JM109 GFP*6His was cultivated to

demonstrate additional applications of the pH sensor unit (chapter 6.2). After induction this bacterial strain expresses the green fluorescence protein. GFP has similar excitation and emission wavelengths as HPTS and can therefore be detected directly with the pH sensor unit. The course of monitored GFP fluorescence proved to be comparable to the bacterial growth curve. This relative information can be circumvented by establishing a proper calibration routine, opening an additional area of application.

Overall the Tristation showed an interesting potential for its application as a parallel reactor system for laboratory usage and scale-up considerations. Conditional upon the accomplished optimizations, calibration routines and software based control, the Tristation was successfully adopted for parallel cultivations. As the Tristation is only comprised of three STRs, this rather small degree of parallelization limits its application for extensive industrial screening purposes. Even though economic effects like total cost of ownership or total cost of operation have not been reviewed in this work, it is believed that especially the cost of labor associated with the labor-intensive setup of the STR units will significantly influence overall cost of operation. By replacing the reusable STR units with single-use and preconfigured vessels, setup time could be reduced. However, the Tristation would need to compete with established and less labor cost influenced screening and optimization systems based on shaking flasks, e.g. Ramos (HiTec Zang GmbH, Herzogenrath, Germany) or microtiter plates, e.g. Biolector (m2p-labs GmbH, Aachen, Germany). Its field of application should therefore be positioned between primary high-throughput-screening of organisms or media compositions and laboratory-scale bioprocess systems.

PART B

8 Ceramic membrane-based bioreactors for microbial biofilm cultivations

The use of membrane reactors, e.g. in industrial waste water treatment has significantly increased over the past two decades. Applications for other areas of biotechnology are promising, however only a few examples are reported up to now.




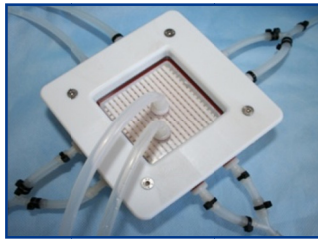
Compared to conventional stirred tank reactors an important advantage of membrane-based bioreactors is the provision of an artificial environment for an increased biomass density and enhanced productivity. Especially shear stress sensitive organisms, which are less productive under the evaluated stress conditions in stirred tank reactors, can be cultivated in such systems as productive biofilms - under less stressful conditions.

The ceramic membrane reactors Quorus LS, GLS, Optimizer and CELL evaluated in this chapter offer in this context a novel approach in productive biofilm cultivation. These systems were kindly provided by Synexa Life Sciences (Pty) Ltd. (Cape Town, South Africa) (Table 6).

Depending on the organism to be cultured, different reactor systems in various sizes for different process scales and modes of operation are available. The Quorus LS (Liquid Solid) is designed for the extended cultivation of microbial organisms growing under (facultative) anaerobic and submerged conditions. Filamentous microorganisms growing under aerobic conditions as a biofilm can be cultivated continuously using the Quorus GLS (Gas Liquid Solid) bioreactor. Both systems are scalable by modification of the total reactor volume and the number of capillary membranes encased. In contrast, the Quorus Optimizer consists of a fixed reactor volume with just one capillary membrane enclosed. This single fiber reactor (SFR) is primarily focused on screening applications to determine optimal growth conditions. It can be operated either in an aerobic or anaerobic mode. The Quorus CELL reactor has been adapted for the cultivation of attachment dependant mammalian cell lines. It consists of multiple membranes layers, which fulfill different and necessary functions such as aeration or medium transportation.

Due to their design and operation all these reactors are primarily focussed on the production of secreted products, such as secondary metabolites, toxic by-products or recombinant proteins. All reactor systems have a similar basic construction. They consist of capillary ceramic membranes encased within a manifold, which effectively forms two separate and distinct compartments: the intra capillary (ICS) and extra capillary space (ECS). While in all cases the cultivation of the organisms is carried out in the ECS, the ICS is either used for product removal, medium supply or aeration. The ceramic capillary membranes provide thereby an ideal platform for the immobilization of shear stress sensitive microorganisms.

Table 6: Area of applications, growth conditions and operation scales of the ceramic membrane-based bioreactors Quorus LS, GLS, Optimizer and CELL.

	Quorus LS	Quorus GLS	Quorus SFR Optimizer	Quorus CELL
				
Target organisms	(facultative) anaerobic organisms	filamentous aerobic organisms	(facultative) anaerobic and filamentous aerobic organisms	adherent mammalian cells
Application	production of secreted products	continuous production of secreted products	screening of optimal process conditions	production of secreted products
Growth conditions	submerged, oxygen-limited	biofilm	submerged, oxygen-limited and biofilm	submerged
Membranes	37-60	25-100	1	58
Reactor size	0.22 – 2 l modules	2 – 25 l modules	0.022 L module	0.12 L module

Within this part of this thesis the bioprocesses of these reactor systems will be described (chapter 8.1, 8.2). Furthermore, a comparative model for the determination of the efficiency and productivity of the Quorus systems will be presented. This model is based on the comparison of the productivity of the Quorus reactors to the ones of shaking flasks and stirred tank reactors (STR) of various sizes under comparable cultivation

conditions. For the aerobic Quorus GLS process the production of recombinant xylanase from the fungi *A.niger* D15 (*xyn2*) (chapter 9.1) and actinorhodin from the filamentous bacteria *S.coelicolor* A3(2) (chapter 9.2) will be investigated. The facultative anaerobic process using the Quorus LS will be investigated by the production of recombinant β -lactamase from *L.lactis* PRA290 (chapter 9.3).

The capabilities of the Quorus Optimizer for preliminary screening purposes will be demonstrated (chapter 8.3) and scale-up determinations from single fibre to production sized reactors will be presented (chapter 8.3.1).

Additional insight into the Quorus processes will be given by comparison of factors contributing towards operating costs, with regard to their percentage composition (chapter 9.4).

Due to the early stage of the development of the Quorus CELL, chapter 10 will primarily focus on the investigation of different process strategies to achieve high numbers of immobilized and viable cells. Results will be discussed based on the cultivations of CHO-K1 and HEK293 cell lines (chapter 10.2).

8.1 Aerobic process for steady-state biofilm cultivations and secreted product recovery

The disposable and scalable Synexa Quorus GLS bioreactors are best suited for the cultivation of aerobic and filamentous growing organisms. Within these systems biomass is immobilized and grown as a biofilm on the outer surface of ceramic membranes. The actual reactor chambers are divided by these ceramic membranes into two distinct compartments. Within the aerated extra capillary space (ECS) the biofilm is grown, while medium supply towards the biofilm is realized from the intra capillary space (ICS).

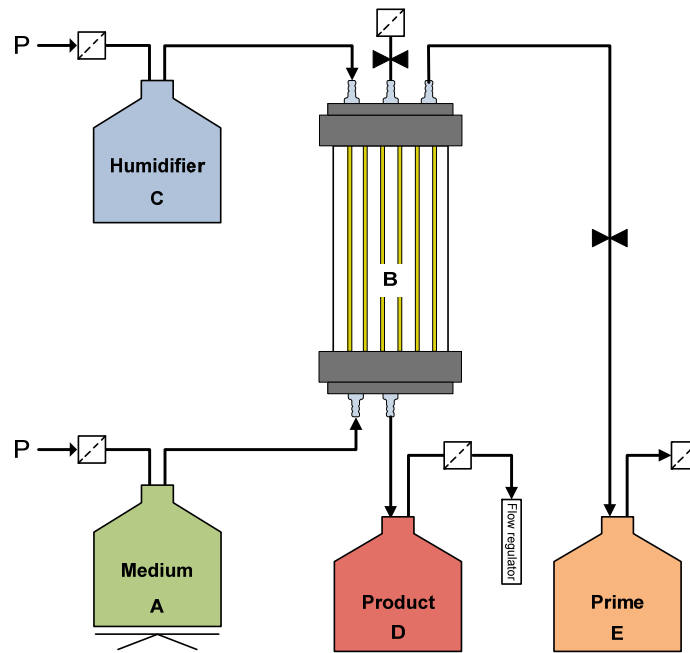


Fig. 37: Quorus GLS bioprocess. By applying pressure onto the medium supply vessel **A**, medium flows unidirectionally into the intra capillary space of the reactor **B**, through the membranes and subsequently through the biofilm. It exits the reactor as used medium enriched with the secreted product into the product collection vessel **D**. Inoculation is accomplished by transferring the inoculum into the extra capillary space with subsequent priming into the intra capillary space.

The whole Quorus GLS bioprocess relies on the use of pneumatic pressure for medium transportation, aeration and product removal. By applying pressure onto a medium supply vessel (MSV) **A**, medium flows unidirectionally into the ICS of the reactor chamber **B** (Fig. 37). The ICS is operated dead-end and therefore medium is transported through the capillary wall of the membranes, through the immobilized microorganisms and emerges from the reactor through the ECS. Aeration of the ECS is accomplished by humidified air **C** flowing through the ECS at a given flow rate and a definable backpressure. Air is supplied via air distribution lines evenly distributed between capillary membranes in the ECS. The pressurized air exits the reactor at the same outlet as the used medium and therefore supports the product removal from the ECS into the product collection vessel (PCV) **D**. As the medium is being distributed from the membranes lumen, the ICS needs to be completely filled with medium to ensure a uniform distribution into each single membrane. Since the accumulation of air within the ICS cannot be fully negated, e.g. during MSV replacement, the system can be primed manually with medium to remove the remaining air and to assure consistent operation. The actual flux of medium is proportional to the pressure differential between the ICS

and the ECS – further stated as trans membrane pressure (TMP). However, factors like ICS and ECS volumes as well as the biofilm density and thickness around the membranes will additionally affect medium flux. With increasing biofilm density and thickness, resistance to flow is increased and medium pressure needs to be adjusted accordingly to maintain constant flux and the steady state of a biofilm cultivation. By measuring the weight loss of the MSV within a defined time frame, an automated flux control is achieved by feeding back this information to the PI-controlled pressure valve.

For inoculation the system is operated inversely. The ECS is aseptically filled with the inoculum followed by the application of pressurized air to remove the carrier medium through the ICS into the prime vessel (PV) E, while the microorganisms are immobilized onto the membranes. Biofilm formation is then induced by supplying medium from the ICS by switching the system back to its regular operation direction. Here nutrient medium flows unidirectionally from the lumen through the porous walls of the membranes and through the biofilm, while in the ECS the biofilm is aerated by air flowing across its surface. By reaching a sufficient thickness of the biofilm, determined by growth-limiting nutrients, a radial nutrient gradient is established across the biofilm (Fig. 38).

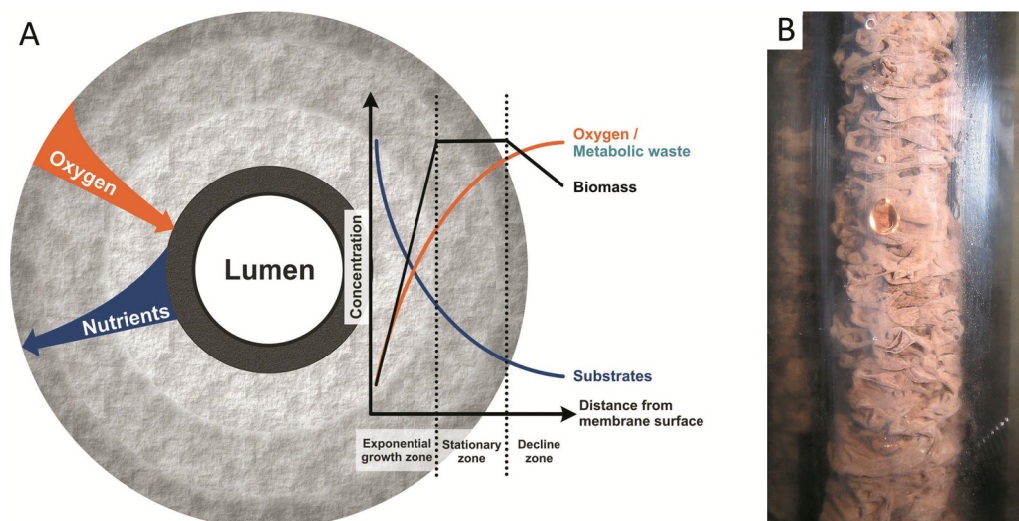


Fig. 38 A: Oxygen and nutrient gradients formed during biofilm formation around the ceramic membranes in the aerobic Quorus GLS bioprocess. Spatially distributed growth zones are observed: exponential growth zone, stationary zone and decline zone. **B:** *A.niger* D15 (xyn2) biofilm after 12 d of cultivation in a Quorus GLS system with an average thickness of 1.0 – 1.5 cm from the membrane surface.

This nutrient gradient is maintained in such a way, that it is high enough to support primary growth of the microorganism close to the membrane surface (exponential growth zone) and low enough to limit growth at a certain distance from the membrane surface and to sustain a stationary phase of the microorganisms e.g. to induce secondary metabolite production (stationary zone). On the exterior of the biofilm, nutrient concentration may be depleted, resulting in sporulation, cell death and lysis (decline zone). Oxygen consumption within the biofilm will increase with biofilm thickness, leading to an oxygen gradient from the exterior of the biofilm towards the lumen. Both gradients will influence the maximum biofilm diameter. Metabolic waste and secreted products are washed from the biofilm with the used medium, flow down the exterior biofilm surface and are transported from the reactor ECS with the airstream into the product collection vessel.

Through a controlled supply of nutrients the biofilm can be maintained at a constant thickness and active biomass as well as product formation is retained in steady-state. Biofilm thickness is furthermore dependent on the operation conditions and the microorganism itself. Ideal process conditions and the most productive biofilm thickness need to be determined in preliminary experiments, as with the Quorus Optimizer (chapter 8.3).

All Quorus GLS production experiments described below were performed in reactor modules with a total capacity of 2 L. Those modules were composed of 25-100 vertically orientated and uniformly spaced ceramic capillary membranes with an average pore size distribution of 40 nm.

8.2 Anaerobic process for submerged biofilm cultivation and secreted product recovery

The Synexa Quorus LS non aerated bioreactors are best suited for the cultivation of anaerobic or microaerophilic organisms such as single celled fungi or shear stress sensitive bacteria. Within this system biomass is immobilized and established as a biofilm on the outer surface of the ceramic membranes in a submerged and oxygen-limited environment. As with the Quorus GLS, the LS process relies on pneumatic pressure as the driving force for medium transportation and product removal - either by the use of air, nitrogen or other gas mixtures. By applying pressure onto the medium

contained within the MSV **A**, medium flows unidirectionally into the reactor chamber **B** (Fig. 39). The actual medium flux is dependent on the applied pressure, reactor volume, membrane surface and the amount of biomass immobilized. Medium supply is via fluid distribution lines evenly distributed within the ECS. With increasing biofilm thickness the resistance to flow is increased and the TMP needs to be adjusted accordingly to maintain a predefined flux rate.

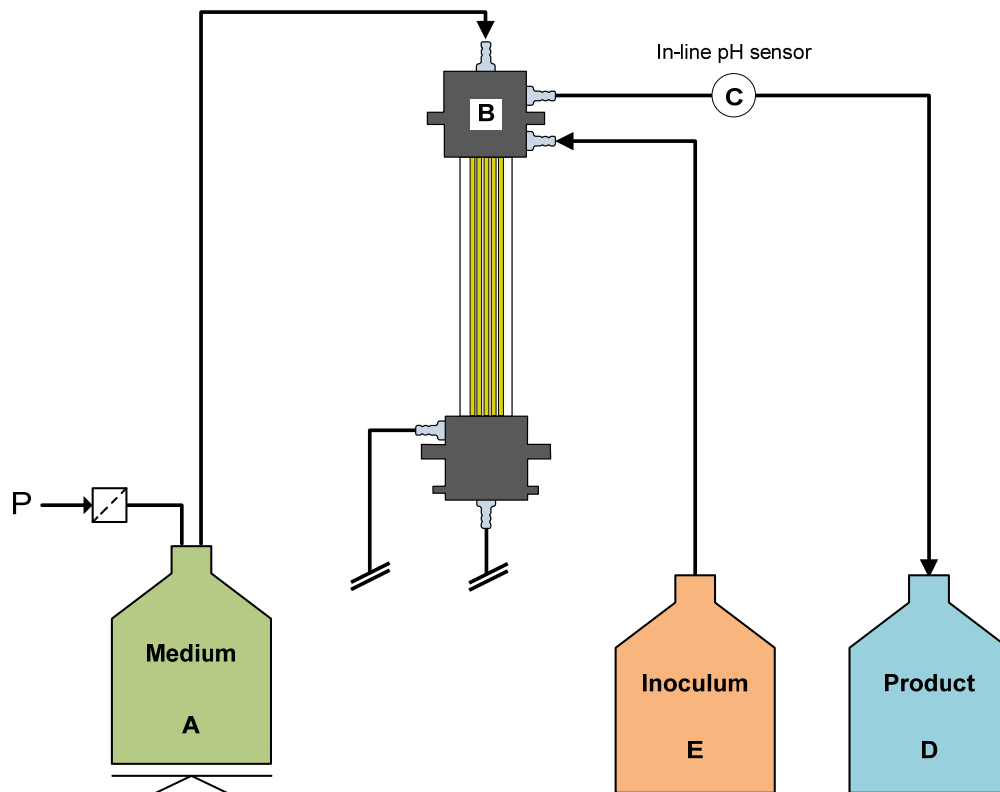


Fig. 39: Quorus LS bioprocess. Depending on applied pressure, medium **A** flows unidirectionally into the extra capillary space of the reactor **B**, through the biofilm and exits the reactor cell-free as used medium enriched with secreted products, into the product collection vessel **D**. Inoculation is accomplished by transferring the inoculum into the extra capillary space with subsequent priming.

An automated flux control is achieved through measurement of the weight loss of the MSV **A** within a certain time frame and feeding back this information to a PI controlled valve to adjust the applied pressure. For pH-sensitive cultivations a pH-controlled process can be applied by placing a pH-sensor **C** into the product stream in close proximity to the reactor exit. Based on the sensor information, the flux controller will automatically in- or decrease medium flux in order to displace metabolic waste e.g. organic acids, thereby maintaining the pH at the preferred settings. Used medium and

secreted products are transported through the capillary wall into ICS and are finally collected in the PCV **D**. For inoculation the ECS is aseptically filled with inoculum followed by subsequent priming with medium from the ECS into the ICS. The microorganisms are thereby immobilized onto the membranes. Medium used for priming is collected in a PV and discharged afterwards. Biofilm formation is lastly induced by constantly supplying medium into the ECS.

The actual Quorus reactor units are designed as disposable modules and can be scaled to various sizes. The modules are additionally equipped with a heat jacket attached to a fan heater for temperature control. All Quorus LS experiments were carried out in 220 mL total volume modules. Those modules are composed of 37 ceramic capillary membranes with an average pore size distribution of 40 nm centered within the reactor chamber. The reactor chamber is thereby divided by the ceramic membranes into two distinct compartments (Fig. 40).

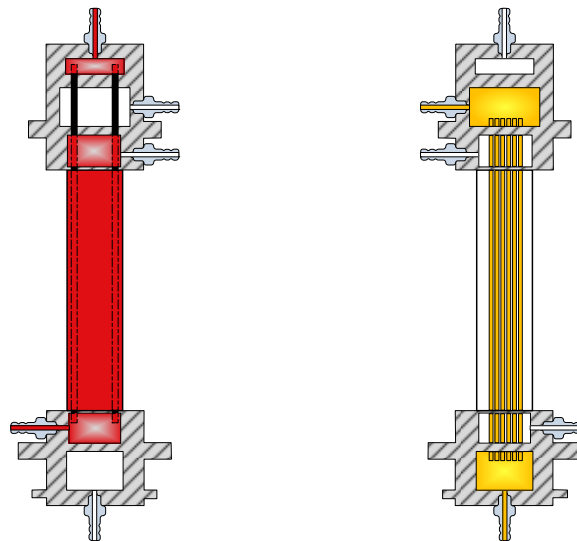


Fig. 40: Schematic representation of the Quorus LS reactor chamber. Medium is supplied through metal distribution pipes into the extra capillary space (red). Used medium, metabolic waste and secreted products are cell-free removed from the intra capillary space (yellow).

In contrast to the Quorus GLS, nutrient supply is achieved, as mentioned above, by a controlled feed directly into the ECS and through the immobilized cells forming the biofilm. With increasing biofilm thickness a radial nutrient gradient is established across the biofilm (Fig. 41). The growing biofilm is thereby separated into three distinct growth-zones: exponential growth takes place on the outer surface of the biofilm, followed at a certain distance by the stationary zone. The decline zone is located adjacent to the outer

surface of the membranes. Nutrient delivery leads to the continuous removal of metabolic waste and secreted products from the biofilm by transportation along with the used medium, through the capillary wall into the ICS.

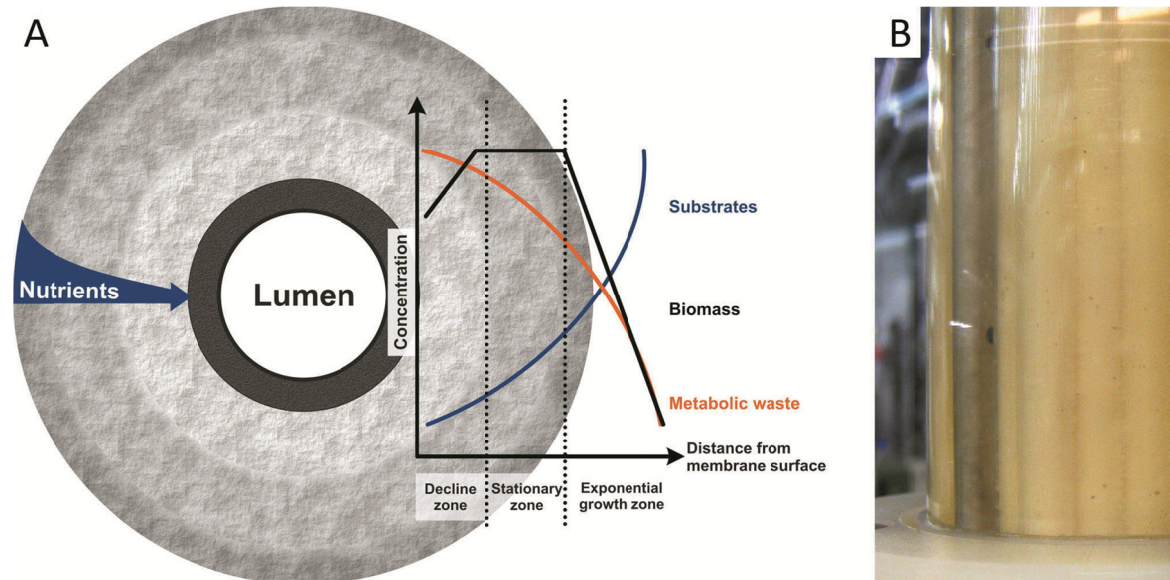


Fig. 41 A: Nutrient gradient formed during biofilm formation around the ceramic capillary membranes in the Quorus LS bioprocess. Spatially distributed growth zones are observed: exponential growth zone, stationary zone and decline zone. **B:** *L.lactis* PRA290 biofilm around the centered membranes after 14 h of cultivation in a Quorus LS.

The resulting product stream emerging from the reactor at the same flux rate as medium is being supplied, is cell-free and therefore incorporates an integrated downstreaming step. The product is collected within a product collection vessel, which can additionally be attached to an automated sampling system. The autosampler transfers fractions of the product to separate sampling vessels of various sizes within a definable time frame.

8.3 Determination of basic process conditions and scale-up considerations

The Synexa Quorus Optimizer is the research and optimization unit among the microbial Quorus reactor family. In contrast to the Quorus GLS or LS, the operable reactor units are comprised of only one ceramic membrane encased within a disposable housing. This housing again forms the two distinct compartments ECS and ICS. The installed ceramic membranes are made of the same material and possess the same physical shape and

characteristics as the ones used in the process scale Quorus GLS/LS units. The Quorus Optimizer can control up to three single fibre reactors (SFR) in parallel.

A valuable feature of the Optimizer is the possibility to easily change its process configuration. The SFRs can thereby be operated either in the aerobic mode (GLS) or anaerobic mode (LS). In contrast to the GLS/LS system, the Optimizer however has no mass balance and therefore lacks advanced controlling features such as flux-control (controlling the pressure to achieve a constant media throughput) or pH-control (control media flux to maintain a constant pH in the product-stream).

Each SFR setup is separated from the others to avoid cross contamination while culturing different organisms (Fig. 42). However, operation parameters such as incubation temperature, ICS and ECS pressures and therefore the resulting flux cannot currently be controlled individually.

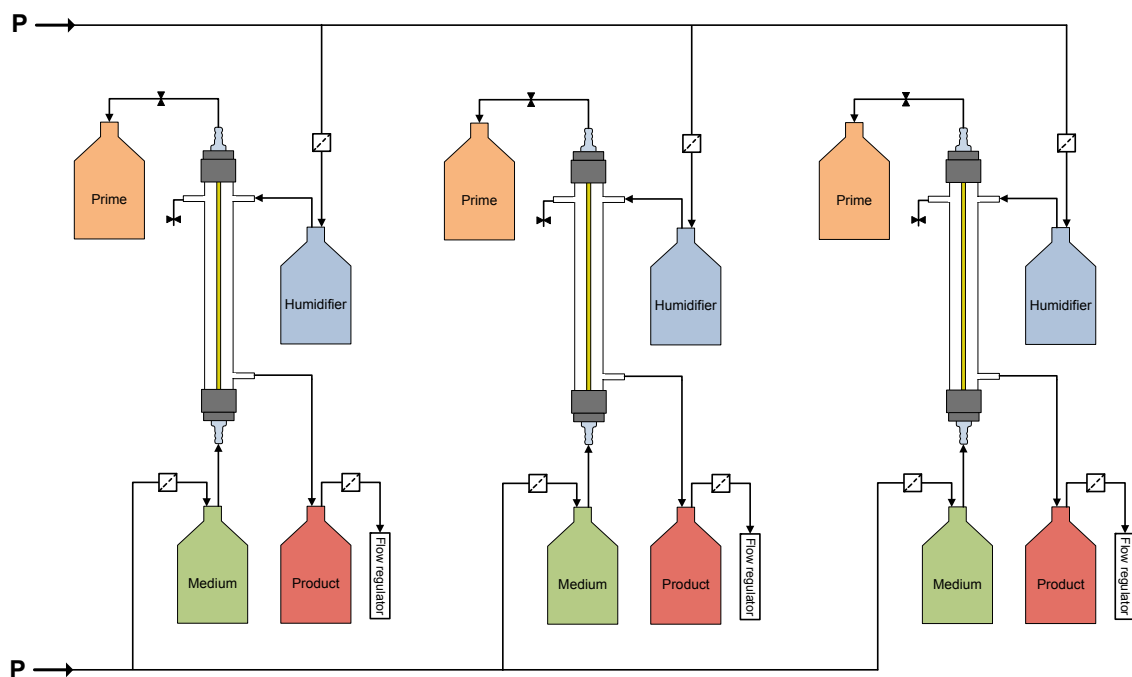


Fig. 42: Quorus Optimizer aerobic process setup. Three single fibre reactors are operated in parallel utilizing the same pressure sources for ECS and ICS pressure.

The Optimizer setup can be used for screening of various organisms under identical growth conditions, screening of the same organism under variation of media composition or conducting experiments in triplicate. But its primary function is the determination of basic process parameters for future scale-up. These parameters

include: incubation temperature, base ECS pressure, airflow and medium flux for optimal growth. Growth rate, biofilm thickness and productivity are directly coupled to each of these parameters. Since the ceramic membranes in the SFR and production units are physically identical and reactor systems differ only in the number of membranes encased within the reactor, the resulting scale-up factor is of linear nature.

Through calculation of the productivity of previously conducted SFR experiments, either as productivity per membrane, per time frame or per cm² membrane surface, the requirements for scaling-up can be defined. The most productive biofilm thickness observed will be of additional importance for the selection of the geometric layout of the future production unit; while the subsequent definition of manufacturing requirements e.g. amount of crude product needed per day, will define the reactor size. For example, in an SFR experiment 0.5 g·d⁻¹ product was produced by an organism with a biofilm radius of 1 mm from the membrane surface and a nutrient delivery rate of 1 mL·h⁻¹. Manufacturing requires a product output of 50 g·d⁻¹. A favourable process reactor would have 100 membranes with a spacing of 4 mm between membrane surfaces (2·biofilm thickness + 2 mm gap for airflow). This geometric layout is most consistent with the 2L GLS₁₀₀ reactor module (10 mm spacing). The necessary nutrient delivery rate would be 100 mL·h⁻¹.

8.3.1 Production of xylanase from *A.niger* D15 as an example for linear scale-up

The linearity of scaling-up SFR cultivations will be demonstrated through the production of the enzyme xylanase from *A.niger* D15. The secretion of recombinant xylanase by *A.niger* D15 (*xyn2*) was achieved by overexpression of the *Trichoderma reesei* xylanase II gene (*xyn2*) in the fungal genome of *A.niger* D15 [50]. This modified strain was provided by Synexa Life Sciences (Pty) Ltd., South Africa, to whom it was given by Professor Wilhelm van Zyl, Stellenbosch University, South Africa.

Detailed results from the scaled production in Quorus GLS units will be described in chapter 9.1.

All SFR and Quorus GLS cultivations were inoculated with identical spore preparations of *A.niger* D15 to a final concentration of 1·10⁵ spores per mL working volume. 2x MM

medium [51-52] was used for nutrient delivery. The reactors were incubated at 30 °C, airflow was set to 1 vvm and the base operating pressure was adjusted to 0.3 bar. SFR cultivations were carried out over a time frame of 18 d, while the Quorus GLS reactors were operated for 40 d.

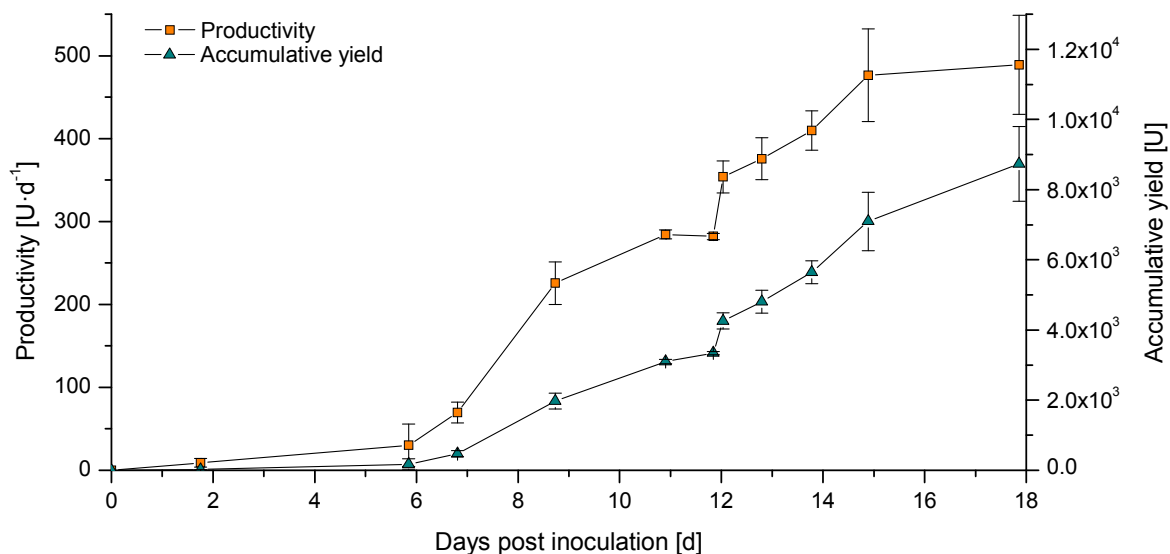


Fig. 43: Time course study of the productivity and accumulative yield from *A.niger* D15 cultivations to produce xylanase. Given data represents the mean values and standard deviations from three SFR cultivations.

The nutrient delivery rate in the SFR units was controlled manually via the TMP and averaged $0.95 \pm 0.5 \text{ mL}\cdot\text{h}^{-1}$. Fig. 43 displays the mean results of three SFR cultivations as a time course study for productivity [$\text{U}\cdot\text{d}^{-1}$] and accumulative yield [U]. Xylanase production started after an approximately 6 d long lag-phase and productivity stabilized after 14.8 d at $488 \text{ U}\cdot\text{d}^{-1}$. The biofilm thickness evened out within the same time frame and finally averaged 1.5 – 2.0 cm. Based on above results, a Quorus GLS₅₀ reactor module comprised of 50 membranes was operated with a scale-up factor of 50. Medium flux was accordingly controlled at $50 \text{ mL}\cdot\text{h}^{-1}$ expecting a 50 times higher product output than in a single SFR. Resulting scale-up factors for the Quorus GLS are illustrated in Fig. 44.

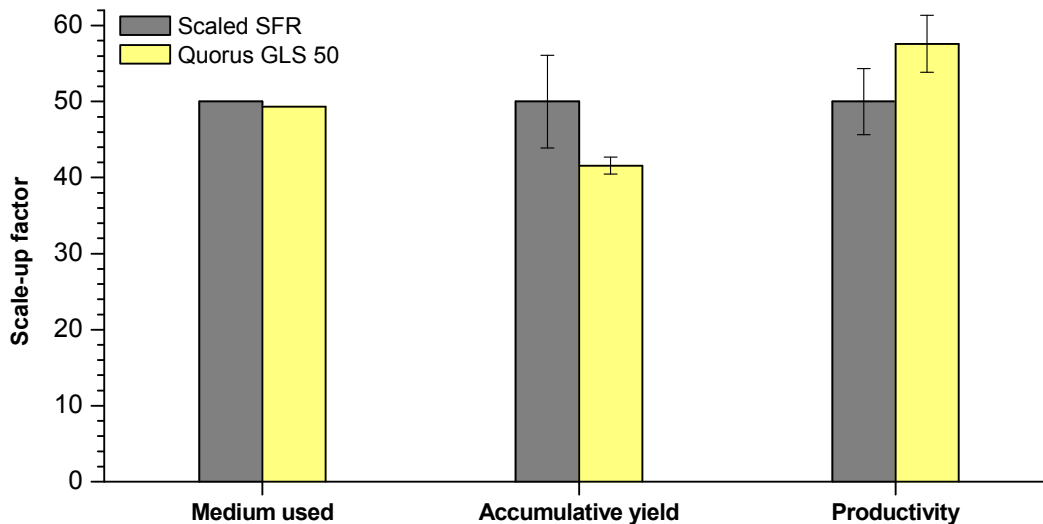


Fig. 44: Scale-up factors of an *A.niger* D15 cultivation to produce xylanase: estimated linear scale-up factors based on SFR results (grey) and experimentally determined factors based on the results of a 50 membrane Quorus GLS process.

Due to the automated flux control in the Quorus GLS₅₀ only a slight variation in medium usage was observed. The accumulated yield using a single SFR averaged $8.7 \pm 1 \cdot 10^3$ U xylanase within 17.8 d. Based on a scale-up factor of 50, $4.4 \pm 0.5 \cdot 10^5$ U xylanase in the 50 membrane Quorus GLS was expected.

Using the Quorus GLS₅₀ $3.6 \pm 0.1 \cdot 10^5$ U xylanase were actually produced, resulting in an experimental scale-up factor (accumulated yield) of 41.6 ± 1.1 . The Quorus GLS showed a higher productivity ($U \cdot d^{-1}$) resulting in an experimental scale-up factor (productivity) of 57.5 ± 3.7 . Overall biofilm thickness in the Quorus GLS was comparable to the ones observed in the SFR. However, the higher productivity scale-up factor can be explained as an artefact of the more variable flux in the SFRs.

However, when assessing the final scale-up factor variations of max. 15 %, it needs to be considered that the cultivations in the Quorus GLS and SFR had slightly different long lag-phases and process operation differed by automated controls. Taking these variations into account, overall scale-up from the SFR to process scale can be considered as linear.

9 Development of a comparative model for efficiency and productivity determination of the ceramic membrane reactors

9.1 Production of fungal xylanase from *A.niger* D15 using the aerobic process

The productivity of the aerobic Quorus GLS process is investigated in this chapter by comparing its results for the production of xylanase by *A.niger* D15 (xyn2) to the ones achieved using conventional batch fermentation systems, such as shaking flasks and stirred tank reactors (STRs).

All cultivations were inoculated with identical spore preparations of *A.niger* D15 to a final concentration of $1 \cdot 10^5$ spores per mL working volume. One 50-membrane and one 100-membrane 2 L Quorus GLS bioreactor modules were used. Reference cultivations were accomplished in 300 mL non-baffled shaking flasks, a 3 L total capacity Biostat A+ (Sartorius Stedim Biotech GmbH, Melsungen, Germany) with a 1.8 L working volume and a 15 L total capacity Biostat C (B.Braun Biotech GmbH, Melsungen, Germany) with a 10 L working volume. Nutrient conditions were identical by the use of freshly prepared and sterile filtrated 2x MM medium. All cultivations were carried out at 30 °C. While growth of biomass using the Quorus GLS bioreactor was controlled through constant nutrient flux, physical operation conditions within the STRs corresponded with literature suggestions. Agitation in the Biostat reactors was set to 400 rpm and aeration was maintained at 1 vvm [53-55]. Aeration within the Quorus units was manually controlled at $2 \text{ L} \cdot \text{min}^{-1}$ (1 vvm) with a backpressure of 0.3 bar. Throughout all cultivations pH control was not utilized. Initial pH in all cases was around 6.0 and remained during fermentation within the range of pH 5.0 – 6.0 as optimal for maximum xylanase activity {Rose, 2002 #1}. Xylanase activity was determined photometrically using the Birchwood azo-xylan assay (Megazyme, chapter 15.5.1).

9.1.1 Fermentation results

Cultivations of *A.niger* D15 in shaking flasks were carried out within a time frame of 8.9 d and reached highest xylanase activity ($41 \pm 2 \text{ U} \cdot \text{mL}^{-1}$) at the end of these cultivations. Benchmark experiments in the Biostat A+ and Biostat C STRs were carried out for a period of 11 d and for 14 d, respectively. Highest xylanase activities of $51 \pm 1.4 \text{ U} \cdot \text{mL}^{-1}$ were reached within the stationary phase after 7.9 d in the Biostat A+ (Fig. 45) and 8.7 d

in the Biostat C (Fig. 46). These timestamps are considered to be the optimal harvesting times and are used for all subsequent calculations.

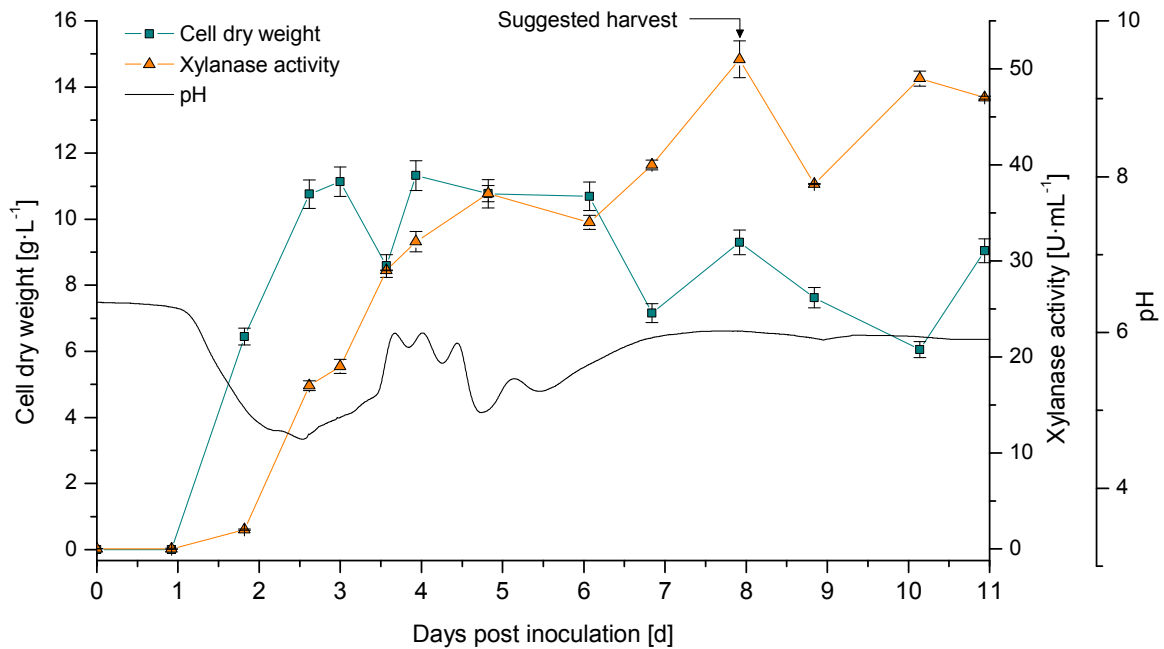


Fig. 45: Results of a 1.8 L Biostat A+ cultivation (30 °C, 400 rpm, 1 vvm) of *A.niger* D15 (xyn2) to produce xylanase. After 7.9 d the highest xylanase activity ($51 \pm 1.9 \text{ U}\cdot\text{mL}^{-1}$) was reached and therefore suggested to be the optimal harvesting time.

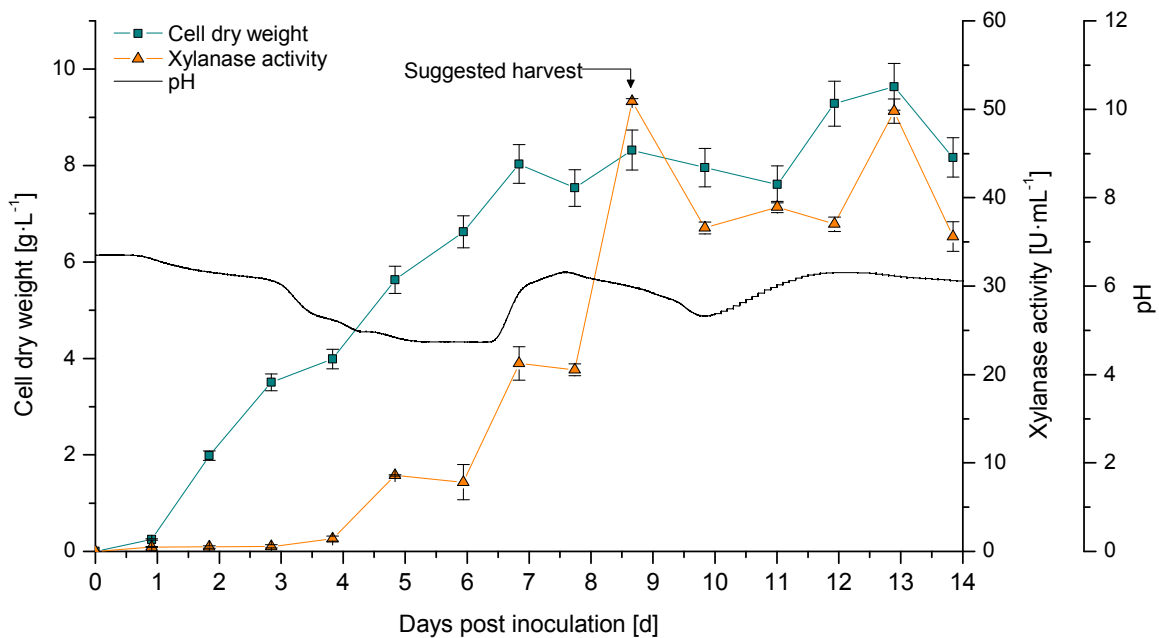


Fig. 46: 10 L Biostat C cultivation (30 °C, 400 rpm, 1 vvm) of *A.niger* D15 (xyn2) to produce xylanase. After 8.7 d the highest xylanase activity ($51 \pm 0.4 \text{ U}\cdot\text{mL}^{-1}$) was reached and therefore suggested to be the optimal harvesting time.

In contrast to STRs the continuous cultivations of *A.niger* D15 using Quorus GLS bioreactors were carried out over a period of 40 d. The 50-membrane Quorus GLS (Fig. 47), which sustained a thicker biofilm, was slightly more productive than the 100 membrane GLS reactor (fermentation graphs not shown). Results from the 50-membrane GLS cultivation were therefore used for all subsequent calculations. After approximately 10 d the cultivation in the GLS₅₀ reactor reached steady-state, where biomass productivity stabilized at approximately $2.1 \cdot 10^4 \text{ U} \cdot \text{d}^{-1}$. Upon entering this stable production-phase the biofilm showed a deep brownish pigmentation with negligible sporulation, which intensified after 25 d of operation. Biofilm thickness stabilized after 15 d and showed a conical increase in diameter from top (1.2 cm) to bottom (2.0 cm) of the vertically orientated membranes. This conical shape is either conditional upon gravimetric conditions or is indicative for growth limiting nutrients not being entirely depleted at the top of the biofilm. Remaining nutrients support more growth as they flow down the biofilm. With an optimized nutrient supply a more evenly distributed biofilm diameter can be achieved.

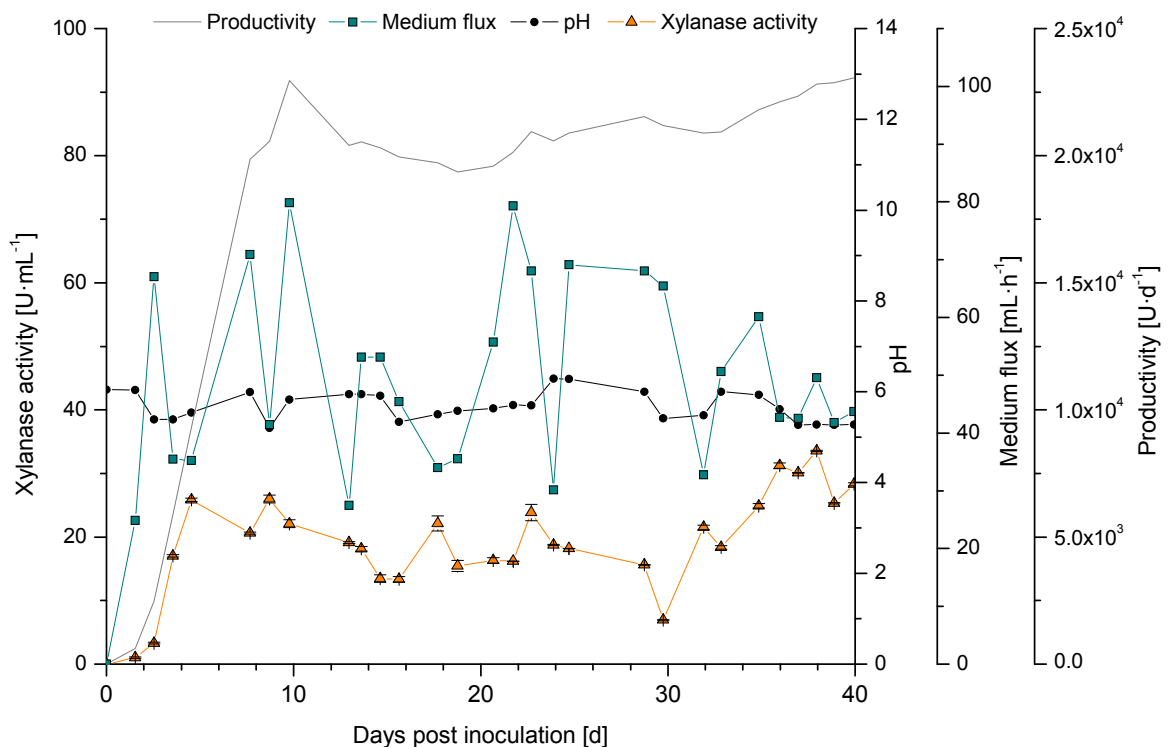


Fig. 47: Continuous production of xylanase by *A.niger* D15 (*xyn2*) using a Quorus GLS 2 L – 50-membrane bioreactor. Displayed are xylanase activity, pH, average medium flux and Quorus GLS productivity. The productivity stabilized after approximately 10 d with a constant production of about $2.1 \pm 0.1 \cdot 10^4 \text{ U}_{\text{Xylanase}} \cdot \text{d}^{-1}$.

Within the first 24 h after inoculation, medium flux was manually limited to $25 \text{ mL}\cdot\text{h}^{-1}$ to prevent spores and freshly grown mycelia being washed off the membranes. From day 2 till the end of the cultivation, medium flux was set to automated control with a setpoint of $50 \text{ mL}\cdot\text{h}^{-1}$: TMP was adjusted automatically and varied between 0.02 – 0.1 bar. Over- and under-fluxing (Fig. 47) resulted from a slow system response. Medium pressure was controlled through a single inlet valve, wherefore overpressure in the MSV could only be released in time with medium transportation, resulting in an under- and overshooting of the controller response. The attachment of an additional automated pressure release valve directly to the MSV is believed to diminish these effects as would further optimization of advanced configuration settings in the control software.

With increasing sporulation, as occurred after 25 d, spores were either washed of the biofilm surface or carried along with the passing airstream resulting in an accumulation of biomass at the reactor bottom. Adjacent mycelia formation led to a blockage of the reactor outlet as observed on day 30. The blocking could, however, be removed by a manual and rapid over pressuring of the ECS. Since sporulation of the biofilm cannot be avoided, a widening of the reactor outlet and attached tubing will lessen the probability of a blockage. The final results of all performed bioprocesses to produce xylanase are summarized in Table 7 and will be part of the discussions in the following chapters.

Table 7: Results from *A.niger D15* (xyn2) cultivations to produce xylanase in various reactor systems.

Reactor system	Days post inoculation [d]	Total yield [U]	Averaged overall activity [$U \cdot L_{\text{Medium}}^{-1}$]
Shaking flasks	8.9	$2.4 \pm 0.1 \cdot 10^3$	$4.0 \pm 0.3 \cdot 10^4$
Biostat A+	7.9	$9.2 \pm 0.3 \cdot 10^4$	$5.1 \pm 0.2 \cdot 10^4$
Biostat C	8.7	$5.1 \pm 0.1 \cdot 10^5$	$5.1 \pm 0.3 \cdot 10^4$
Quorus GLS 2 L (50 membranes)	40	$9.2 \pm 0.3 \cdot 10^5$	$1.9 \pm 0.4 \cdot 10^4$
Quorus GLS 2 L (100 membranes)	40	$7.7 \pm 0.4 \cdot 10^5$	$1.6 \pm 0.3 \cdot 10^4$

9.1.2 Bioreactor efficiency and productivity

Product formation is typically based on the accumulation or presence of biomass. Because aerobic biomass formation in conventional batch fermentation will cease with the depletion of nutrients or oxygen, it will accumulate towards a maximum for a given nutrient supply, with a specific amount of product output, which is allowed to accumulate within the culture vessel to a maximum concentration. This is illustrated by the similar maximum xylanase concentrations obtained for the Biostat A+ and C bioprocesses.

Similarly, biomass generation in the Quorus GLS bioreactor is obtained through the formation of a stable biofilm around the ceramic membrane surfaces. Biofilm growth reaches a maximum thickness, which is regulated and maintained by the amount of nutrients supplied to the biomass through nutrient flux. Since oxygen supply and nutrient delivery can be adjusted to fit actual needs, biofilm thickness is limited by the organism itself and by the extent of available space around the membranes. The optimal biofilm thickness and the optimal number of membranes fitted into the available space to sustain a biofilm of that thickness is process dependent and can generally be adjusted to suit process needs. In contrast to STRs, product is not allowed to accumulate, but rather continuously removed from the biomass in order to sustain maximum productivity of the biofilm. This will result in a lower volumetric productivity when compared to a STR, but it needs to be beared in mind, that the biofilm is kept in an active state allowing the same amount of biomass to produce more product over a longer period.

Since the total product output or total yield of a cultivation will typically increase with reactor size or working volume, a direct comparison of the different STRs and the Quorus systems based on those values is not valid. Furthermore, Quorus GLS operation results in a continuous product stream of a constant concentration, while the product concentration in STRs is a direct result of the accumulation of product in a fixed working volume and is not necessarily an accurate reflection of the actual productivity of the system.

9.1.2.1 Volumetric productivity

A valid factor for the comparison of reactor systems is the volumetric production rate [Eq. 16], which takes the volume of medium used and the fermentation time into account.

$$\text{Volumetric productivity} = \frac{P}{V_{\text{Medium}} \cdot t} \quad [\text{Eq. 16}]$$

t = considered time frame; P = Product amount generated in t ; V_{Medium} = Volume medium used in t

But since the Quorus system has not only used more medium (V_{Medium}) but more importantly was operated for a longer time t than a single defined batch, the volumetric productivity over the whole process time is not comparable. While in batch fermentation the volume of the used medium is fixed by the STR's working volume, media volume in Quorus operation will increase with time and therefore decrease volumetric productivity. For a more suitable comparison the volumetric production rate for the Quorus system was instead calculated using a defined volume of medium: as the Biostat C working volume was 10 L, the volumetric productivity of the Quorus GLS was calculated over a period of time within the stable production phase, where 10 L of medium were used. With an average volumetric production rate of $2.4 \cdot 10^3 \text{ U} \cdot \text{L}_{\text{Medium}}^{-1} \cdot \text{d}^{-1}$ within this timeframe, conditional upon its lower daily production rate, the Quorus GLS system cannot compete with the other systems under the chosen cultivation conditions (Table 8).

9.1.2.2 Productivity per reactor capacity

Another valid factor for the comparison of reactor systems is the efficiency of a reactor system itself, which is depicted by the productivity rate per reactor capacity or space-time-yield (STY) [Eq. 17], where the productivity is normalized to 1 L of reactor capacity.

$$\text{Productivity per reactor capacity} = \frac{P}{V_{\text{Reactor}} \cdot t} \quad [\text{Eq. 17}]$$

t = considered time frame; P = product amount generated in t ; V_{Reactor} = total reactor capacity

Even though productivity and volumetric productivity of the Quorus GLS were comparably lower than in the much larger Biostat C, the capability of the biofilm cultivation can be shown by calculation of the productivity per reactor capacity. With a STY of $1.1 \cdot 10^4 \text{ U} \cdot \text{L}_{\text{Reactor}}^{-1} \cdot \text{d}^{-1}$ the Quorus GLS process is 3.3 times more efficient than even the very productive (based on the preceding comparisons) Biostat C (Table 8).

Table 8: Results from *A.niger* D15 (xyn2) cultivations to produce xylanase in various fermentation vessels. All values are averaged to the whole process time. Given values represent mean values and standard deviations

	Days post inoculation [d]	Average overall productivity [$\text{U} \cdot \text{d}^{-1}$]	Average volumetric production rate [$\text{U} \cdot \text{L}_{\text{Medium}}^{-1} \cdot \text{d}^{-1}$]	Average production rate per reactor capacity. [$\text{U} \cdot \text{L}_{\text{Reactor}}^{-1} \cdot \text{d}^{-1}$]
Shaking flasks	8.9	$2.0 \pm 0.1 \cdot 10^2$	$4.5 \pm 0.1 \cdot 10^3$	$5.1 \pm 0.2 \cdot 10^2$
Biostat A+	7.9	$1.2 \pm 0.1 \cdot 10^4$	$6.4 \pm 0.1 \cdot 10^3$	$3.9 \pm 0.2 \cdot 10^3$
Biostat C	8.7	$5.9 \pm 0.1 \cdot 10^4$	$5.1 \pm 0.1 \cdot 10^3$	$3.9 \pm 0.1 \cdot 10^3$
Quorus GLS 2 L (50 membranes)	40	$2.3 \pm 0.1 \cdot 10^4$	$2.5 \pm 0.1 \cdot 10^3$ **	$1.1 \pm 0.1 \cdot 10^4$

** based on the use of 10 L medium within a stable production phase to compare to STR batches.

9.1.3 Modeling of long term operation

One of the advantages of the Quorus GLS system lies in its continuous operation. To compare each reactor system in long term operation a feasible time frame of 180 d is considered. To estimate the period of a single run, a process and reactor dependent cycle-time is defined. Each production cycle consists of a standardized 24 h downtime for setting up the reactor, a reactor specific unproductive lag-phase as well as a reactor specific production-phase [Eq. 18].

$$t^{\text{cycle}} = t^{\text{down}} + t^{\text{lag}} + t^{\text{production}} \quad [\text{Eq. 18}]$$

t^{cycle} = cycle-time; t^{down} = duration of downtime; t^{lag} = duration of lag-phase; $t^{\text{production}}$ = duration of production-phase

The compositions of such production cycles for the compared bioreactors are illustrated in Fig. 48.

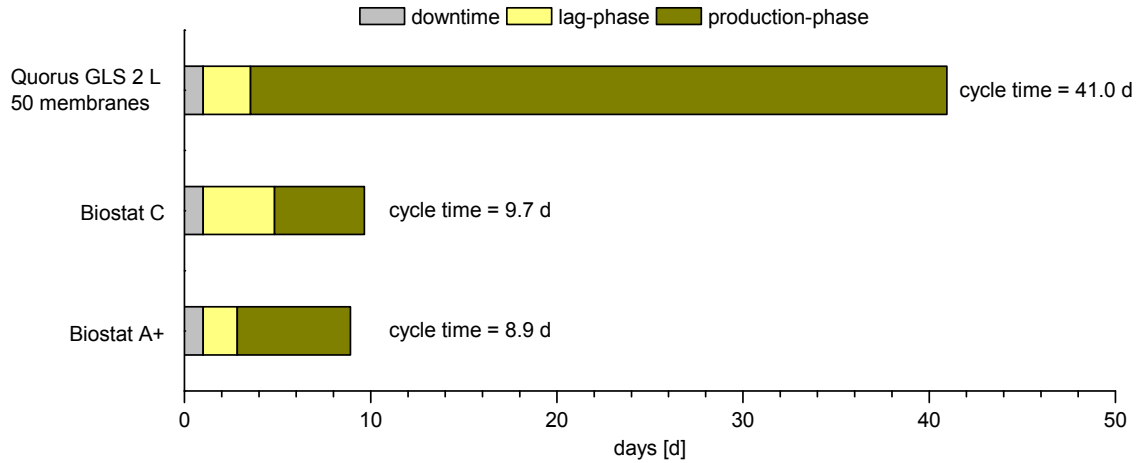


Fig. 48: Total cycle time of the reactor specific production cycles for the compared bioreactors. Each production cycle is composed of downtime, lag-phase and production-phase.

In the current experiment xylanase production in the Quorus GLS was stopped after 40 d, which included a 37.4 d uninterrupted production-phase. Due to the continuous operation of the Quorus GLS, product removal can be accomplished continuously within this production phase. Harvesting in the STR's Biostat A+ and C can only be performed once and therefore define the end of a production cycle. 1 d downtime was assumed for the setup of each reactor cycle.

Within the previously defined 41 d Quorus GLS production cycle 4.2 Biostat C and 4.6 Biostat A+ production cycles can be undertaken (Fig. 49).

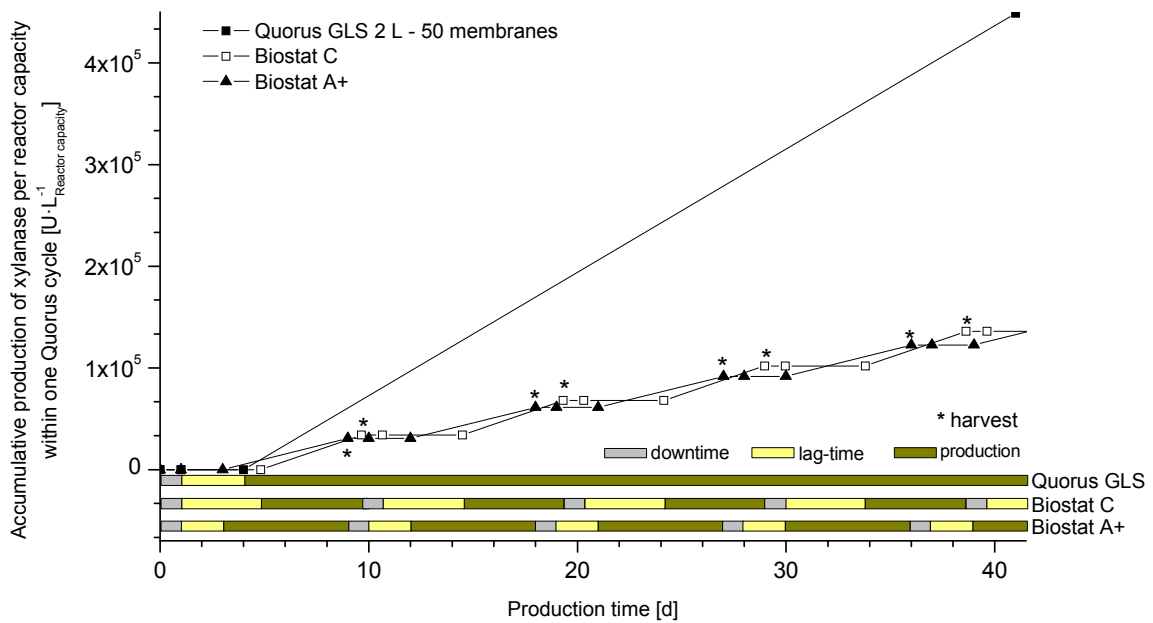


Fig. 49: Detailed plot of the accumulative production of xylanase from *A.niger* D15 (xyn2) per 1 L reactor capacity within one Quorus GLS cycle. Additionally an overview of the duration downtimes, lag-phases and production-phases is given.

Based on the achieved results of single runs (Table 8), the accumulative productivity per reactor capacity ($U \cdot L_{\text{Reactor}}^{-1} \cdot d^{-1}$) of each reactor system within the considered time frame of 6 month can be calculated by simply adding up single batches or runs up to a total time of 180 d resulting in a linear relationship (Fig. 50).

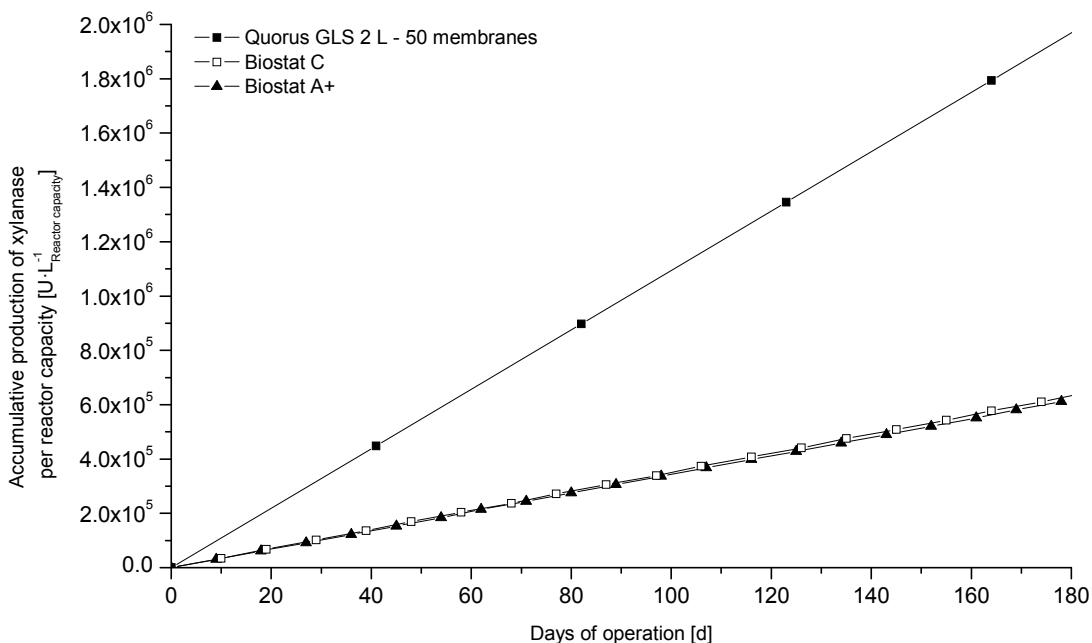


Fig. 50: Accumulative production of xylanase from *A.niger* D15 (*xyn2*) normalized to 1 L reactor capacity using various bioreactors. The plots are based on the estimation of maximum possible repeated production cycles within a 180 d period.

As already reported for a single cycle, the Quorus GLS bioreactor surpasses all batch processes in long term operation when comparing the productivity per reactor capacity. However, when directly comparing the total product output (U) the Biostat C would produce the most xylanase within the estimated time frame of 6 months (data not shown).

9.1.4 Variation of production time

While total production time in the STRs is fixed by a specific point for cell broth harvest, the end of the production-phase can be varied in the Quorus GLS bioreactors. Such a variation will impact on the total number of production cycles that can be undertaken within a 180 d period. The overall productivity of the Quorus system within this time frame will be affected accordingly. The influence on productivity of such variation is

shown in Fig. 51. In this graph the Quorus product output was normalized against the total amount of xylanase produced in a Biostat C (stated as productivity ratio R_i), so that the productivity of the Quorus GLS system can be modelled and directly compared to the STR [Eq. 19]. This is achieved by calculating the product output of the Quorus system, when the Quorus production-phase is increased from $t = 0$ d up to $t = 180$ d.

$$R_i = \frac{P_{\text{exp}}^{\text{Quorus}} \cdot t_i^{\text{production}} \cdot \text{cyc}_i^{\text{Quorus}}}{t_{\text{exp}}^{\text{production}}} \cdot \frac{1}{P^{\text{STR}} \cdot \text{cyc}^{\text{STR}}} \quad [\text{Eq. 19}]$$

R_i = productivity ratio Quorus to STR

$P_{\text{exp}}^{\text{Quorus}}$ = experimental Quorus productivity

$t_{\text{exp}}^{\text{production}}$ = duration experimental Quorus production-phase

$t_i^{\text{production}}$ = duration of production-phase (0..t)

$\text{cyc}_i^{\text{Quorus}}$ = number of possible Quorus cycles in t

P^{STR} = experimental STR productivity

cyc^{STR} = number of possible STR cycles in t

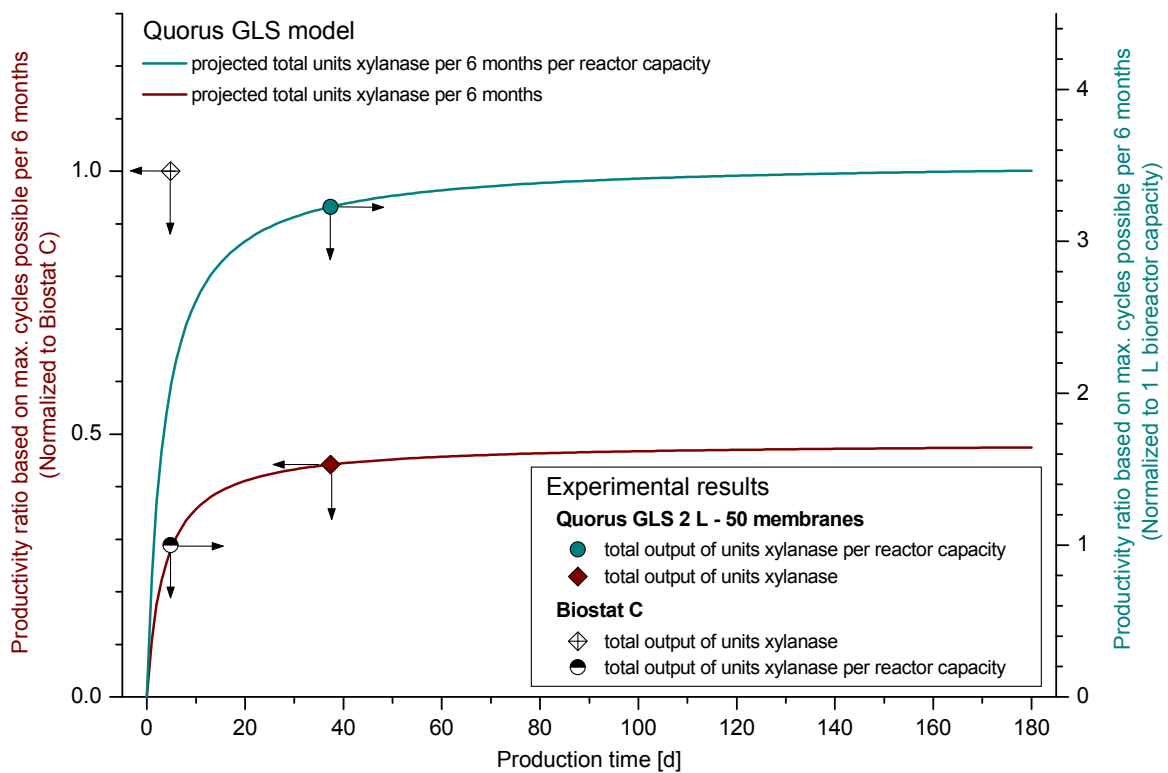


Fig. 51: Modeling of a Quorus GLS cultivation of *A.niger* D15 (xyn2) to produce xylanase. Impact of increasing Quorus GLS production-phase up to 180 d onto the total product output (brown squares) and space-time-yield (cyan circles) of the Quorus process. This data is superimposed on the actual Quorus GLS and Biostat C results. This model can be used to estimate the break-even point for the expected duration of the Quorus production time required for the Quorus to equal the Biostat C in total product output and space-time-yield. All values are normalized to the accumulative output of the maximum number of Biostat C batches in 180 d.

Fig. 51 displays a dual comparison normalized to the Biostat C: the total product output of xylanase in U (brown squares) and the productivity based on reactor capacity in $U \cdot L_{\text{Reactor}}^{-1}$ (cyan circles). The final product output and space-time-yield of the experimental Quorus GLS process (~41 d cycle time) and Biostat C (~10 d cycle time) over a 180 d period are marked. As the Biostat C cycle-time is fixed, its productivity remains constant and is used as a baseline for comparison. From the model data superimposed in Fig. 51 it becomes clear that with shorter Quorus production phases the impact of additional downtime and lag-phase at the start-up of each cycle is apparent. With longer production-phases fewer cycles are achieved and the impact of downtime and lag-phase on productivity is less significant. In this case the product output and space-time-yield level off as the production phase extends beyond 60 d, while total product output of the Quorus GLS will reach not more than 44 % of a Biostat C. Space-time-yield breaks even after a production time frame of 2 d and triplicates in comparison to the Biostat C when operated with production times longer than 20 d.

Based on the same assumptions as above, Fig. 52 shows the impact of varying Quorus GLS production time on productivity compared to the Biostat A+.

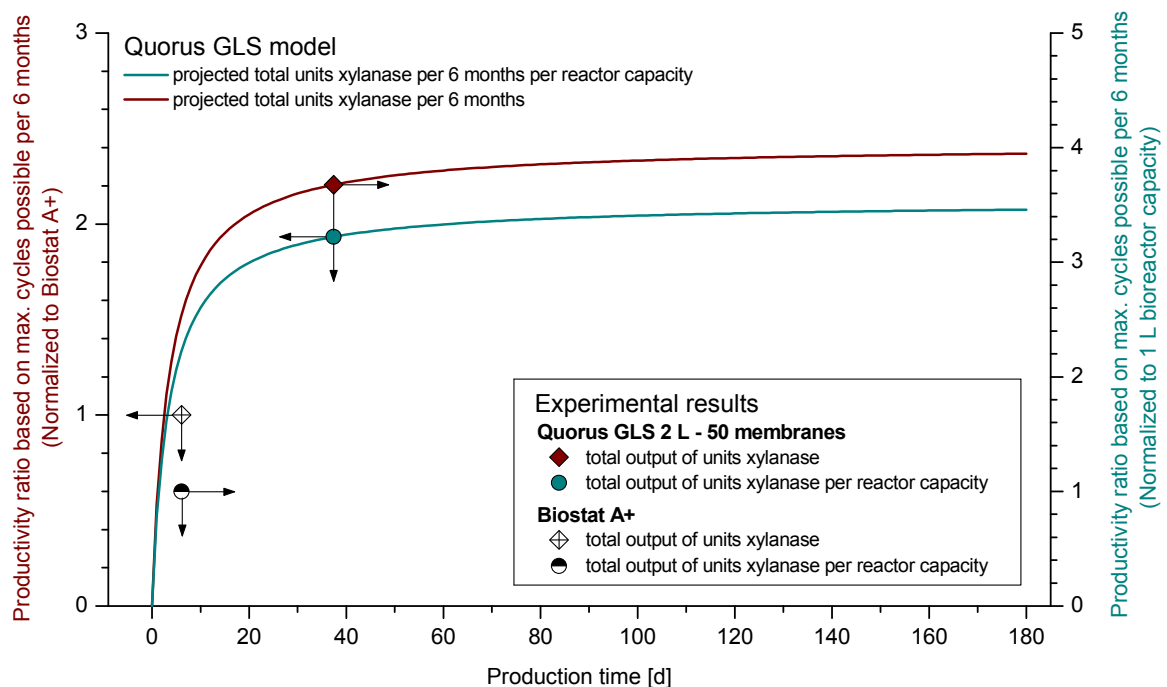


Fig. 52: Modeling of a Quorus GLS cultivation of *A.niger* D15 (*xyn2*) to produce xylanase. Impact of increasing Quorus GLS production time up to 180 d onto the total product output (brown squares) and space-time-yield (cyan circles) of the Quorus process. This data is superimposed on the actual Quorus GLS and Biostat A+ results. All values are normalized to the accumulative output of the maximum number of Biostat A+ batches in 180 d.

In this comparison the product output and space-time-yield even out as the production phase is extended beyond 80 d. The total product output of the Quorus GLS breaks even with the Biostat A+ after production times of about 3 d – which can be expected, since the Biostat A+ process was less productive than the Biostat C batch. With production times longer than 80 d the total xylanase output of the Quorus GLS would be about 2.3 times higher than the one of a Biostat A+. Space-time-yield breaks even after a production time frame of 2 d and triplicates in comparison to the Biostat A+ when operated with production times longer than 21 d.

9.2 Production of actinorhodin from filamentous *S.coelicolor* A3(2) using the aerobic process

Streptomyces coelicolor is a Gram-positive, filamentous bacteria belonging to the order Actinomycetales. The *S.coelicolor* A3(2) strain is known to produce at least five different secondary metabolites: undecylprodigiosin, calcium-dependant antibiotic (CDA), methylenomycin, chlorobiocin and actinorhodin. The productivity analysis in this work will only be focused on the secondary metabolite and polyketide antibiotic actinorhodin. This strain was supplied by Synexa Life Sciences [Pty] Ltd., South Africa.

Inoculation of all cultivations has been carried out using 1 % (v/v) of 3 d shaking flask cultures from the same source. Continuous cultivation of *S.coelicolor* A3(2) in the Quorus GLS system was performed using a 2 L total capacity module equipped with 25 membranes. Benchmark cultivations were conducted in 500 mL baffled shaking flasks, a 3 L total capacity Biostat A+ with a 1.8 L working volume and a 15 L total capacity Biostat C with a 10 L working volume. Nutrient conditions were identical by the use of freshly prepared and sterile filtrated ISP2 broth. pH was initially adjusted to 7.2 and then allowed to follow its natural course [56]. All cultivations were operated at the same temperature of 30 °C. Aeration of the STR cultures were set to 1 vvm and agitation was controlled automatically within the range of 200–350 rpm [57] to maintain a pO₂ saturation at a lower threshold of 40 %. Flask culture agitation was set to 200 rpm using an orbital shaker as suggested by Zhang *et al.* [58]. Quorus GLS medium flux was set to 20 mL·h⁻¹. Actinorhodin quantification was conducted using a photometric assay published by Doull *et al.* [59] (chapter 15.5.1).

9.2.1 Fermentation results

Cultivations of the filamentous bacteria *S.coelicolor* A3(2) in baffled shaking flasks were undertaken within a time frame of 5.8 d reaching highest actinorhodin concentrations at the end of the cultivation ($38 \text{ mg}\cdot\text{L}^{-1}$). Fermentations in the STRs were carried out within 6 d (Biostat A+) and 12 d (Biostat C). Both Biostat cultivations showed comparable profiles: rapid growth and oxygen consumption within the first 48 h of the cultivation and an adjacent pH shift to a more alkaline level. The increase in pH was consistent with the change of culture broth colorization to violet and therefore indicates the production of actinorhodin after 2 d. Highest actinorhodin concentrations were determined after 4.7 d in the Biostat A+ ($104 \text{ mg}\cdot\text{L}^{-1}$, Fig. 53) and after 8.9 d in the Biostat C ($81 \text{ mg}\cdot\text{L}^{-1}$, data not shown). These timestamps are considered to be the optimal harvesting times and are used for all subsequent calculations.

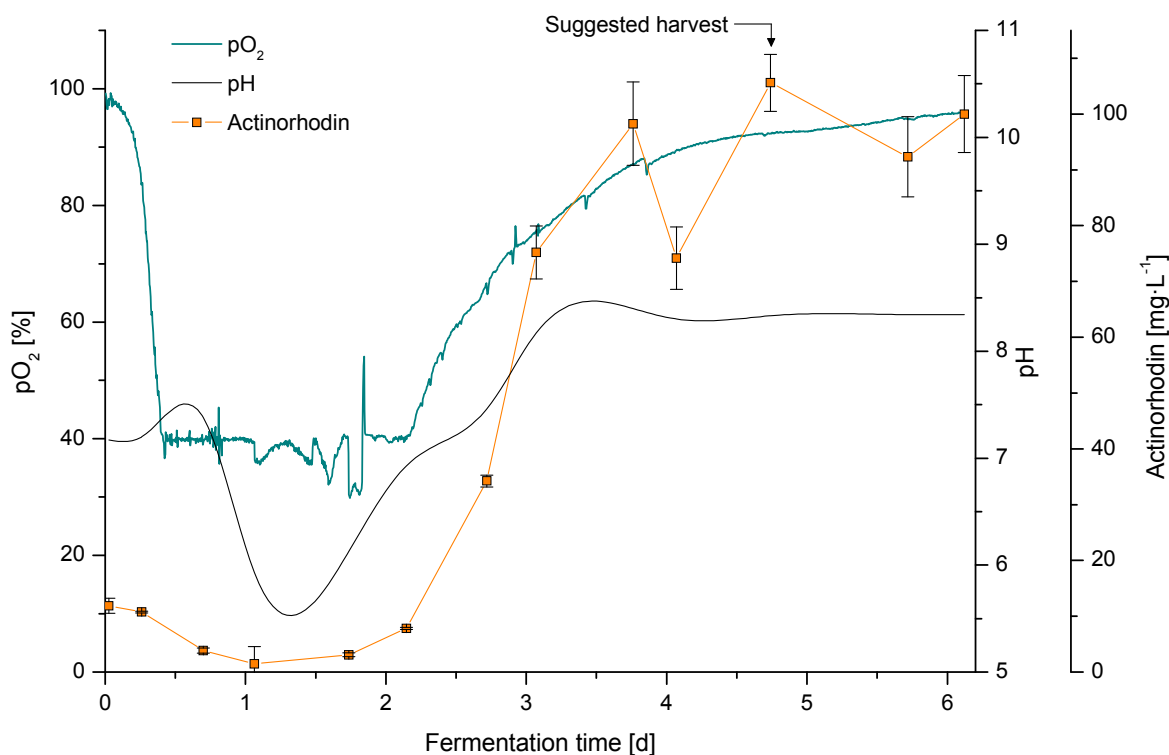


Fig. 53: 1.8 L Biostat A+ cultivation (30 °C, 200-350 rpm, 1 vvm) of *S.coelicolor* A3(2) to produce actinorhodin. After 4.7 d the highest actinorhodin concentration ($104 \text{ mg}\cdot\text{L}^{-1}$) is reached and therefore suggested to be the optimal harvesting time.

In contrast to STRs, the continuous cultivation of *S.coelicolor* A3(2) in the Quorus GLS 2 L – 25 membrane system was carried out for 28 d. Visible biofilm formation started after approximately 24 h of operation with a distinct growth of beige mycelia on the

membrane surface. With increasing biofilm thickness, formation of yellow and red pigmentation was observed from day 3. After 9 d biofilm surface was fully coated in grey-white spores, while actinorhodin production increased as permeate colorization turned visibly deep purple. Maximum biofilm growth stagnated after 12 d reaching an overall thickness of approximately 0.5 cm from membrane surface. As already observed for *A.niger* (chapter 9.1.1) the biofilm was conically shaped with increasing diameter from top to bottom.

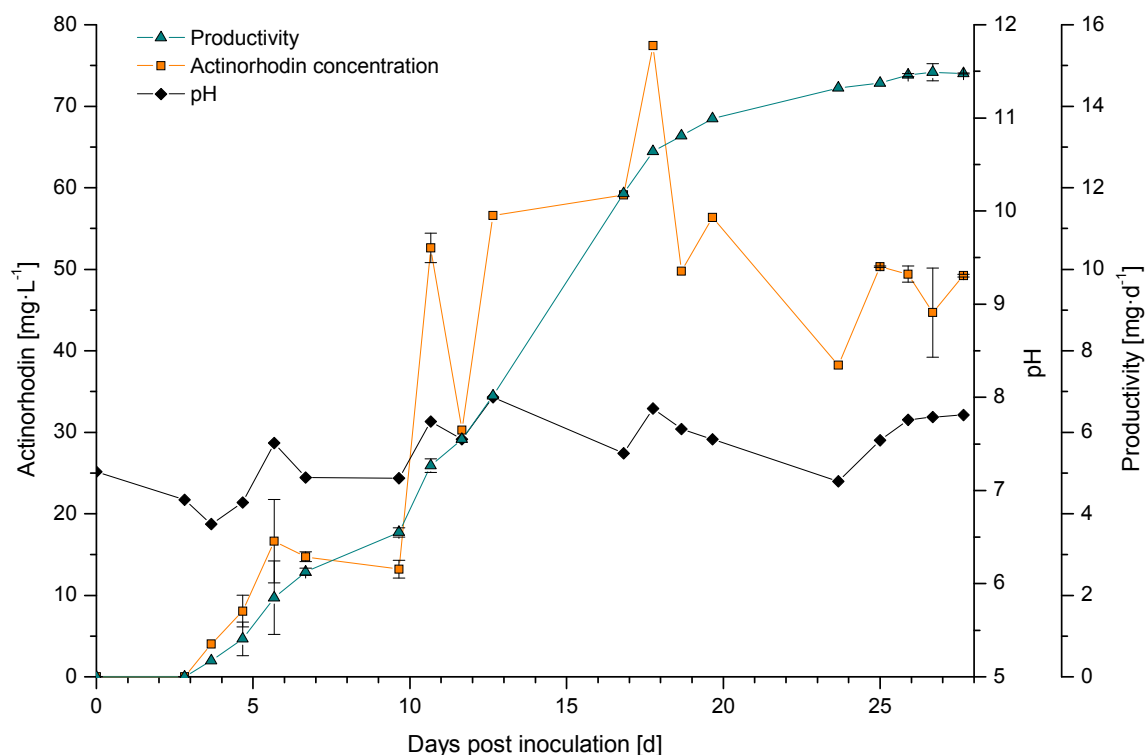


Fig. 54: Continuous production of actinorhodin by *S.coelicolor* A3(2) using a Quorus GLS 2 L – 25 membrane bioreactor. Displayed are actinorhodin concentration, pH and Quorus GLS productivity. The productivity stabilized after approximately 20 d with a constant production of about 14 mg·d⁻¹.

However, in contrast to the *A.niger* D15 cultivation a blockage of the reactor outlet was not observed. A stable production phase with a product output of 14 mg·d⁻¹ was reached after 20 d, while product concentration stabilized at 51 mg·L⁻¹ after 10 d (Fig. 54). Relevant production results of all conducted cultivations are listed in Table 9 and are the basis for the following discussions.

Table 9: Results from *S.coelicolor* A3(2) cultivations to produce actinorhodin in various fermentation vessels. All values are averaged to the whole process time. Given values represent mean values and standard deviations.

	Days post inoculation [d]	Total yield [mg]	Average volumetric production rate [$mg \cdot L_{\text{Medium}}^{-1} \cdot d^{-1}$]	Average production rate per reactor capacity. [$mg \cdot L_{\text{Reactor}}^{-1} \cdot d^{-1}$]	Average product concentration [$mg \cdot L_{\text{Medium}}^{-1}$]
Shaking flasks	5.8	3.8 ± 1	6.6 ± 2	1.3 ± 0.4	37.8 ± 9
Biostat A+	4.7	187 ± 9	22.2 ± 1	13.3 ± 0.6	104.0 ± 5
Biostat C	8.9	811 ± 7	9.1 ± 1	6.1 ± 0.1	81.1 ± 1
Quorus GLS 2 L (25 membranes)	27.7	410 ± 17	1.6 ± 1**	7.2 ± 0.3	37.3 ± 5

** based on the use of 10 L medium within a stable production phase to compare to a 10 L Biostat C batch

Following the same argument as in chapter 2.1.3 the Quorus GLS system could not compete with STRs in volumetric productivity. With a volumetric production rate of $1.6 \text{ mg} \cdot L_{\text{Medium}}^{-1} \cdot d^{-1}$ the Quorus performs less than the Biostat C ($9.1 \text{ mg} \cdot L_{\text{Medium}}^{-1} \cdot d^{-1}$) and the Biostat A+ ($22.2 \text{ mg} \cdot L_{\text{Medium}}^{-1} \cdot d^{-1}$). Focussing on the efficiency of the reactor itself, it becomes obvious that the Quorus GLS productivity per reactor capacity of $7.2 \text{ mg} \cdot L_{\text{Medium}}^{-1} \cdot d^{-1}$ lies between the Biostat A+ ($13.3 \text{ mg} \cdot L_{\text{Reactor}}^{-1} \cdot d^{-1}$) and the Biostat C ($6.1 \text{ mg} \cdot L_{\text{Reactor}}^{-1} \cdot d^{-1}$).

9.2.2 Modeling of long term operation

To compare the reactor systems in long term operation a total time frame of 180 d is considered. By fitting as many production-cycles as possible of each reactor type into this time frame, the accumulative productivity per reactor capacity based on the results in Table 9 can be calculated. The corresponding cycle times of each reactor system are illustrated in Fig. 55. Within one Quorus GLS production cycle 3.2 Biostat C and 5.0 Biostat A+ production cycles can be undertaken (Fig. 56).

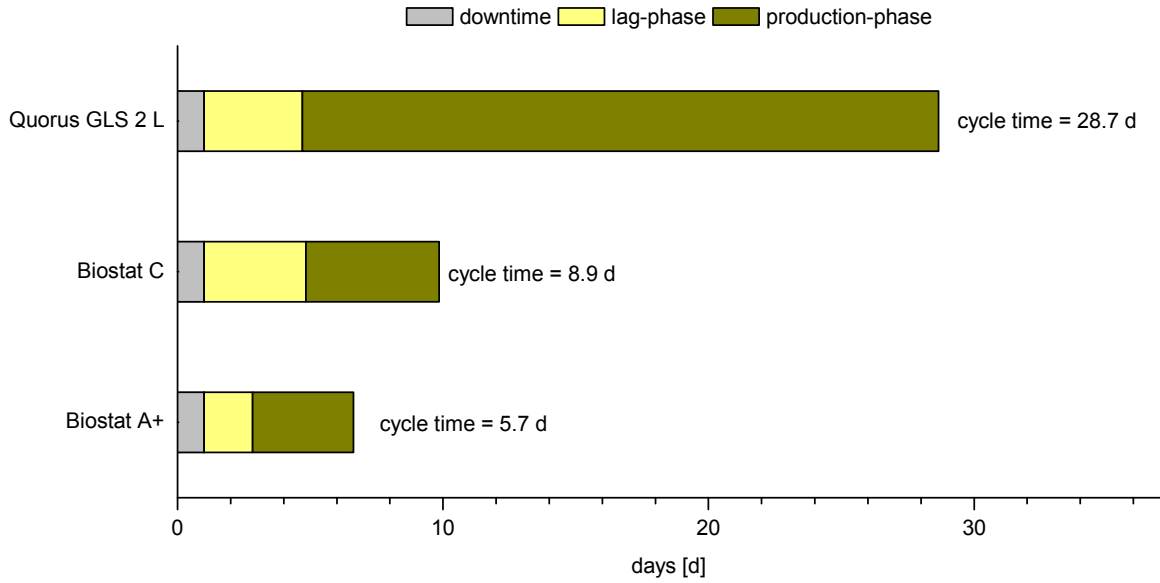


Fig. 55: Total cycle time of the reactor specific production cycles for the compared bioreactors. Each production cycle is composed of downtime, lag-phase and production-phase.

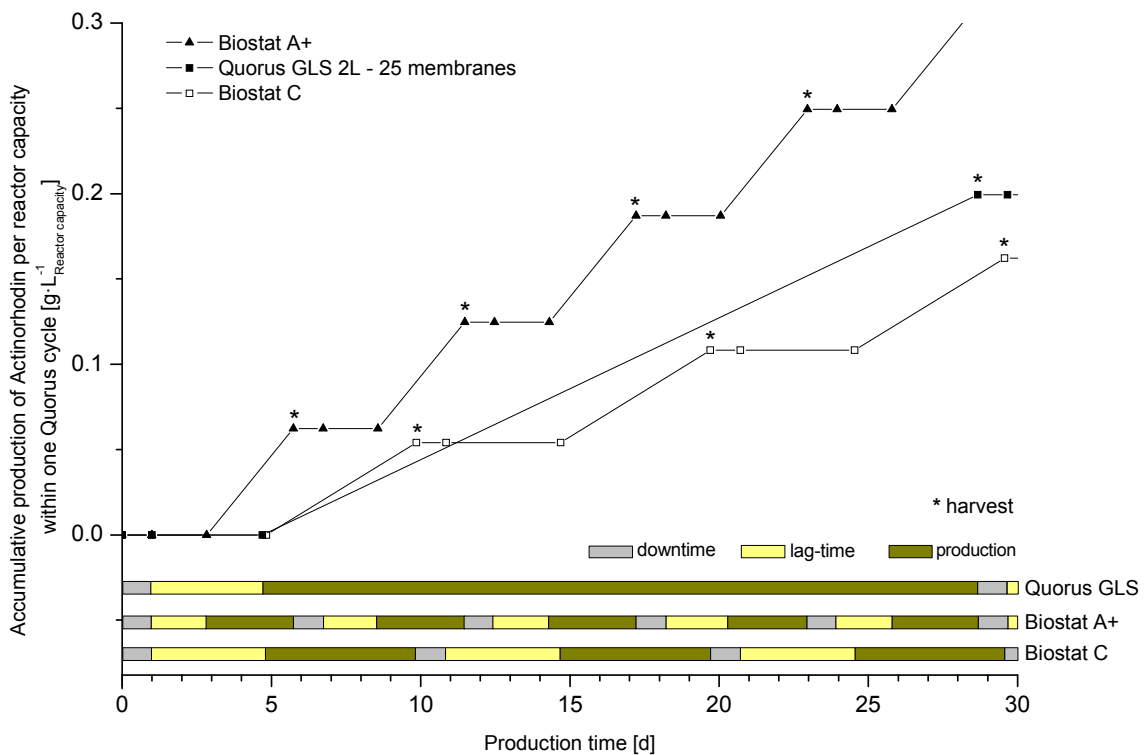


Fig. 56: Detailed plot of the accumulative production of actinorhodin from *S.coelicolor* A3(2) per 1 L reactor capacity within one Quorus GLS cycle. Additionally an overview of downtimes, lag-times and production-times is given.

Actinorhodin production in the Quorus GLS was stopped after 28.7 d which included a 25.1 d production-phase. Due to the continuous operation of the Quorus GLS, product removal can be accomplished at any time within this production phase. Harvesting in the

STRs Biostat A+ and C can only be performed once and therefore defines the end of a production cycle.

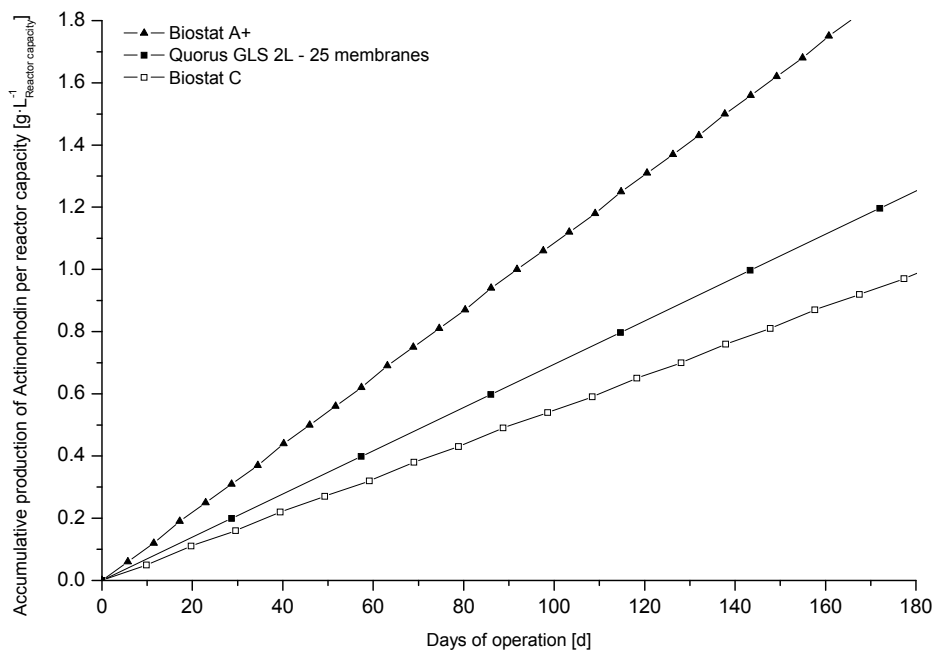


Fig. 57: Accumulative production of actinorhodin from *S.coelicolor* A3(2) normalized to 1 L reactor volume using various bioreactors. The plots are based on the estimation of maximum possible repeated production cycles within a 6 month period.

As already stated for volumetric productivity, the Quorus GLS space-time-yield lies between the better performing Biostat A+ and the Biostat C (Fig. 57). However, when directly comparing the total product output [g], the Biostat A+ would produce the most actinorhodin within the estimated time frame of 6 months, followed by the Quorus GLS and Biostat C (data not shown).

9.2.3 Variation of production time

Modeling the Quorus GLS production time over a period of 180 d while cultivating *S.coelicolor* A3(2) to produce actinorhodin is a valuable method to estimate the productivity compared to a benchmark system in long term operation. As a result the break-even of the Quorus system with a STR used for benchmarking and stable production-phases can be abstracted. Normalizing those values to the specific benchmark systems Biostat C (Fig. 58A) and Biostat A+ (Fig. 58B) will allow a direct comparison over a long period of time. Based on the same assumptions as described in chapter 9.1.4 and [Eq. 19] above, figures display a dual comparison normalized to the Biostat C and A+ data: the total product output ratio of actinorhodin (brown squares)

and the productivity ratio based on reactor capacity (cyan circles). The actual product output and space-time-yield of the Quorus GLS, Biostat A+ and C are marked.

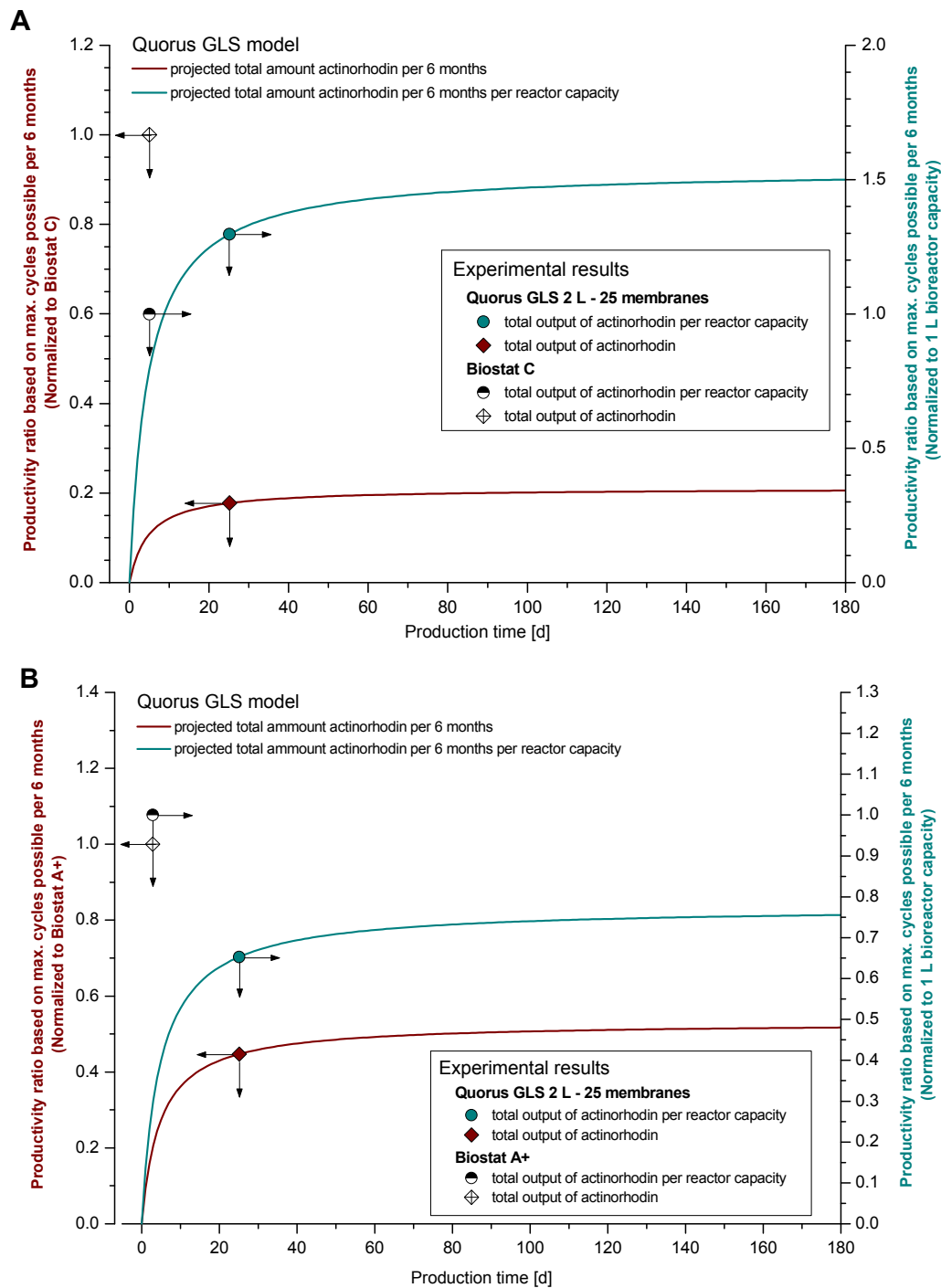


Fig. 58: Modeling of a Quorus GLS cultivation of *S.coelicolor* A3(2) to produce actinorhodin. Effect of varied Quorus GLS production time up to 180 d onto the total product output (brown squares) and space-time-yield (cyan circles) of the Quorus process. This data is superimposed on the actual Quorus GLS and Biostat results.. All values are normalized to the accumulative output of the maximum number of Biostat batches in 180 d. **A:** Productivity ratio of the Quorus GLS based on the Biostat C. **B:** Productivity ratio of the Quorus GLS based on the Biostat A+.

It becomes obvious, that Quorus GLS product output and space-time-yield will enter, compared to a Biostat C, a stable production phase after about 40 d (Fig. 58 A). While the total product output of the Quorus GLS will not reach more than 20 % of a Biostat C, the space-time-yield breaks even after a production period of about 9 d. Compared to the Biostat C the Quorus space-time-yield will reach 150 % with production times longer than 60 d.

In contrast the productivity model normalized to the results of the Biostat A+ showed that the Quorus GLS will not exceed Biostat A+ productivity at any time (Fig. 58B). Due to the high productivity and especially the short lag-phase of the Biostat A+ a break-even of the Quorus GLS in total output and space-time-yield is not expected.

9.3 Production of β -lactamase from *L.lactis* PRA290 as an example for the anaerobic process

To evaluate the conditions and productivity of the anaerobic Quorus LS process and furthermore compare the achieved results to conventional batch bioprocesses, the strain *L.lactis* PRA290 was used as a model organism.

Lactococcus lactis is a Gram-positive lactic acid bacterium growing under facultative anaerobic conditions. In this example the P170 expression system of *L.lactis* (Bioneer A/S, Horsholm, Denmark) was used to secrete the recombinant protein β -lactamase. This strain was provided by Synexa Life Sciences (Pty) Ltd., South Africa.

All cultivations were inoculated with 1 % (v/v) static overnight flask cultures from the same source. One 0.22 L Quorus LS bioreactor unit was used for evaluation. Benchmark cultivations were conducted in 500 mL baffled shaking flasks, a 3 L Biostat A+ with a 2 L working volume and a 15 L Biostat C with a 10 L working volume. Nutrient conditions were identical by the use of freshly prepared and sterile filtrated LM5-V100-G75 medium (pH=7.6) (chapter 15.3.4) [60]. All cultivations were operated at the same temperature of 30 °C. STR cultures were not aerated, while agitations were maintained at 50 rpm [61]. 2 M KOH was used in all STR cultivations to control the pH not to drop below a setpoint of 6.0. pH control in the Quorus process was realized through an automated in- or decrease of medium flux rate to maintain a pH at a lower threshold of

6.0. Flask cultures were agitated at 50 rpm using an orbital shaker or left static. β -lactamase activity was determined using a spectrophotometric assay based on the enzymatic hydrolyzation of nitrocefin (chapter 15.5.3).

9.3.1 Fermentation results

The cultivations of *L.lactis* in shaking flasks were conducted over a time frame of 22 h, reaching the highest β -lactamase activities of $3.3 \cdot 10^3 \text{ U} \cdot \text{L}^{-1}$ after 15.2 h. Static submerged flask cultures showed the highest enzyme activities of $2.5 \cdot 10^3 \text{ U} \cdot \text{L}^{-1}$ after 9.2 h. Both STR cultivations were monitored over a period of 24 h and showed comparatively long lag-phases of 5 h, whereas β -lactamase production started in both cases after 8.2 h. While the optimal harvesting time with a β -lactamase activity of $7.3 \cdot 10^3 \text{ U} \cdot \text{L}^{-1}$ in the Biostat A+ was reached after 17.7 h (Fig. 59), highest activity of $7.2 \cdot 10^3 \text{ U} \cdot \text{L}^{-1}$ in the Biostat C was obtained after 20.3 h (data not shown).

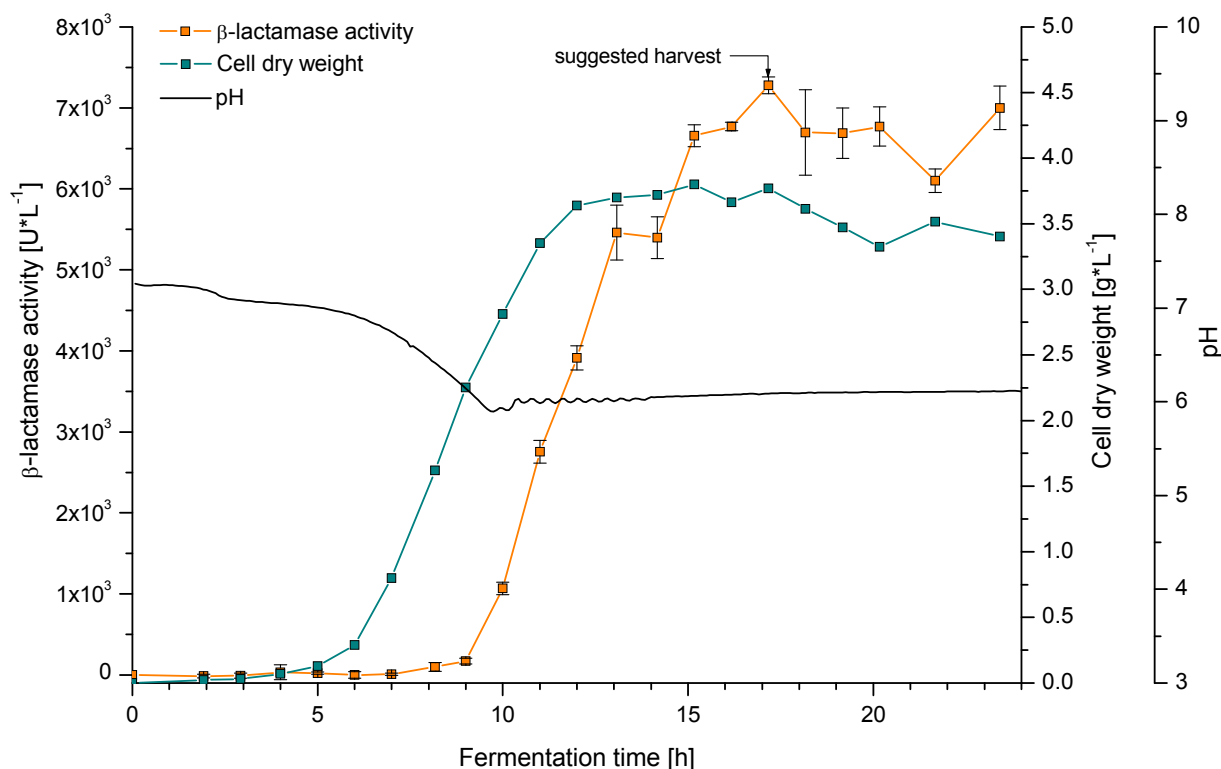


Fig. 59: Results of a 2 L Biostat A+ cultivation of *L.lactis* PRA290. After 17.7 h the highest β -lactamase activity ($7.3 \cdot 10^3 \text{ U} \cdot \text{L}^{-1}$) is reached and therefore defined as harvesting time.

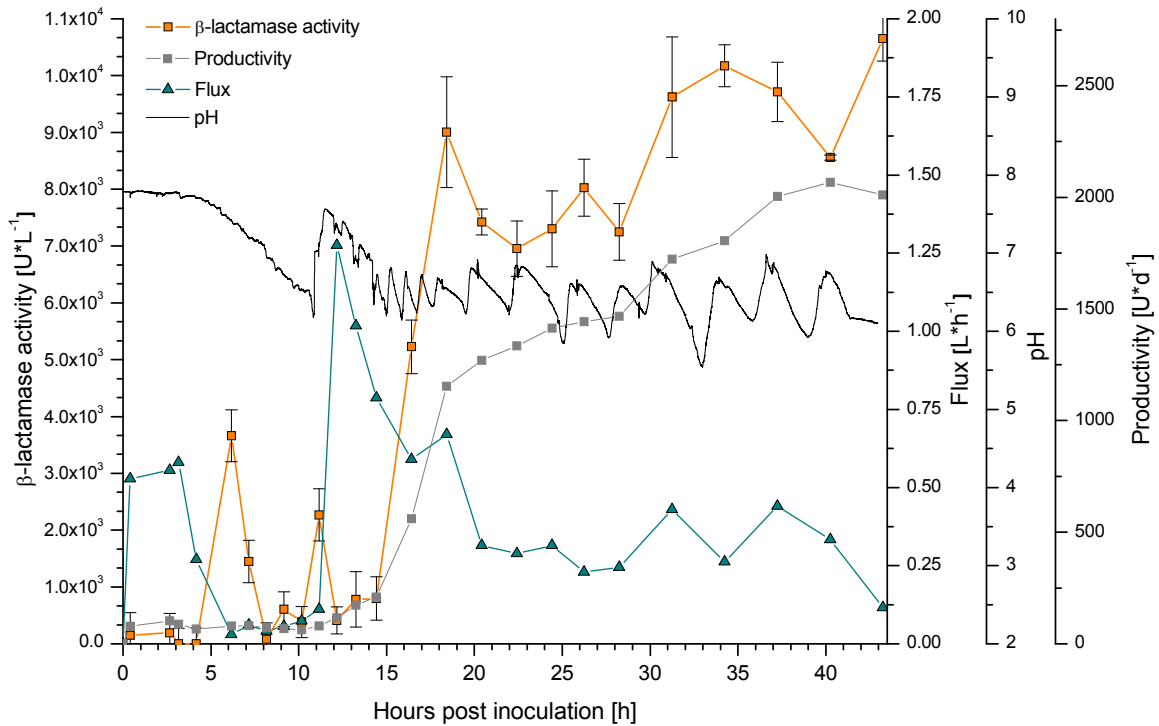


Fig. 60: Production of β -lactamase from *L.lactis* PRA290 using a 0.22 L Quorus LS bioreactor. Displayed are β -lactamase activity, pH, productivity and medium flux. The Quorus LS productivity stabilized after approximately 36 h with a production of about $2 \cdot 10^3 \text{ U} \cdot \text{h}^{-1}$.

After 5 h of culturing *L.lactis* PRA290 in the Quorus LS bioreactor (Fig. 60) pH started to decrease over an additional period of 5 h until the lower set threshold of 6.0 was reached. The automated flux controller responded by increasing medium flux to maintain the pH of the culture above 6.0 till the end of the cultivation. β -lactamase production started 14.4 h post inoculation with a rapid increase in enzyme activity. Productivity stabilized after 36 h with decreasing flux at an average production rate of $2 \cdot 10^3 \text{ U} \cdot \text{h}^{-1}$.

In contrast to the Quorus GLS the Quorus LS process cannot be operated over a comparatively long time frame. As stated above, a submerged biofilm is formed on the membrane surfaces within the ECS, supplied with a constant nutrient feed. As the density of the biofilm will increase with ongoing cultivation, it will not – compared to the Quorus GLS – be maintained at a constant thickness. While the biomass accumulates, medium pressure needs to be increased constantly to maintain flux in order to supply increasing amounts of nutrients to maintain metabolism of accumulating cells and/or displace metabolic waste such as lactic acid to maintain a desired pH. The cultivation of *L.lactis* in the Quorus LS bioreactor was stopped after 43.3 h. However, it could

conceivably have been maintained at least for another 24 h, since the applied pressure had not reached the predefined maximum of 1.2 bar. This maximum is precautionary set to prevent bursting of the MSV, hose couplings or the reactor chamber. Overpressure would immediately be released by a security valve.

Table 10: Results from *L.lactis* PRA290 cultivations to produce β -lactamase in various fermentation systems. All values are averaged to the whole process time.

	Hours post inoculation [h]	Total yield [U]	Average volumetric production rate [$U \cdot L_{\text{Medium}}^{-1} \cdot h^{-1}$]	Average production rate per reactor capacity. [$U \cdot L_{\text{Reactor}}^{-1} \cdot h^{-1}$]	Average activity [$U \cdot L_{\text{Medium}}^{-1}$]
Static flasks	9.2	158 ± 6	287 ± 11	57 ± 2	2.5 ± 0.1 · 10 ³
Shaking flasks	15.2	194 ± 13	212 ± 14	42 ± 3	3.2 ± 0.2 · 10 ³
Biostat A+	17.7	1.7 ± 0.1 · 10 ⁴	411 ± 6	325 ± 5	7.3 ± 0.01 · 10 ³
Biostat C	20.3	8.0 ± 0.3 · 10 ⁴	356 ± 12	263 ± 9	7.2 ± 0.2 · 10 ³
Quorus LS 0.22 L	43.3	8.6 ± 1.0 · 10 ⁴	128 ± 14	9.1 ± 1 · 10 ³	5.5 ± 0.6 · 10 ³

Even though the productivity in the Quorus LS depends, like in the STRs on the accumulation of biomass, the Quorus LS volumetric productivity of 128 $U \cdot L^{-1} \cdot h^{-1}$ could not exceed the reference cultivations (Table 10). This is primarily due to the unusually long lag-phase observed in this experiment. No more work was done to improve this run, while much effort was put into increasing STR performance. The total amount of medium used during LS process amounted to 15.8 L. With reference to the average STY the systems show an inverse performance: as all flask cultivations performed at 42 - 57 $U \cdot L_{\text{Reactor}}^{-1} \cdot h^{-1}$ and the STRs at approximately 7 · 10³ $L_{\text{Reactor}}^{-1} \cdot h^{-1}$, highest STY of 9.1 · 10³ $L_{\text{Reactor}}^{-1} \cdot h^{-1}$ was achieved with the Quorus LS process. Considering that the total capacity of the Quorus LS reactor is only 11 % of the Biostat A+ or 2.2 % of the Biostat C working volume, the Quorus LS production rate is remarkable. Taking the total reactor capacity into account, the Quorus LS bioreactor outperforms the STRs even with a much longer lag-phase at least by the factor 28.

9.3.2 Modeling of long term operation

A comparison of the productivity of each reactor system in a 30 d long period can be accomplished by fitting as many production cycles of each reactor system as possible into this time frame. As a result the total product output or accumulative productivity per reactor capacity can be assessed by adding up the productivities of each cycle up to 30 d. The necessary cycle-times of each reactor system are illustrated in Fig. 61. Within one Quorus LS cycle 1.6 Biostat A+ and 1.5 Biostat C production-cycles can be undertaken (Fig. 62).

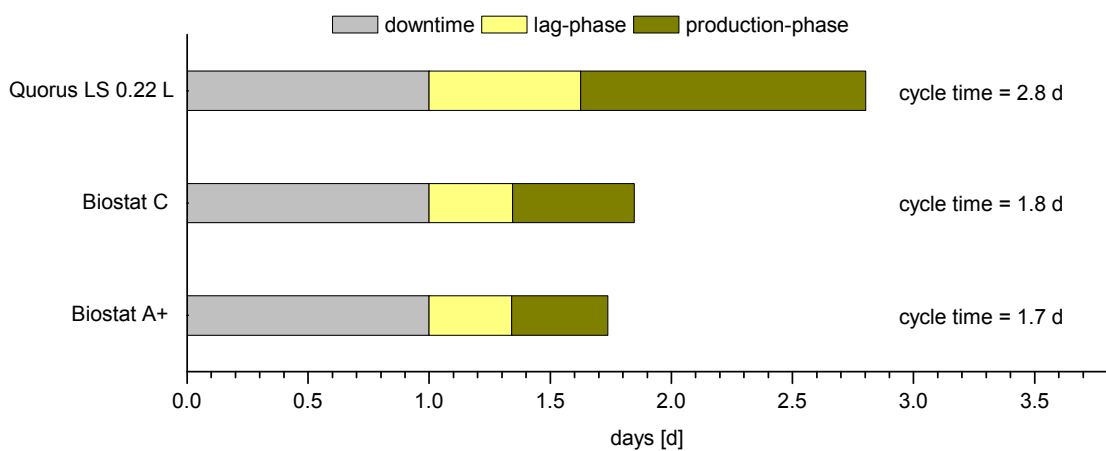


Fig. 61: Total cycle-time of the reactor specific production-cycles for the compared bioreactors. Each production cycle is composed of downtime, a lag-phase and production-phase.

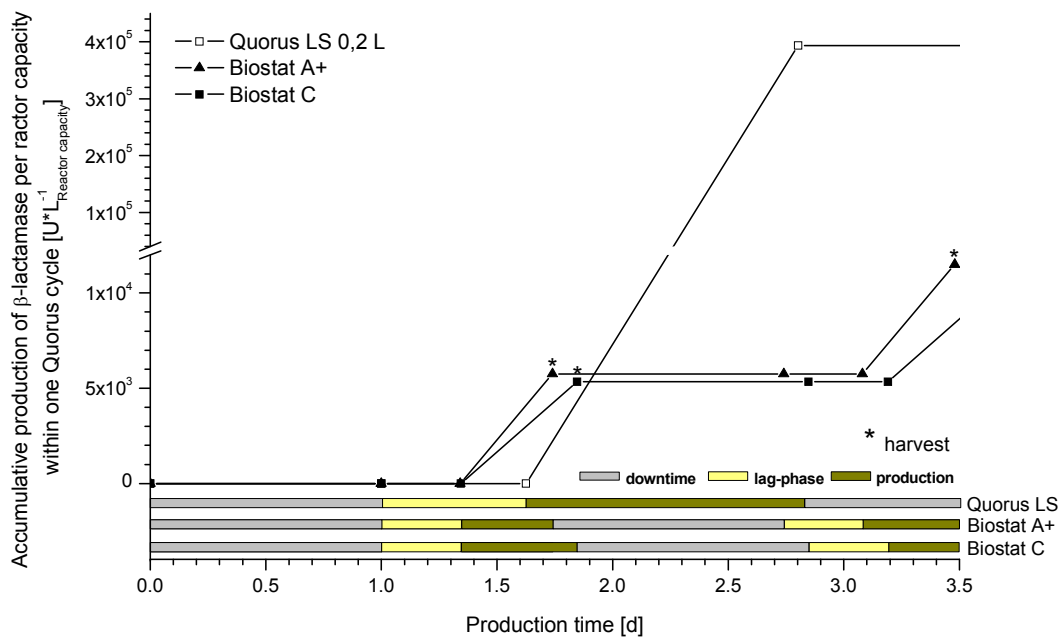


Fig. 62: Detailed plot of the accumulative production of β -lactamase from *L.lactis* PRA290 per L reactor capacity within one Quorus LS cycle. Additionally an overview of downtimes, lag-times and production-times is given.

The production of β -lactamase from *L.lactis* PRA 290 in the Quorus LS was stopped after a 28.3 h production-phase, which correlated with the use of 15.8 L medium. While product removal from the Quorus LS system is either automated or can manually be accomplished at any interval, harvesting in the Biostat reactors can only be performed once and therefore defines the end of each production-cycle. The accumulation of product output normalized to reactor capacity of as many production cycles as possible within a time frame of 30 d is illustrated in Fig. 63.

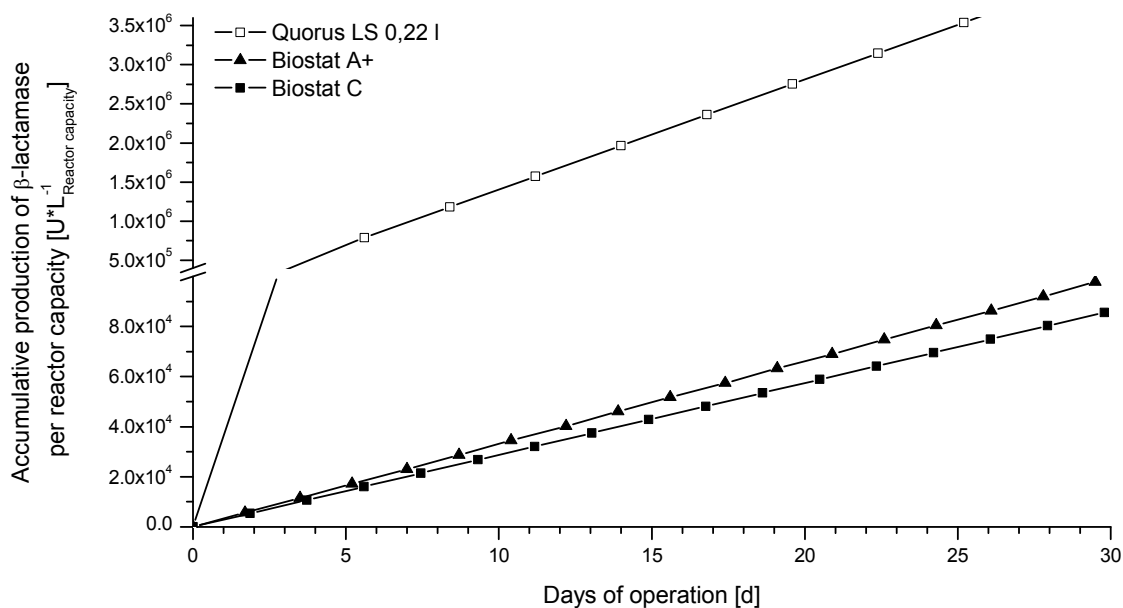


Fig. 63: Accumulative production of β -lactamase from *L.lactis* PRA290 normalized to 1 L reactor volume in various bioreactors. The plots are based on the estimation of maximum possible repeated production cycles within a 30 d period.

Even though the STR processes were optimized towards shorter lag-phases from initially 15 h to 6 h and higher product outputs by the use of a more concentrated inoculum, they cannot compete with the space-time-yield of the Quorus LS. In this context the LS will exceed the most productive STR (Biostat A+) already after 0.9 d post inoculation (Fig. 62). By examination of total product output within this time-frame, highest production would however be achieved using a Biostat C, followed by the Quorus LS and Biostat A+ (data not shown).

9.3.3 Variation of production time

As the production times of the STRs are fixed by their harvesting time, product removal in the Quorus LS can be achieved constantly. Taking into consideration that all batch

fermentations will consist of a 24 h downtime, identical lag-phases and production times with the same product output per batch, the total amount of β -lactamase produced in 30 d, can be estimated.

By determining the product output of the Quorus LS with production-phases from 0 – 60 h and normalizing the results to the totally produced amount of β -lactamase of as many batches as possible in 30 d in the STRs, the monthly productivity of the Quorus LS system can be modelled and directly compared. Furthermore, the break-even with the reference cultivations can be specified.

A dual comparison normalized to the Biostat A+ and C results is shown in Fig. 65 A and B: the total product output ratio of β -lactamase in U (brown squares) and the productivity based on reactor capacity in $U \cdot L_{\text{Reactor}}^{-1}$ (cyan circles). The actual product output and space-time-yield of the Quorus LS and STRs used for benchmarking are marked.

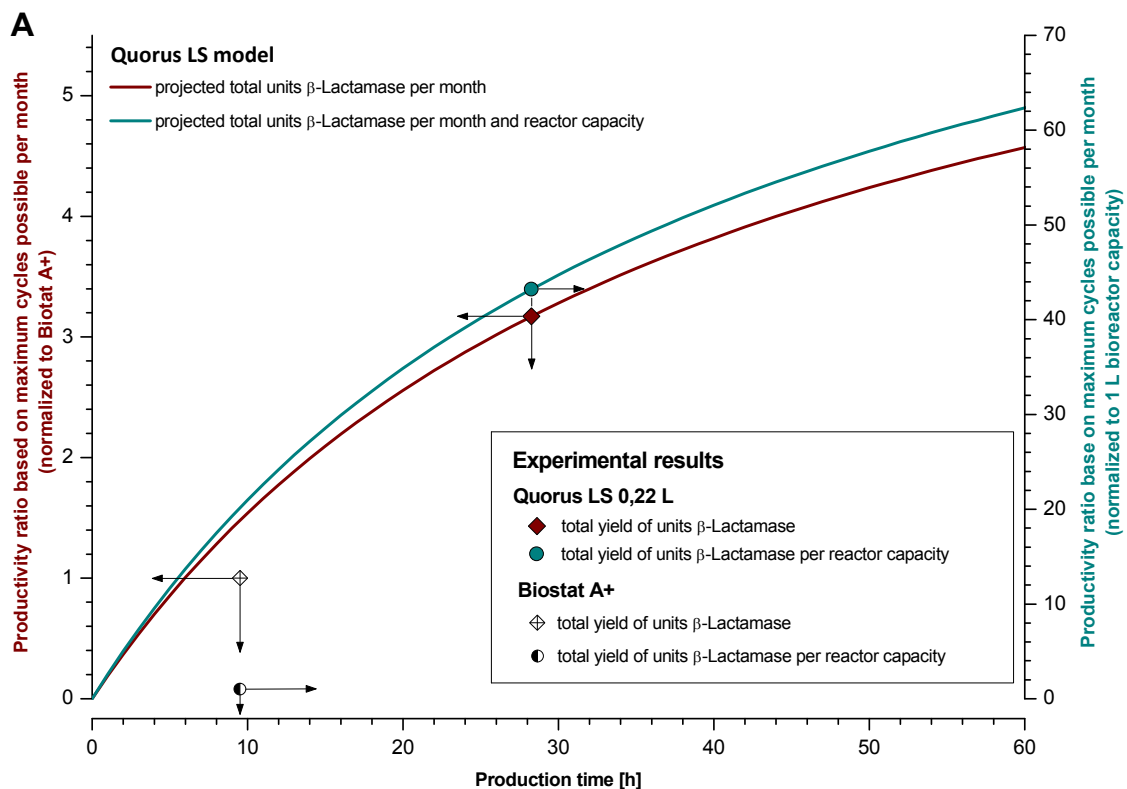


Fig. 64 A: Modeling of a Quorus LS cultivation of *L.lactis* PRA290 to produce β -lactamase. Effect of varied Quorus LS production time up to 30 d onto the total product output (white squares) and space-time-yield (black triangles) for the Quorus process. This data is superimposed on the actual Quorus LS and Biostat A+ results. All values are normalized to the accumulative output of the maximum number of Biostat A+ batches in 30 d. Here: productivity ratio of the Quorus LS based on the Biostat A+.

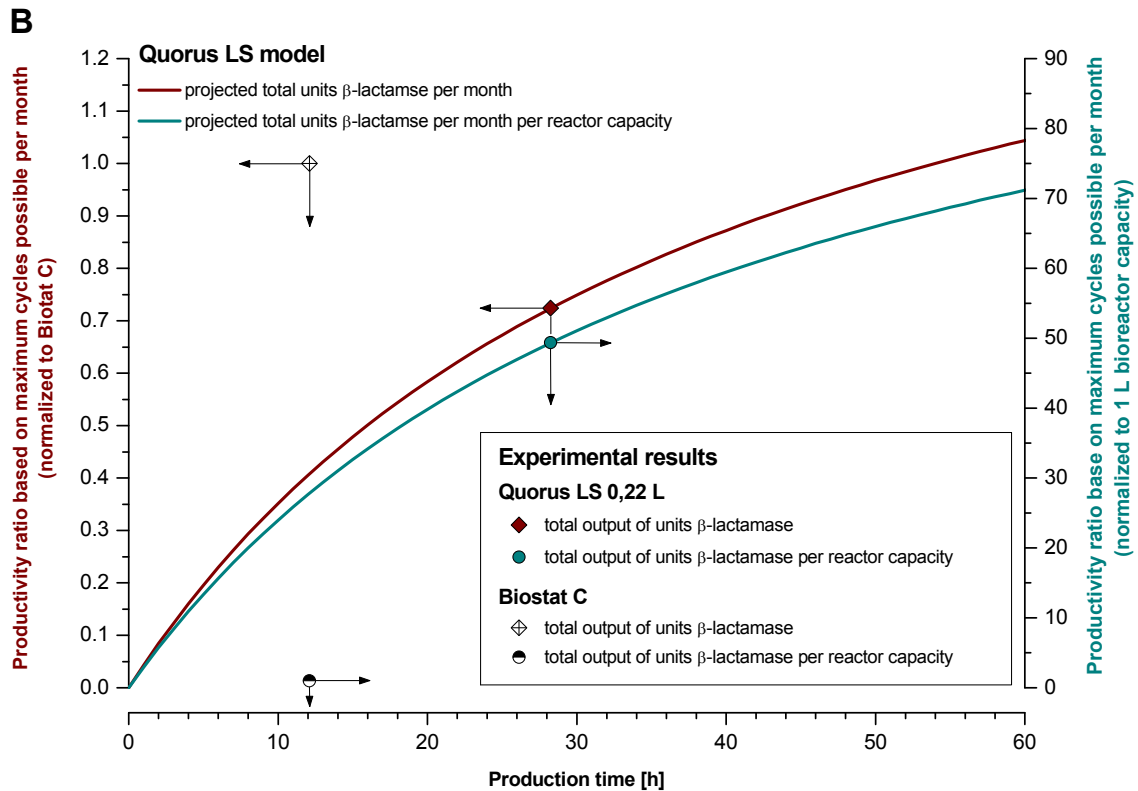


Fig. 65 B: Productivity ratio of the Quorus LS based on the Biostat C.

An extension of the Quorus LS production-phase up to 60 h is possible. Since the submerged biofilm is not maintained at a constant thickness it will accumulate with ongoing fermentation leading to a substantial increase in productivity. A productivity-plateau as previously shown for the Quorus GLS is not expected within the theoretically considered time frame.

A break even of the Quorus LS in total product output and space-time-yield with the Biostat A+ is reached after less than 6 h of Quorus production time. As the cultivation of *L.lactis* was stopped after 28 h of production time, it was already reaching three times the total product output and a 34 times higher space-time-yield than the Biostat A+. Highest product output was achieved using a Biostat C, however, by extending the Quorus LS production-phase to more than 54 h it would overtake the Biostat C product output. A break-even between Quorus LS and Biostat C STY is obtained with production-phases longer than 12 h.

9.4 Cost influencing factors in operation

Process productivities and furthermore the costs to achieve such are other important factors in comparing different process strategies. The amount of used media, product titer, unproductive downtime and downstream processing (DSP) are just a few examples of many process variables, but such with crucial impact on total cost of process operation [62].

Within this chapter the evaluated Quorus GLS and LS processes will be compared on a basic level of operational cost to the STR benchmarking systems. As an example for the aerobic Quorus GLS process, results from the production of xylanase from *A.niger* D15 (chapter 9.1.2) will be applied. The production of β -lactamase from *L.lactis* (chapter 9.3.1) will be correlated to operational costs as an example for the anaerobic Quorus LS process. For this comparison the prices are limited to downtime, medium and downstreaming, and are estimated as follows:

Cost of unproductive downtime was defined as 100 € per d plus additional 10 € per litre reactor capacity for cleaning, sterilization and validation of the reactor units. As the Quorus reactors are disposable, these additional assets do not apply. Corresponding costs of labour are already incorporated within this factor. Medium costs are mainly determined by materials and preparation. They are considered as 5 € per litre. In conventional bioprocesses 50 - 70 % of total costs are allotted to DSP, whereas in cultivations employing recombinant organisms up to 90 % is possible [63]. Within this context, DSP costs for this comparison are assumed as 40 € per processed litre culture broth. Quorus LS DSP costs were reduced since the cell-free product removal (chapter 8.2) represents an integrated downstreaming step. Specific values are given in Table 11.

Table 11: Estimated cost factors of downtime, medium and DSP for the applied reactor systems.

	Quorus GLS	Quorus LS	Biostat A+	Biostat C
Downtime [€·d⁻¹]	100	100	120	200
Medium [€·L⁻¹]	5	5	5	5
Downstreaming [€·L⁻¹]	40	36	40	40

9.4.1 Cost distribution for the production of xylanase from *A.niger* D15

For cost analysis the Quorus GLS process-phase was realistically extended to a single continuous process lasting 179 d (total cycle time of 180 d, including 1d downtime). The Biostat's accumulative totals were estimated based on the maximum possible full cycles that can be undertaken within the same 180 d period. Relevant parameters such as medium used, downtime, production time and total yield are listed in Table 12.

Table 12: Estimation of production parameters for the production of xylanase by *A.niger* D15 (xyn2) within 180 days.

	Quorus GLS	Biostat A+	Biostat C
Number of cycles	1	20	18
Downtime [d]	1	21	19
Total production time [d]	179	159	161
Total volume of medium [L]	216	36	186
Average product concentration [U·L⁻¹]	$1.9 \cdot 10^4$	$2.6 \cdot 10^4$	$4.0 \cdot 10^4$
Total yield [U]	$4.1 \cdot 10^6$	$9.7 \cdot 10^5$	$7.5 \cdot 10^6$

By summing up all costs, the proportions of downtime, medium and DSP can be calculated (Fig. 66). In doing so it becomes clear that a cost intensive factor during accumulative operation of the Biostat reactors is downtime, especially for the Biostat A+ and Biostat C, where it accounts for close to 60 % and 30 %, respectively, of the total cost of operation.

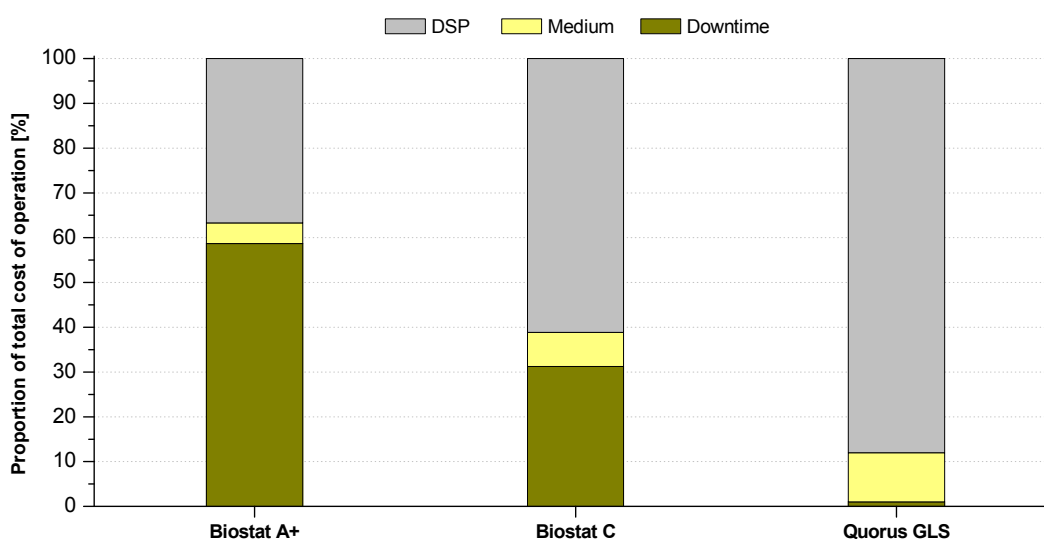


Fig. 66: Percentage composition of the cost intensive factors downstream processing, medium and downtime while production of xylanase from *A.niger* D15 over a period of 180 d. Results are based on Table 11 and Table 12.

Since the Quorus system is operated constantly, just one set-up time is necessary. In this context, medium cost is negligible and does not exceed more than 11 % (Quorus GLS) of total cost. Most notably, 61 % (Biostat C) and 88 % (Quorus GLS) of operational cost are allotted to DSP. Further, with increased use of medium in relation to total product output the impact of DSP costs becomes more relevant. With the lower product concentration obtained from the Quorus GLS product stream, primary concentration steps will impact even more on the Quorus DSP costs.

9.4.2 Cost distribution for the production of β -lactamase from *L.lactis* PRA290

Various cost impacting parameters such as used medium, downtime and total yield have been calculated based on the number of Biostat and Quorus LS cycles that can be accomplished within a total time frame of 30 d. For this comparison the Quorus LS production-phase was realistically extended to a time frame of 60 h, resulting in an overall downtime of 9 d out of 30 d. All calculated parameters are stated in Table 13.

Table 13: Estimation of production parameters for the production of β -lactamase from *L.lactis* PRA290 within 30 d.

	Quorus LS	Biostat A+	Biostat C
Number of cycles	8.6	17	16
Downtime [d]	9	17	16
Total production time [d]	21	12	13
Total volume of medium [L]	183	33	153
Average product concentration [U·L⁻¹]	$5.5 \cdot 10^3$	$8.6 \cdot 10^3$	$8.0 \cdot 10^3$
Total yield [U]	$1.0 \cdot 10^6$	$2.8 \cdot 10^5$	$1.2 \cdot 10^6$

As for the previous comparison a limiting factor in using multiple cycles is unproductive and therefore expensive downtime (Fig. 67). This is most relevant for the Biostat A+, where downtime accounts for 55 % of operating expenses. While Biostat C batches add up to a comparable long downtime, these larger batches utilize more medium, which has a greater impact on DSP cost (61 %) and proportionately reduces overall Biostat C downtime to only 31 % of total cost.

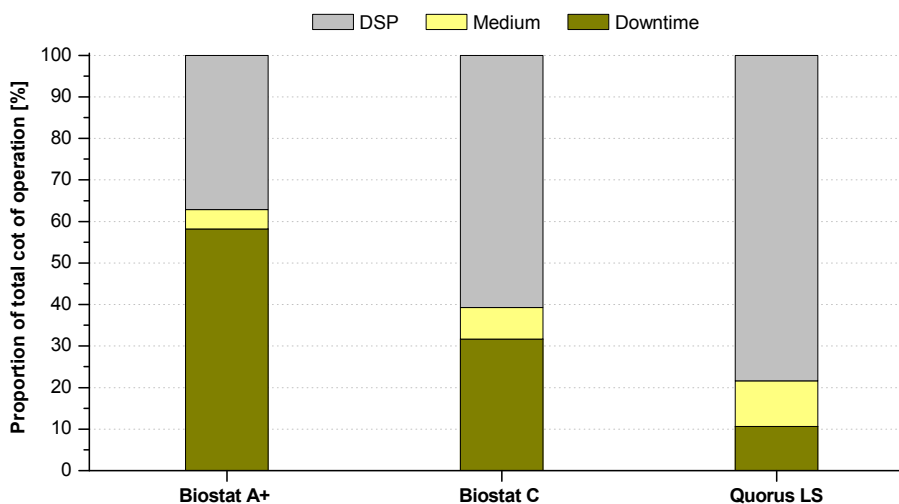


Fig. 67: Percentage composition of the cost intensive factors downstreaming, medium and downtime while production of β -lactamase from *L.lactis* PRA290 over a period of 30 days. Results are based on Table 11 and Table 13.

Since the Quorus system is operated with longer production cycles, less downtime in the considered time frame is necessary. Furthermore, an increase of the Quorus LS production-time, if possible, will result in fewer cycles and lead to a less impact of downtime on total cost. DSP cost becomes more relevant for the Biostat C and Quorus LS, with increasing use of medium and final total product output. The Quorus system uses on the one hand more medium than the Biostat C, but on the other hand has the crucial advantage of an integrated DSP step resulting in a cell-free product stream. Compared to the Biostat downstream-strategies, separation of biomass from the supernatant by centrifugation is not necessary and will therefore decrease DSP expense. This advantage was already considered by decreasing Quorus LS DSP cost (Table 11). The smaller product titer in the Quorus product stream is an additional influence on DSP cost (78 %). However, because of the continuous product output, with a nearly constant product concentration, the downstream process can be adapted accordingly, which may in turn reduce overall DSP cost.

10 Membrane bioreactor prototype for mammalian cultivations

The cultivation of adherent cell lines on a laboratory scale is routinely done in static systems such as T-flasks. For scaling up adherent cultures, cells can be grown in a controlled reactor, either attached to static matrices or suspended on microcarriers.

The ceramic membrane reactors Quorus CELL (Synexa Life Sciences, Cape Town, South Africa) provide in this context a novel and compact method for the mass culture of attachment dependent mammalian cell lines. These reactors utilize ceramic membranes as a surface for cell attachment and continuously perfuse the cells with fresh medium for increased cell productivity. Recovery of valuable secreted products is enabled through constant permeate removal.

10.1 Reactor and process description

The main purpose of Synexa's ceramic membrane based Quorus CELL reactors is the provision of a controlled environment for the cultivation of adherent mammalian cell cultures and the recovery of secreted products. The basic operation principle is based on the previously described Quorus microbial processes. The Quorus CELL reactors consist of multiple, horizontally orientated ceramic membranes. These membranes are encased within a manifold, which effectively forms at least two separate and distinct compartments. Adherent cells are grown in the extra capillary space on the outer surface of the ceramic membranes, while the intra capillary space of the membranes is used for nutrient delivery, aeration and permeate removal.

The nutrient delivery rate is based on the TMP between the ICS of the membranes delivering the medium, the reactors ECS and the ICS of cross-flow operated permeate membranes (Fig. 68). In its simplest configuration the ECS is aerated bubble-free by supplying humidified air from the ICS of permeate membranes at a constant pressure and air flow rate (Fig. 68). Medium flux from the ICS (medium membranes) through the adherent cell layer and into the ECS is achieved by adjusting medium pressure, while ECS pressure and ICS of permeate membranes is kept constant. For a pH-controlled process, the TMP is automatically varied to in- or decrease medium flux and thus displace

accumulating lactic acid from the ECS, thereby changing the pH of the medium within the ECS.

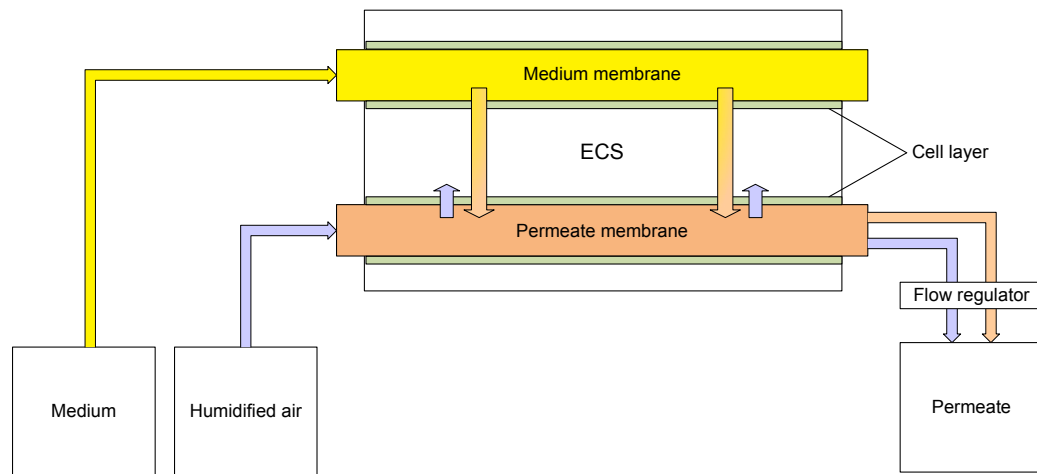


Fig. 68: Schematic representation of the Quorus CELL basic operation principle. Medium (orange) is pressurized and flows unidirectionally from the lumen of the fibre into the ECS. Humidified air (blue) is used for ECS-aeration and permeate removal (orange) through the ICS of the permeate membrane.

During operation, used media, metabolic waste and secreted products are removed from the ECS by transportation through the capillary wall of the permeate membrane and into a permeate collection vessel, along with the flow regulated air. Due to the membranes average pore size distribution, the removed permeate is cell-free.

The evaluated Quorus CELL prototypes exist in different reactor sizes and shapes. They are currently divided into transverse-flow production scaled disposable reactor-modules (Quorus CELL) and small scale R&D modules (Quorus miniCELL and maxiCELL) used for preliminary process evaluation and development.

10.1.1 Quorus miniCELL and maxiCELL reactors

To establish an initial process, various experiments have to be performed. To evaluate the effects of changing process parameters, such as different aeration rates or varying medium flux, the developmental small scale reactor units Quorus miniCELL and maxiCELL were used.

While the miniCELL (Fig. 69 A) reactors were operated by a manual control of pressure differentials, the maxiCELL reactors (Fig. 69 B) were operated semi-automatic within the Quorus CELL Optimizer housing. This housing is similar to the Quorus microbial

Optimizer and contains the necessary equipment for pressure and temperature control. Many adjustments over the Quorus Optimizer have been implemented, including more uniform temperature distribution within the incubation chamber, e.g. a mass balance to determine flux rates and integrated pH sensors. It is furthermore suitable for housing the actual Quorus CELL reactor (chapter 10.1.2).

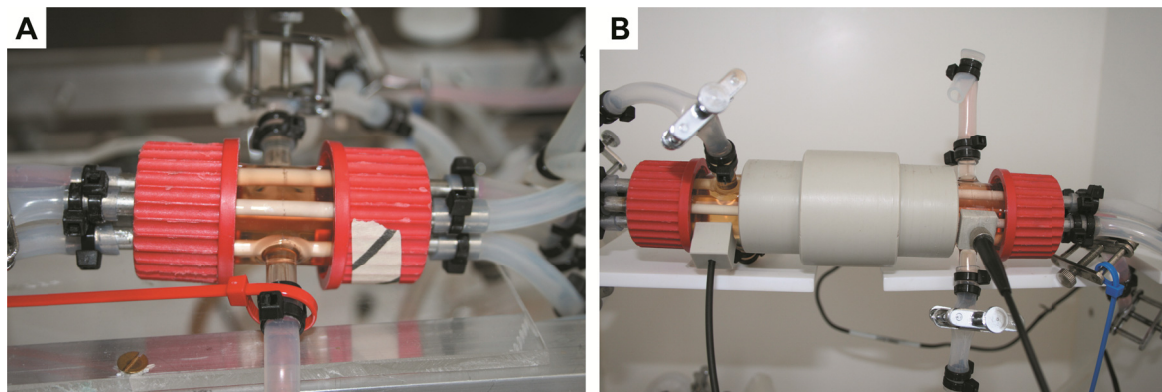


Fig. 69: Membrane reactor units for process evaluation and development: Quorus miniCELL (A) and Quorus maxiCELL (B).

While the miniCELL working volume sizes 25 cm³ and surface-area reaches 26 cm², the maxiCELL is a linear scale-up with a working volume of 50 cm³ and a membrane-surface-area of 56 cm². Therefore both reactors possess similar surface-area to working-volume ratios (SVR) of 1.04 cm⁻¹ and 1.12 cm⁻¹, respectively.

Even though both developmental reactor types do not represent the full capability of the Quorus CELL, especially when directly comparing the SVRs (chapter 10.1.2), they are a valuable tool for preliminary process development and optimization. Results from such experiments can be directly applied to the Quorus CELL. In contrast to the miniCELL reactors, the maxiCELLs do not only differ in reactor-volume and membrane-surface-area, they are also equipped with a port for the inclusion of an invasive pH-electrode into the ECS. Information from this sensor formed the basis for the pH-controlled process.

Both reactor types are based on 4 ceramic membranes which are encased within a reusable glass manifold. Each of these membranes is configured to be used for a specific purpose such as medium supply, aeration and permeate removal.

10.1.2 Quorus CELL

The actual production sized disposable reactor Quorus CELL design is more advanced than the development modules, consisting of 4 transversely stacked ceramic membrane layers with a total of 58 membranes. Each of these layers is equipped with an individual entry- and exit-connection for independent aeration, nutrient delivery or permeate/product recovery. Two ports opening directly into the ECS can be used for inoculation or sampling (Fig. 70 A). The membranes used have different characteristics for bubble-free aeration or to prevent membrane fouling by serum components e.g. for nutrient delivery or product recovery.

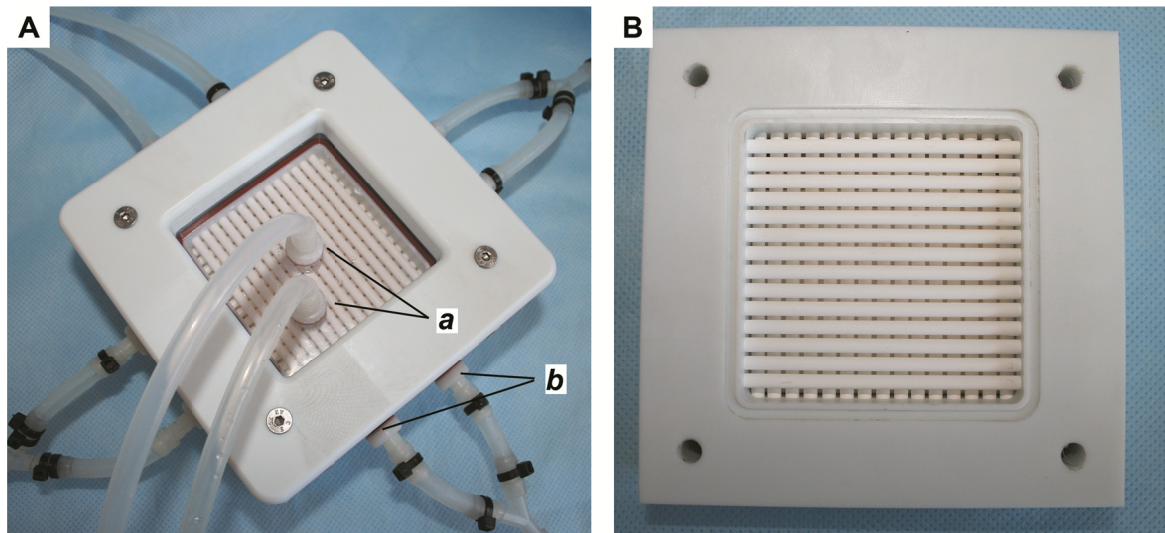


Fig. 70: Fully assembled Quorus CELL reactor (A) with ECS connections for inoculation and sampling (*a*). Entry- and exit connections for nutrient supply or product recovery (*b*). Membrane insert of the Quorus CELL (B).

The reactor units are thereby separated into two basic modules: the membrane module (Fig. 70 B) and its housing. The membranes are molded into the manifold with an epoxy-glue to guarantee stability during mechanical stress, e.g. by movement or pressure. The housing is attached to this module by screws and is sealed with gaskets to ensure sealing, enabling pressure stability up to 1.5 bar. The internal membrane surface sizes 519 cm² and the working-volume reaches 119 cm³ resulting in a SVR of 4.4 cm⁻¹. The ceramic membranes in each layer are distributed evenly, center to center (Fig. 71).

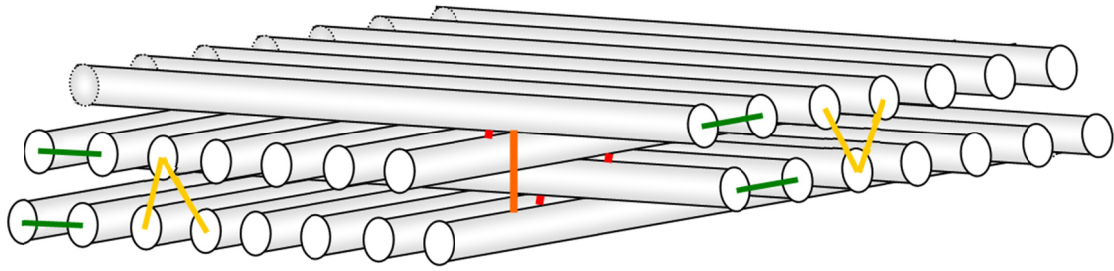


Fig. 71: Geometrical alignment of the Quorus CELL membranes. Membrane layers are separated by gaps which vary depending on their orientation to one another. Vertical distance between successive membrane layers (red). Horizontal center to center distance between adjacent membranes (green). Proportional distance between membrane layers within an insert (orange and yellow)

Comparing the current Quorus CELL design on a SVR basis to existing technology reveals that a single Quorus CELL module has a higher SVR than for example a Nunclon Cell Factory (Thermo Electron LED GmbH, Langenselbold, Germany) (Fig. 72). However, surface-area to working-volume ratios of 5.0 cm^{-1} like the Corning Hyperflask bottles (Corning Incorporated, New York, USA) or the Cellcube 10 (Corning Incorporated, New York, USA) cannot be reached at this stage. By interconnection of multiple Quorus CELL membrane inserts within a single module through stacking, the SVR can be increased significantly, but this option needs to be further evaluated in order to determine possible scale-up limitations.

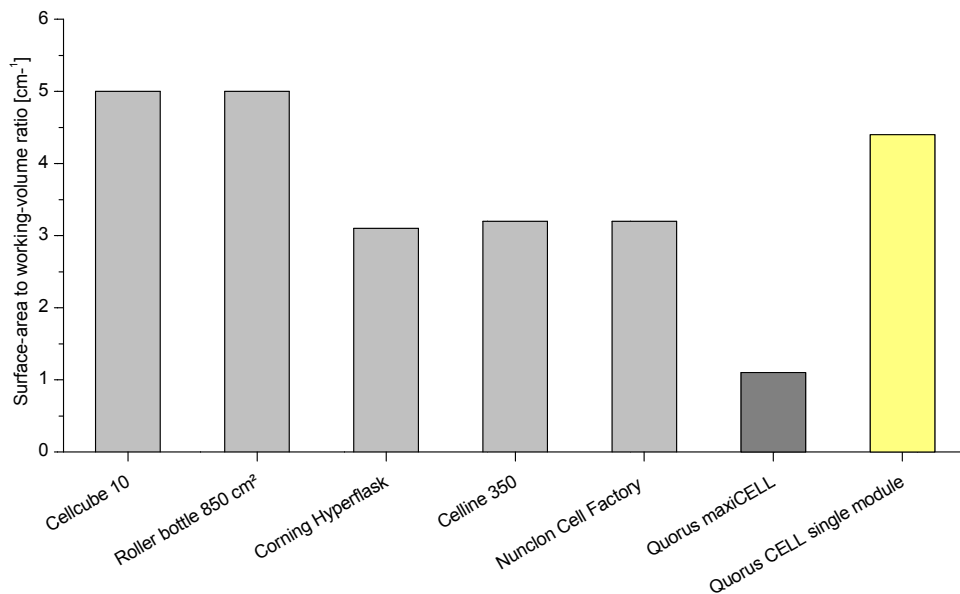


Fig. 72: Comparison of the surface-area to working-volume ratios of existing cultivation devices to the Quorus CELL prototype.

10.2 Example cultivations of CHO-K1 and HEK-293

Preliminary cultivations for process analysis and development using Quorus reactors were undertaken using the adherent mammalian cell lines HEK-293 and CHO-K1.

The HEK-293 cell line (ACC 305) was purchased from DSMZ (Braunschweig, Germany) and the CHO-K1 cell line was provided by Synexa Life Sciences (Pty) Ltd., Cape Town, South Africa. These cell lines were cultivated using DMEM-Ham's F-12 containing 2 mM L-glutamine supplemented with 10 % (v/v) fetal bovine serum (FBS) and 1 % (v/v) Pen/Strep. Cells were initially grown in 75 cm² and 175 cm² T-flasks. All subsequent cultivations were carried out at 37 °C.

Due to the early stage of process development, process analysis in this work is focused solely on biomass production. Concentrations of cells suspended within the ECS were investigated by removing the remaining medium and manual cell counting. Concentrations of cells adherent to the reactor housing and membranes were determined by dismantling the reactor and trypsination of these components. Vitalities were determined by vital staining using trypan blue.

For reactor inoculation cells were suspended in 15-20 mL DMEM-Ham's F-12 supplemented with FBS and Pen/Strep and aseptically injected into the ECS. Approximately $2 \cdot 10^6$ cells (miniCELL), $4 \cdot 10^6$ cells (maxiCELL) and $3 \cdot 10^7$ cells (Quorus CELL) were used for inoculation. Suspended cells in the ECS were immobilized onto the membranes by supplying medium directly into the ECS and removing it through the ICS of all membranes, immobilizing and encouraging cell attachment on all membrane surfaces.

10.3 Effects of variation of membrane setups and aeration strategies

Different membrane setups and aeration strategies were studied to find an optimal process configuration. Initially two membranes for medium feed and two membranes for aeration and permeate recovery were used.

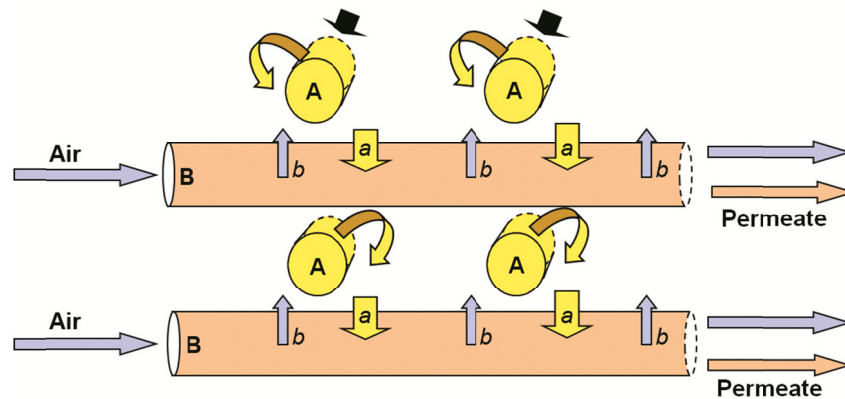


Fig. 73: Initial process setup utilizing two membranes for medium supply **A** and two membranes for aeration and permeate removal **B**. Medium *a* is supplied into the ECS and removed as permeate, while pressured air *b* is used for aeration and permeate transport.

As shown in Fig. 73 pressurized medium flows into the lumen of the dead-end operated membranes **A**. Fresh medium perfuses from within the ICS of the medium membranes, to cells attached to the outer surface of these membranes, and disperses into the ECS. Membranes **B** are operated in crossflow mode. Pressured air is constantly passed through the permeate membranes ICS, resulting in diffusive aeration *b* of the ECS and, conditional upon a lower pressure than the medium supply, a continuous removal of permeate *a*.

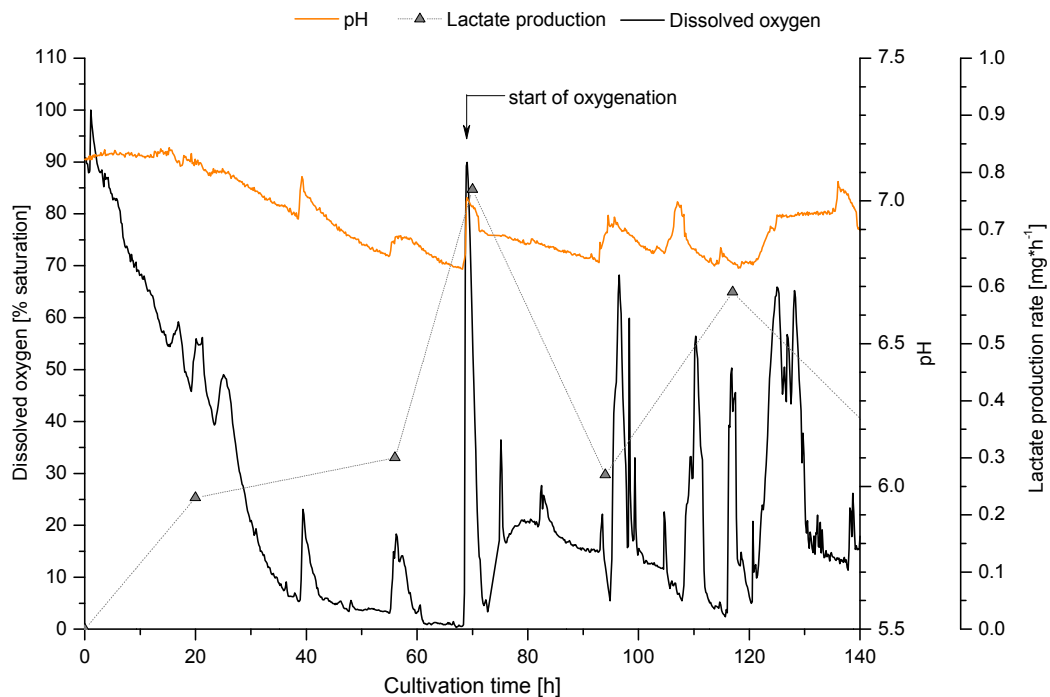


Fig. 74: Results of a CHO-K1 cultivation in a Quorus maxiCELL reactor. After 68 h a depletion of dissolved oxygen was detected and oxygen was introduced into the air stream used for aeration (black arrow).

By way of example, process data of a CHO-K1 cultivation in a maxiCELL reactor using this membrane setup is illustrated in Fig. 74. Process data from the ECS, such as dissolved oxygen (DO) and pH were detected using optical sensors (Presens pH-mini & Fibox, Regensburg, Germany) attached to the glass manifold. An invasive pH probe was used for pH-regulation (data not shown).

pH regulation was achieved through the automated in- or decrease of the media supply rate, displacing lactic acid from the ECS. After about 68 h oxygen limitation and increased lactate production was observed. To counteract these limiting factors, oxygen was introduced into the airstream of the permeate lines. Spiking in the cultivation data results from manual ECS sampling and manually adjusted oxygen flow, which could be due to a pressure drop and subsequently increased freshly aerated medium supply. However, spiking from increased flow may indicate better oxygen transfer across membranes at higher flow rates due to increased turbulence within the ICS.

A parallel time course study in miniCELL bioreactors using similar conditions (no oxygenation) gave a maximum cell yield on day 4, followed by a steady decline in total cell numbers with longer operation (Fig. 75). The DO limitation in the maxiCELL after 72 h coincides with cell loss recorded in the miniCELL reactors.

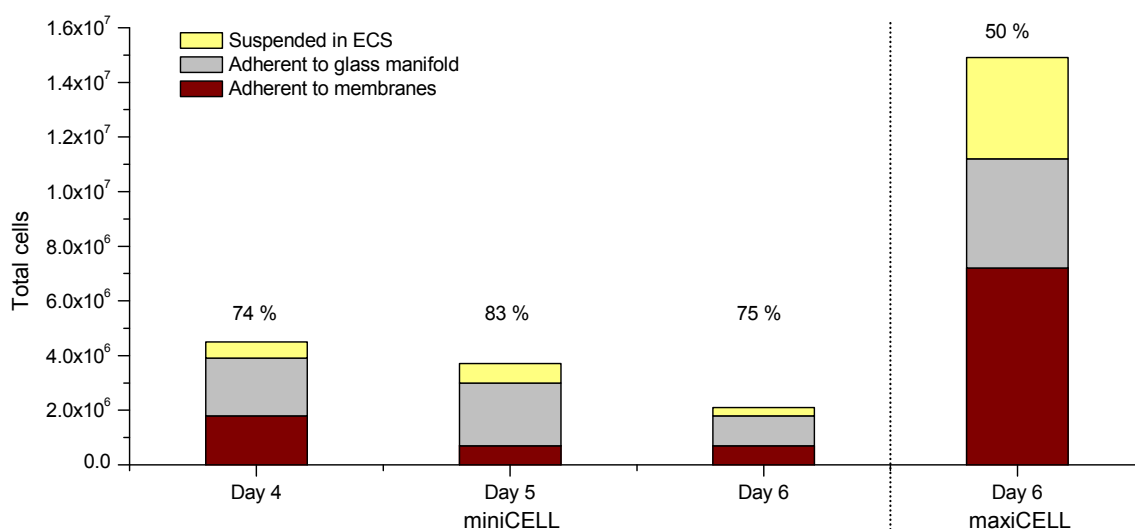


Fig. 75: Cell yield of CHO-K1 cultivation using two membranes for medium supply and two membranes for aeration/oxygenation. Cell distribution is shown for a time course study in miniCELL reactors and maxiCELL cultivation. Values in % specify the overall vitality of all cells in the corresponding reactor.

Determination of cell numbers in the maxiCELL reactor was performed after 6 d of cultivation. Cell numbers in the maxiCELL quadrupled to a final amount of $1.5 \cdot 10^7$ cells with an overall vitality of 50 %. 48 % of those cells grew adherent to the membranes, which correlates to a cell concentration of $1.3 \cdot 10^5$ cells per cm^2 membrane surface. Remaining cells were suspended in the ECS or adherent to the glass manifold.

By identifying fast oxygen depletion as a limiting factor when using only compressed air for aeration (Fig. 74), the membrane configuration was altered accordingly (Fig. 76).

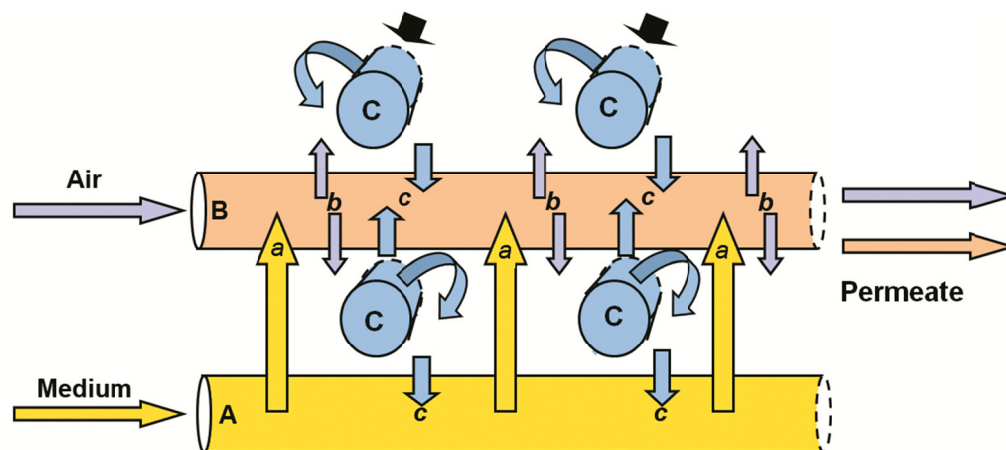


Fig. 76: Altered process setup utilizing two membranes for oxygenation C, one membrane for aeration and permeate removal B and one membrane for medium supply A. Medium *a* is supplied into the ECS and removed as permeate, oxygen *c* is used for additional oxygenation, while pressured air *b* is used for aeration and permeate transport.

Two membranes C were configured dead-end for oxygenation. Standard medium supply A and aeration/permeate recovery B were each reduced to one membrane.

Cultivations of HEK-293 and CHO-K1 in maxiCELL reactors using this setup showed an increase in cell numbers by a factor of five. Overall vitality amounted to 67% for the CHO-K1 and 74% for the HEK-293 cells. Concentrations of cells growing adherent to the membranes were measured as $7.7 \cdot 10^4$ cells/ cm^2 (CHO-K1) and $1.5 \cdot 10^5$ cells/ cm^2 (HEK-293).

This setup was transferred to the production scale disposable Quorus CELL reactor for further investigation. Two membrane layers were used for oxygenation, one for medium supply and one for aeration and permeate removal. A cultivation of CHO-K1 cells using

this setup showed an increase in cell numbers by a factor of 6 after 6 d of operation when compared to the maxiCELL experiments. While overall vitality was only 45 %, close to 90 % of the cells were attached to the membrane layers.

Comparing these results to recently published data of CHO-K1 cultivations in standard T175 flasks and Corning Hyperflasks [64] the Quorus CELL reactor shows a significantly increased cell concentration per cm^2 available surface area (Fig. 77).

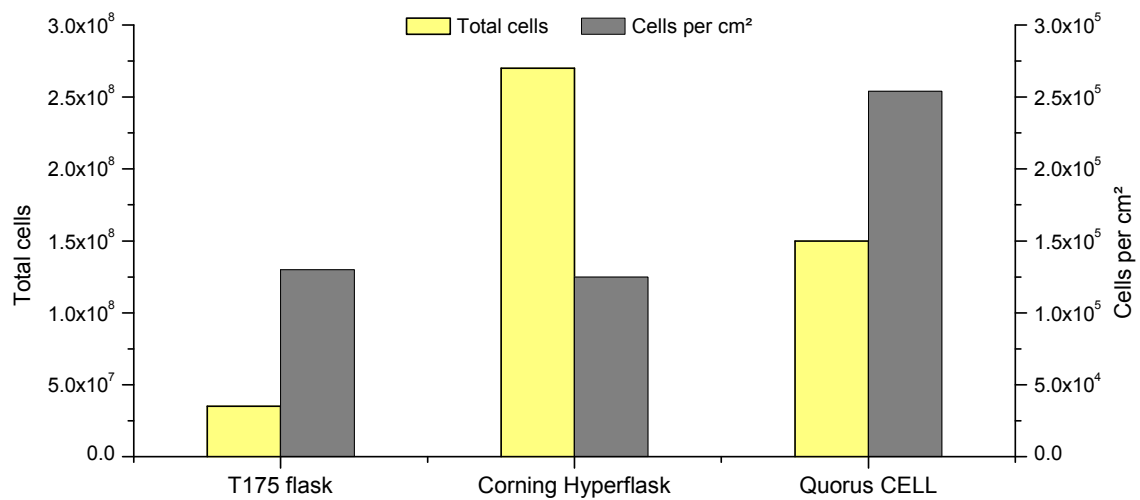


Fig. 77: Total cell numbers and cell concentrations per surface area of a CHO-K1 cultivation in a standard T175 flask, Corning Hyperflask and Quorus CELL reactor.

11 Conclusion part B

Various ceramic capillary membrane based bioreactors, utilizing different process strategies for microbial and mammalian cell cultivation, have been evaluated. All reactors consist of ceramic membranes encased within a disposable housing. The reactor chamber is separated by those membranes into two distinct compartments – the extra and intra capillary space. Even though all reactors have this basic physical setup in common, they differ by number of encased membranes, membrane orientation and procedural function of the extra and intra capillary space.

The ceramic membrane reactors for microbial applications offer two different process modes: aerobic biofilm cultivation (Quorus GLS) and submerged (facultative) anaerobic biofilm cultivation (Quorus LS). The Quorus Optimizer SFRs can be operated with either process. These single fibre reactors are the small scale versions of the production sized Quorus GLS and LS reactors. Within the Quorus Optimizer housing up to three SFRs can be operated in parallel. The importance of this system for screening applications and more importantly for scale-up considerations has been demonstrated with the cultivation of *A.niger* D15 (chapter 8.3.1). Process parameters defined by those experiments, such as base operating pressure or medium supply rate, have been successfully scaled to a production sized Quorus GLS with a near linear scale-up factor.

The Quorus GLS reactor system is suited for the continuous cultivation of aerobic and filamentous growing organisms (chapter 8.1). In contrast to batch operated stirred tank reactors, productive biomass is not accumulated towards a maximum, but instead immobilized and then grown as a biofilm on the surface of the ceramic membranes. The biofilm is thereby grown towards a productive thickness and then maintained in steady-state by a controlled and constant supply of nutrients. The GLS process follows the gradostat concept, relying on the formation of nutrient and oxygen gradients over the cross-section of the biofilm. Products secreted by these microorganisms are transported with the used medium out of the reactor. To evaluate this bioprocess, cultivations of the fungi *A.niger* D15 (*xyn2*) to produce xylanase (chapter 9.1) and the bacteria *S.coelicolor* A3(2) to produce actinorhodin (chapter 9.2) have been monitored. The productivities of these cultivations have been assessed and compared to benchmark cultivations

conducted in shaking flasks and stirred tank reactors such as the Biostat A+ and Biostat C. Product titers in the Quorus GLS cultivations were generally lower than in the benchmark cultivations, but stabilized upon the biofilm entering steady-state. Due to the continuous product output an adapted downstreaming process could however positively benefit from this circumstance. Further research in the downstreaming of the Quorus product stream would give an additional insight into the product dependent processes.

Different productivities have been discussed: while the volumetric productivity is generally considered as a suitable method for the comparison of identical cultivation methods, the use of productivity per reactor capacity or space-time-yield is believed to better bridge comparisons between batch and Quorus bioprocesses (chapter 9.1.3).

When culturing *A.niger* D15 for the production of xylanase, the Quorus GLS bioreactor showed a 2.8 times higher space-time-yield when compared to a Biostat A+ or C (chapter 9.1.2). During the production of actinorhodin from *S.coelicolor* A3(2) the Quorus GLS outperformed the Biostat C by a factor of 1.2 but was 46 % less productive than the Biostat A+ regarding space-time-yield (chapter 9.2.1).

When considering long term or accumulative operation of each reactor system a cycle-time, consisting of downtime, lag-phase and production-phase has been defined (chapter 9.1.3). While the cycle-times for batch operated reactor systems is determined by their individual harvesting times, cycle-times in the Quorus GLS can be varied by extension of their production-phase. Such variation has a significant impact on Quorus GLS productivity when directly compared to STRs. By plotting such data as a time course study, break-even points between the compared reactors can be estimated (chapter 9.1.4). Furthermore, stable production-phases, where the expansion of production-time will have no increasing effect on productivity can be assessed e.g. within an assumed 180 d period during the production of actinorhodin from *S.coelicolor* A3(2), Quorus GLS space-time-yield will break even with a Biostat C when production-phases last at least 9 d (chapter 9.2.3). By directly comparing Quorus GLS productivity with a Biostat C, Quorus productivity will level off with production-phases longer than 60 d.

It is believed that further optimization of the parameters for biofilm cultivation of *A.niger* D15 and especially *S.coelicolor* A3(2) would result in increased product titers and

space-time-yield. Monitoring the formation of nutrient and oxygen gradients within the biofilm would aid process development, particularly regarding optimal and most productive biofilm thickness. Furthermore, a reduction of used medium can potentially increase product titre and enhance overall productivity. Up-scaling of the performed experiments onto 10 L or 25 L GLS units would additionally give valuable insight into possible scale-up limitations and better define the linearity of up-scaling.

The Quorus LS bioreactor is operated in the anaerobic mode and is best suited for the submerged cultivation of (facultative) anaerobic or microaerophilic bacteria or single celled fungi. Even though the bioprocess relies on the formation of a biofilm on membrane surfaces, the biofilm is however not retained in steady-state (chapter 8.2). Here the biofilm growth and thickness will increase in time as nutrients are supplied continuously, until either this supply is no longer sufficient (pressure required to drive flow through the biofilm reaches its maximum safety cut-off) or available space in the reactor chamber is exhausted. The Quorus LS process can therefore not be operated over similarly long time frames as the Quorus GLS process. In contrast to the GLS process, nutrients are not supplied from the intra capillary space, through the capillary wall and through the biofilm, but from the opposite direction resulting in a cell-free product stream emerging the reactor from within the capillary lumen.

Productivity of the Quorus LS process was evaluated with the production of β -lactamase from *L.lactis* PRA290 and comparison the productivities of batch operated Biostat A+ and C reactors (chapter 9.3.1). The analysis of the results showed that the Quorus LS space-time yield was 28 times higher than in the Biostat A+ and 34 times higher than in Biostat C. However, average product concentration from the Quorus LS was approximately 24 % lower than in both STRs. Through further optimization of the Quorus LS feeding strategy, the initial lag in production can be reduced and the product titer can be increased.

Application of the previously established model to determine breakeven points by variation of Quorus production-phases revealed that the Quorus LS outperformed the Biostat A+ in total amount of produced product and in space-time-yield (chapter 9.3.3). With production-phases of less than 6 h the Quorus LS productivity breaks even with the Biostat A+ within an estimated time-frame of as many production cycles as possible in

30 d. Within the same time-frame the Quorus LS total product output would break even with a Biostat C when expanding the production-phases beyond 50 h. The Quorus LS showed a remarkably high efficiency and outperformed to Biostat A+ in almost all comparisons. Once again, further experiments using larger reactor modules would grant a valuable insight into the scale-up considerations of the Quorus LS system. Besides process optimizations e.g. a more precise pH-control by implementation of pH-sensors into the reactor chamber, additional experiments to determine optimal feeding strategies would also increase process productivity. Benchmark cultivations in STRs equipped with perfusion units would provide valuable information and a more relevant process comparison.

Operating costs have been investigated at a basic level in relation to overall percentage composition (chapter 9.4). In this context, medium cost is considered to be negligible, however the amount of used medium impacts on downstreaming costs - and becomes the dominating factor in all Quorus processes. In contrast to the STRs, where reduction of reactor capacity will go along with an increase of expensive downtime, Quorus downtime has much less impact in this consideration – even for comparably short Quorus LS production cycles. As already mentioned above, optimization towards less medium usage and/or increased product titer would not only increase overall productivity, but moreover decrease downstreaming costs associated with Quorus processes. All Quorus reactor units are disposable and therefore offer a major advantage over the stainless steel Biostat fermenters because cost intensive cleaning, sterilization and validation do not apply. Additionally, the disposable Quorus GLS units are operated continuously and therefore minimize the risk of contamination of multiple batches, which would disrupt the subsequent downstreaming chain resulting in expensive downtime.

The Quorus CELL reactors consist of multiple horizontally oriented membrane layers encased within a disposable housing (chapter 10.1). Adherent mammalian cell lines can be cultivated within this reactor system on the surface of the membrane layers. The membrane layers are used for different purposes, such as aeration, medium supply or product recovery. Various cultivations of CHO-K1 and HEK-293 cells in the Quorus CELL reactors have been performed using different membrane setups (chapter 10.2). Through

the use of optical sensor technology fast oxygen depletion could be identified as a limiting factor under the chosen cultivation conditions. By altering the membrane configuration and supplying oxygen in addition to the initial aeration, cell viability could be increased while total cell concentration was maintained (chapter 10.3). For further enhancement and longer sustainment of the cell viability, the oxygen supply needs to be regulated to avoid oxidative stress.

Current pH-control is achieved through in- or decreasing the medium flux. pH is measured within the ECS and correlating information is fed back into the medium supply algorithms to maintain the pH set-point. For sustaining cell viability and reducing medium usage this control has to be optimized or alternate strategies e.g. mixing chambers, have to be evaluated. For further process optimization a basic reactor characterization including residence time distributions and oxygen transfer capabilities have to be performed.

Overall the Quorus ceramic membrane reactors performed well and represent an innovative approach for the cultivation of microbial organisms or attachment depended mammalian cell-lines. The anaerobic Quorus LS process in particular, showed considerably higher productivities than conventional batch processes. The focusing on organisms producing valuable secreted products is adequate and fits the chosen reactor configurations. Upon further process improvement, achieved productivities could realistically be increased and therefore position the Quorus systems as an interesting alternative to conventional cultivation techniques would be even more favourable with respect to the cultivation of shear stress sensitive organisms.

12 Outlook

A high degree of parallelization is essential for time and cost saving bioprocess development. However, the need for reliable and comprehensive process information, especially in the later stages of process development, often outweighs a high experimental throughput. In this context and especially because stirred tank reactors are mostly the preferred choice for industrial processes, a parallelized and miniature scaled counterpart is of considerable importance to bridge between parallel operation and significant process information. Even though a few systems of this kind have been presented in literature or are already available on the market, the reactor system described in the first part of this thesis is an interesting addition to this field of application. Based on the implemented optical sensor technology and conditional upon the suggested optimizations, e.g. replacement of the reusable reactor units by single-use vessels, this reactor system would undoubtedly be an interesting substitute for small scale experiments. However, a profound investigation of cost factors, such as cost of ownership or cost of labour associated with the operation of such system would be, if compared to the overall costs of established miniature screening techniques, of trend-setting information.

Even though the biotechnological landscape is dominated by stirred tank reactor systems, numerous niche applications exist, where specialized reactor designs are necessary. Shear stress sensitive organisms, e.g. filamentous bacteria or adherent growing mammalian cell-lines are less productive under the stress elevated conditions in stirred tank reactors. The ceramic membrane reactor prototypes, which have been characterized in the second part of this thesis, offer an interesting approach for productive biofilm cultivation. Due to the continuous removal of metabolic waste and secreted products, these systems could e.g. be used for the production of toxic products or, based on the aerobic process, for the production of valuable volatiles. The anaerobic process showed a remarkable high productivity and should be evaluated further – especially in fields of application, where currently perfusion based systems are established. Based on their pressure driven operation, these systems offer advantages

over more susceptible pump operated systems and qualify therefore as an interesting alternative to conventional cultivation techniques of shear-stress sensitive organisms.

Even though the ceramic membrane reactor for the cultivation of adherent mammalian cell-lines is currently in an early stage of development, the advantages of this system have been outlined. Especially because of its high surface area to volume ratio and the perfusion like operation, this system shows interesting potential for the highly productive cultivation of adherent cell-lines. A more profound understanding of the flow characteristics would allow a more precise pH control and therefore a reduced usage of expensive cell culture medium. A detailed investigation of the oxygen distribution within this system would grant additional information to optimize the aeration strategies, resulting in higher cell viabilities and possibly in higher productivities.

In summary, various innovative bioreactor systems in different scales have been presented, extensively characterized and numerous suggestions for further improvement and new fields of application have been outlined.

13 List of abbreviations

2D	two dimensional
dpp	4,4'-diphenylphenanthroline
HPTS	8-hydroxy-1,3,6-pyrene-trisulphonic-acid-trisodium salt
pKa	acid dissociation constant
Bo	Bodenstein number
CHO	Chinese hamster ovary
CSTR	continuously stirred tank reactor
cot	cotangens
d	day
DO	dissolved oxygen
d-H ₂ O	deionized water
DSP	downstream processing
DLR	dual lifetime referencing
Eq.	equation
<i>E.coli</i>	<i>Escherichia coli</i>
ECS	extra capillary space
Fig.	figure
FDA	food and drug administration
FD	frequency domain
GLS	gas liquid solid
GFP	green fluorescence protein
Hz	Hertz
HTS	high throughput screening
h	hour
HEK	human embryonic kidney
I/O	input output
ISP2	International Streptomyces Project 2
ICS	intra capillary space
LED	light emitting diode
LS	liquid solid
L	litre
MFC	mass flow controller
max	maximum
t'	mean residence time
MSV	medium supply vessel
m	meter
MTP(s)	microtiter plate(s)
MM	minimal medium
min	minute
M	mole
NADH	nicotinamide adenine dinucleotide
OD	optical density
OD ⁶⁰⁰	optical density at 600 nm
pO ₂	partial pressure of oxygen

PFR	plug flow reactor
PV	prime vessel
PAT	process analytical technology
P	product
PCV	product collection vessel
PI	proportional integral
PID	proportional integral derivative
R&D	research and development
RTD	residence time distribution
rpm	rotations per minute
SSB	Sartorius Stedim Biotech
s	second
R	signal intensity ratio
SFR	single fibre reactor
STY	space time yield
STR(s)	stirred tank reactor(s)
SVR	surface area to volume ratio
Tab.	table
tan	tangens
t	time
TD	time domain
V_{reactor}	total reactor capacity
TMP	trans membrane pressure
TTL	transistor-transistor-logic
USA	United States of America
U	units
USB	universal serial bus
V_{Medium}	volume of medium
v/v	volume per volume
vvm	volume per working volume per minute

14 Bibliography

1. Gapes, J., Nimcevic, D., and Friedl, A. (1996) Long-Term Continuous Cultivation of *Clostridium beijerinckii* in a Two-Stage Chemostat with On-Line Solvent Removal. *Appl. Environ. Microbiol.* 62, 3210-3219
2. Villain, L., Meyer, L., Kroll, S., Beutel, S., and Scheper, T. (2008) Development of a Novel Membrane Aerated Hollow-Fiber Microbioreactor. *Biotechnology Progress* 24, 367-371
3. Brecht, R. (2010) Disposable Bioreactors: Maturation into Pharmaceutical Glycoprotein Manufacturing. In *Advances in Biochemical Engineering/Biotechnology* 1-31, Springer
4. Langhammer, S., Riedel, M., Bushnaq-Josting, H., Brecht, R., Poertner, R., and Marx, U. (2007) Evaluation of a Scalable Disposable Bioreactor System for Manufacturing of Mammalian Cell Based Biopharmaceuticals. In *Cell Technology for Cell Products*, 623-628, Springer Netherlands
5. Ntwampe, S.K.O., Sheldon, M.S., and Volschenk, H. (2007) The Membrane Gradostat Reactor: Secondary metabolite production, bioremediation and commercial potential. *African Journal of Biotechnology* 6, 1164-1170
6. Yang, W., Cicek, N., and Ilg, J. (2006) State-of-the-art of membrane bioreactors: Worldwide research and commercial applications in North America. *Journal of Membrane Science* 270, 201-211
7. Inloes, D.S., Michaels, A.S., Robertson, C.R., and Matin, A. (1985) Ethanol production by nitrogen-deficient yeast cells immobilized in a hollow-fiber membrane bioreactor. *Applied Microbiology and Biotechnology* 23, 85-91
8. Reimann, A., Biebl, H., and Deckwer, W.D. (1998) Production of 1,3-propanediol by *Clostridium butyricum* in continuous culture with cell recycling. *Applied Microbiology and Biotechnology* 49, 359-363
9. Inloes, D.S., Smith, W.J., Taylor, D.P., Cohen, S.N., Michaels, A.S., and Robertson, C.R. (1983) Hollow-fiber membrane bioreactors using immobilized *E. coli* for protein synthesis. *Biotechnology and Bioengineering* 25, 2653-2681
10. Fey-Lamprecht, F., Albrecht, W., Groth, T., Weigel, T., and Gross, U. (2003) Morphological studies on the culture of kidney epithelial cells in a fiber-in-fiber bioreactor design with hollow fiber membranes. *Journal of Biomedical Materials Research Part A* 65A, 144-157
11. Cadwell, J.J.S. (2004) New Developments in Hollow-Fiber Cell Culture. *American Biotechnology Laboratory* 22, 14-17
12. Betts, J.I., and Baganz, F. (2006) Miniature bioreactors: current practices and future opportunities. *Microbial Cell Factories* 5, -
13. Kumar, S., Wittmann, C., and Heinzle, E. (2004) Minibioreactors. *Biotechnology Letters* 26, 1-10
14. Hanson, M.A., Ge, X., Kostov, Y., Brorson, K.A., Moreira, A.R., and Rao, G. (2007) Comparisons of optical pH and dissolved oxygen sensors with traditional electrochemical probes during mammalian cell culture. *Biotechnology and Bioengineering* 97, 833-841
15. De Jesus, M.J., Girard, P., Bourgeois, M., Baumgartner, G., Jacko, B., Amstutz, H., and Wurm, F.M. (2004) TubeSpin satellites: a fast track approach for process

- development with animal cells using shaking technology. *Biochemical Engineering Journal* 17, 217-223
16. Stettler, M., De Jesus, M., Ouertatani-Sakouhi, H., Engelhardt, E.M., Muller, N., Chenuet, S., Bertschinger, M., Baldi, L., Hacker, D., Jordan, M., and Wurm, F.M. (2007) 1000 non-instrumented bioreactors in a week. *Cell Technology for Cell Products*, 489-495
 17. Weuster-Botz, D. (2006) Mikro-Bioverfahrenstechnik. *Chemie Ingenieur Technik* 78, 256-260
 18. Samorski, M., Muller-Newen, G., and Buchs, J. (2005) Quasi-continuous combined scattered light and fluorescence measurements: A novel measurement technique for shaken microtiter plates. *Biotechnology and Bioengineering* 92, 61-68
 19. Kensy, F., John, G.T., Hofmann, B., and Buchs, J. (2005) Characterisation of operation conditions and online monitoring of physiological culture parameters in shaken 24-well microtiter plates. *Bioprocess Biosyst Eng* 28, 75-81
 20. Kensy, F., and Buechs, J. (2006) Online-Monitoring von Mikrofermentationen. *Laborwelt* 7, 6-9
 21. Buchs, J. (2001) Introduction to advantages and problems of shaken cultures. *Biochemical Engineering Journal* 7, 91-98
 22. Zang, A. (2009) RAMOS Respiration Activity Monitoring System. *Hi-Tec Zang GmbH*
 23. Weuster-Botz, D., Puskeiler, R., Kusterer, A., Kaufmann, K., John, G.T., and Arnold, M. (2005) Methods and milliliter scale devices for high-throughput bioprocess design. *Bioprocess and Biosystems Engineering* 28, 109-119
 24. Harms, P., Kostov, Y., French, J.A., Soliman, M., Anjanappa, M., Ram, A., and Rao, G. (2006) Design and performance of a 24-station high throughput microbioreactor. *Biotechnology and Bioengineering* 93, 6-13
 25. Ge, X., Hanson, M., Shen, H., Kostov, Y., Brorson, K.A., Frey, D.D., Moreira, A.R., and Rao, G. (2006) Validation of an optical sensor-based high-throughput bioreactor system for mammalian cell culture. *J Biotechnol* 122, 293-306
 26. Qualitz, J.E., Rao, G., D'Angelo, M.R., and Lakowicz, J.R. (2009) Cellstation, High-Throughput Bioreactors. *Fluorometrix* 2009
 27. FDA, and Administration, U.S.F.a.D. (2004) Guidance for Industry - PAT - A Framework for Innovative Pharmaceutical Development, Manufacturing, and Quality Assurance. <http://www.fda.gov/Drugs/GuidanceComplianceRegulatoryInformation/Guidances/default.htm>
 28. Eibl, R., and Eibl, D. (2009) Disposable Bioreactors in Cell Culture-Based Upstream Processing. *BioProcess International* 7, 18-23
 29. Endres, C., Haake, C., Landgrebe, D., Beutel, S., Stahl, S., Hitzmann, B., Scheper, T., and Friehs, K. (2009) Moderne Bioprozessanalytik - eine kurze Übersicht. *Biospektrum* 06, 662-665
 30. Proulx, S.P., and Furey, J.F. (2007) Disposable, pre-sterilized fluid receptacle sampling device. Millipore Corporation
 31. Bernard, F., Chevalier, E., Cappia, J.-M., Heule, M., and Paust, T. (2009) Disposable pH Sensors. *BioProcess International* 9, 32-36
 32. Joo, S., and Brown, R.B. (2008) Chemical Sensors with Integrated Electronics. *Chemical Reviews* 108, 638-651

33. Schick, K., and Uhen, D. (2006) Disposable conductivity sensor comprising memory means and temperature sens for calibration. (WIPO, ed)
34. Roychoudhury, P., Harvey, L.M., and McNeil, B. (2006) At-line monitoring of ammonium, glucose, methyl oleate and biomass in a complex antibiotic fermentation process using attenuated total reflectance-mid-infrared (ATR-MIR) spectroscopy. *Analytica Chimica Acta* 561, 218-224
35. Schuegerl, K. (2001) Progress in monitoring, modeling and control of bioprocesses during the last 20 years. *Journal of Biotechnology* 85, 149-173
36. Hantelmann, K., Kollecker, M., Huell, D., Hitzmann, B., and Scheper, T. (2006) Two-dimensional fluorescence spectroscopy: A novel approach for controlling fed-batch cultivations. *Journal of Biotechnology* 121, 410-417
37. Rao, G., Kostov, Y., Moreira, A., Frey, D., Hanson, M., Jornitz, M., Reif, O.W., Baumfalk, R., Qualitz, J. (2009) Non-Invasive Sensors as Enablers of "Smart" Disposables. *Bioprocess International* 7, 24-27
38. Scheper, T., Hitzmann, B., Staerk, E., Ulber, R., Faurie, R., Sosnitza, P., and Reardon, K.F. (1999) Bioanalytics: detailed insight into bioprocesses. *Analytica Chimica Acta* 400, 121-134
39. Glindkamp, A., Riechers, D., Rehbock, C., Hitzmann, B., Scheper, T., and Reardon, K. (2010) Sensors in Disposable Bioreactors Status and Trends. 145-169
40. Kermis, H.R., Kostov, Y., Harms, P., and Rao, G. (2002) Dual Excitation Ratiometric Fluorescent pH Sensor for Noninvasive Bioprocess Monitoring: Development and Application. *Biotechnology Progress* 18, 1047-1053
41. Kostov, Y., and Rao, G. (2003) Ratio measurements in oxygen determinations: wavelength ratiometry, lifetime discrimination, and polarization detection. *Sensors and Actuators B: Chemical* 90, 139-142
42. Klimant, I., Huber, C., Liebsch, G., Neurauter, G., Stangelmayer, O., and Wolfbeis, S. (2001) Dual Lifetime Referencing (DLR) - A New Scheme for Converting Fluorescence Intensity into a Frequency-Domain or Time-Domain Information. In *New Trends in Fluorescence Spectroscopy* (Valeur, B., and Brochon, J.C., eds), 257-274, Springer Verlag
43. Andrzejewski, D., Klimant, I., and Podbielska, H. (2002) Method for lifetime-based chemical sensing using the demodulation of the luminescence signal. *Sensors and Actuators B: Chemical* 84, 160-166
44. Neurauter, G., Klimant, I., and Wolfbeis, O.S. (1999) Microsecond lifetime-based optical carbon dioxide sensor using luminescence resonance energy transfer. *Analytica Chimica Acta* 382, 67-75
45. Kumar, S., Wittmann, C., and Heinzle, E. (2004) Review: Minibioreactors. *Biotechnology Letters* 26, 1-10
46. Agayn, V.I., and Walt, D.R. (1993) Fiber-optic Sensor for Continuous Monitoring of Fermentation pH. *Nat Biotech* 11, 726-729
47. Dela Cruz, J.M., Pastirk, I., Comstock, M., Lozovoy, V.V., and Dantus, M. (2004) Use of coherent control methods through scattering biological tissue to achieve functional imaging. *Proceedings of the National Academy of Sciences of the United States of America* 101, 16996-17001
48. Morin, A.M., Xu, W., Demas, J.N., and DeGraff, B.A. (2000) Oxygen Sensors Based on a Quenching of Tris-(4,7-diphenyl-1,10-phenanthroline)ruthenium(II) in Fluorinated Polymers. *Journal of Fluorescence* 10, 7-12

49. Phillips, G.J. (2001) Green fluorescent protein; a bright idea for the study of bacterial protein localization. *FEMS Microbiology Letters* 204, 9-18
50. S. Rose, W.v.Z. (2002) Constitutive expression of the *Trichoderma reesei* β -1,4-xylanase gene (*xyn2*) and the β -1,4-endoglucanase gene (*egl*) in *Aspergillus niger* in mola. *Applied Microbiology and Biotechnology* 58, 461-468
51. Punt, P., and van den Hondel, C. (1992) Transformation of filamentous fungi based on hygromycin B and phleomycin resistance markers. *Methods Enzymol.* 216, 447-457
52. Wang, L., Ridgway, D., Gu, T., and Moo-Young, M. (2005) Bioprocessing strategies to improve heterologous protein production in filamentous fungal fermentations. *Biotechnology Advances* 23, 115-129
53. El-Enshasy, H., Kleine, J., and Rinas, U. (2006) Agitation effects on morphology and protein productive fractions of filamentous and pelleted growth forms of recombinant *Aspergillus niger*. *Process Biochemistry* 41, 2103-2112
54. Siedenberg, D., Gerlach, S.R., Weigel, B., Schugerl, K., Giuseppin, M.L.F., and Hunik, J. (1997) Production of xylanase by *Aspergillus awamori* on synthetic medium in stirred tank and airlift tower loop reactors: the influence of stirrer speed and phosphate concentration. *Journal of Biotechnology* 56, 103-114
55. Yuan, Q.P., Wang, J.D., Zhang, H.A., and Qian, Z.M. (2005) Effect of temperature shift on production of xylanase by *Aspergillus niger*. *Process Biochemistry* 40, 3255-3257
56. Elibol, M., and Mavituna, F. (1998) Effect of sucrose on actinorhodin production by *Streptomyces coelicolor* A3(2). *Process Biochemistry* 33, 307-311
57. Ozergin-Ulgen, K., and Mavituna, F. (1998) Oxygen transfer and uptake in *Streptomyces coelicolor* A3(2) culture in a batch bioreactor. *Journal of Chemical Technology and Biotechnology* 73, 243-250
58. Zhang, H.C., Zhan, J.X., Su, K.M., and Zhang, Y.X. (2005) A kind of potential food additive produced by *Streptomyces coelicolor*: Characteristics of blue pigment and identification of a novel compound, lambda-actinorhodin. *Food Chemistry* 95, 186-192
59. Doull, J.L., and Vining, L.C. (1990) Nutritional control of actinorhodin production by *Streptomyces coelicolor* A3(2): suppressive effects of nitrogen and phosphate. *Applied Microbiology and Biotechnology* 32, 449-454
60. Bioneer (2004) Heterologous Protein Production using *Lactococcus lactis* - P170 Expression System. *P170 Expression System Handbook* 1
61. Zannini, E., Santarelli, S., Osimani, A., Dell'Aquila, L., and Clementi, F. (2005) Effect of process parameters on the production of lactic acid bacteria in batch fermentation. *Annals of Microbiology* 55, 273-278
62. Farid, S. (2008) Process Economic Drivers in Industrial Monoclonal Antibody Manufacture. In *Process Scale Purification of Antibodies* (Gottschalk, U., ed), 239-261, John Wiley & Sons, Inc.
63. Blanch, H.W., and Clark, D.S. (1997) *Biochemical Engineering*. Marcel Dekker
64. Upton, T., Pardo, A.M.P., Sherman, H.A., Martin, G., and Tanner, A. (2006) A Novel Flask Design for High Density Cell Culture. *Corning publication*, 1

15 Appendix

15.1 Chemicals

Unless stated otherwise, all chemicals were obtained from Sigma-Aldrich Chemie GmbH (Munich, Germany).

Agar	
Ammonium heptamolybdate	
Azo Xylan (Birchwood)	Megazyme International Ireland Ltd. (Wicklow, Ireland)
Bacteriological peptone enzymatic hydrolysate	
Biotin	
Boric acid	
Calciumchloride dihydrate	
Calcium-Pantothenate	
Casamino acids	Difco (Otto Nordwald, Hamburg, Germany)
Chloramphenicol	
Citric acid	
Cobalt nitrate	
Copper(II)sulfate pentahydrate	
Dipotassium hydrogen phosphate	
DMEM:F12 with L-glutamine	Lonza Cologne AG (Cologne, Germany)
Erythromycin	
Ethylenediaminetetraacetic acid	
Ferrous(II)sulfate heptahydrate	
Folic Acid	
Glucose monohydrate	
Glycerine	
Hydrochloric acid (1 M)	
Kobalt(II)chloride hexahydrate	
L-arabinose	
L-arginine	
L-glutamine	
L-proline	
L-serine	
L-riboflavine	
M17 broth	Oxoid Deutschland GmbH (Wesel, Germany)
Magnesium chloride	
Malt extract	
Manganese(II)chloride tetrahydrate	
Methylenblue	
Niacinamide	
Nitrocefin	Oxoid Deutschland GmbH (Wesel, Germany)
Potassium sulfate	
Pyrodixal hydrochloride	
Riboflavin	
Sodium acetate	
Sodium chloride	
Sodium hydroxide	
Sodium hydroxide	
Sodium molybdate dihydrate	
Sodium nitrate	
Sodium sulfite	
Sulfuric acid (38%)	
Thiamine hydrochloride	
Yeast extract	
Zinc(II)sulfate	

15.2 Devices

Device	Model	Vendor/Manufacturer
Bioreactor	Biostat C	B.Braun GmbH, Melsungen, Germany
Bioreactor	Biostat A+	Sartorius Stedim Biotech GmbH, Goettingen, Germany
Bioreactor	Cultibag RM	Sartorius Stedim Biotech GmbH, Goettingen, Germany
Centrifuge	Biofuge pico	Thermo Fisher Scientific, Waltham, USA
Centrifuge	Multifuge 3s	Thermo Fisher Scientific, Waltham, USA
Cooling unit	Frigomix 1000	Sartorius Stedim Biotech GmbH, Goettingen, Germany
Exhaust analytics	AO2020	ABB Ltd, Zurich, Switzerland
Exhaust analytics	S710	Sick Maihak GmbH, Reute, Germany
Fluorescence spectrophotometer	F-4500	Hitachi High-Technologies Corporation, Tokyo, Japan
Gas blending system	Hitec E-7110	Bronkhorst Maettig GmbH, Kamen, Germany
Glucose analysis	YSI2700 Select	YSI Incorporated, Ohio, USA
Mass flow controller	F-201C	Bronkhorst Maettig GmbH, Kamen, Germany
Microscope	BX41	Olympus Deutschland GmbH, Hamburg, Germany
Multi I/O boxes	USB1208	PLUG-IN Electronic GmbH, Eichenau, Germany
	USB1024	
	USB-Temp	
	USB1608	
Optical oxygen sensor	Oxy-4 Fibox	Presens GmbH, Regensburg, Germany
Optical pH sensor	pH-mini	Presens GmbH, Regensburg, Germany
Peristaltic pump	ISM930C	Ismatec, Wertheim-Mondfeld, Germany
pH sensor	pH605	METROHM GmbH & Co. KG, Filderstadt, Germany
Power supply (5V)	PSE60-105	Powersolve Electronics Ltd, Newbury, UK
Power supply (universal)	Voltcraft TNG245	Conrad Electronic SE, Hirschau, Germany
Spectrophotometer	Cary50 Scan	Varian Inc., Palo Alto, USA
Spectrophotometer	Multiscan Spectrum	Thermo Fisher Scientific, Waltham, USA
Temperature sensor	Modig 008V2	Megatron, Putzbrunn, Germany

15.3 Growth media

15.3.1 Lysogeny broth – LB medium:

Yeast extract $5 \text{ g}\cdot\text{L}^{-1}$, tryptone $5 \text{ g}\cdot\text{L}^{-1}$, NaCl $1 \text{ g}\cdot\text{L}^{-1}$

15.3.2 2x Minimal medium

Yeast extract $20 \text{ g}\cdot\text{L}^{-1}$, glucose monohydrate $22 \text{ g}\cdot\text{L}^{-1}$, NaNO_3 $120 \text{ g}\cdot\text{L}^{-1}$, bacterial peptone $1 \text{ g}\cdot\text{L}^{-1}$, trace element 100x stock $1 \text{ mL}\cdot\text{L}^{-1}$

Trace element 100x stock

$\text{ZnSO}_4\cdot 2 \text{ H}_2\text{O}$ $20.13 \text{ g}\cdot\text{L}^{-1}$, $\text{MnCl}_2\cdot 2 \text{ H}_2\text{O}$ $4.95 \text{ g}\cdot\text{L}^{-1}$, $\text{FeSO}_4\cdot 7 \text{ H}_2\text{O}$ $5.04 \text{ g}\cdot\text{L}^{-1}$, $\text{CoCl}_2\cdot 6 \text{ H}_2\text{O}$ $1.69 \text{ g}\cdot\text{L}^{-1}$, $\text{CuSO}_4\cdot 5 \text{ H}_2\text{O}$ $1.6 \text{ g}\cdot\text{L}^{-1}$, $\text{NaMoO}_4\cdot 2 \text{ H}_2\text{O}$ $1.5 \text{ g}\cdot\text{L}^{-1}$, Na-EDTA $129.54 \text{ g}\cdot\text{L}^{-1}$

15.3.3 ISP2 broth

Yeast extract 5 g·L⁻¹, malt extract 10 g·L⁻¹, glucose monohydrate 4.4 g·L⁻¹

15.3.4 LM5-V100-G75

Buffer capacity	200 mmol amount per L	400 mmol amount per L
dd-H ₂ O	740 mL	540 mL
MeCit 1000x stock	5 mL	5 mL
Micro 1000x stock	5 mL	5 mL
KPP buffer 1 M	200 mL	400 mL
Vita 100x stock	50 mL	50 mL
K ₂ SO ₄	0.24 g	0.24 g
Na-acetate * 3H ₂ O	2 g	2 g
L-cysteine	0.25 g	0.25 g
L-tyrosine	0.125 g	0.125 g
L-arginine	1 g	1 g
L-glutamine	0.5 g	0.5 g
L-serine	1.5 g	1.5 g
Yeast extract	15 g	15 g
Glucose monohydrate	82.5 g	82.5 g
Erythromycin	1 mL	1 mL

15.3.4.1 Stock solutions

MeCit 1000x

FeSO₄*7 H₂O 2.78 g·L⁻¹, CaCl₂*2 H₂O 73.5 mg·L⁻¹, MgCl₂*6 H₂O 108 g·L⁻¹, Citric acid*H₂O 21 g·L⁻¹

Micro 1000x

(NH₄)₆Mo₇O₂₄*4 H₂O 3.7 mg·L⁻¹, H₃BO₃ 24.8 mg·L⁻¹, CoCl₂*6 H₂O 7.1 mg·L⁻¹, CuSO₄*5 H₂O 2.5 mg·L⁻¹, MnCl₂*4 H₂O 15.8 mg·L⁻¹, ZnSO₄*7 H₂O 2.9 mg·L⁻¹

Vita 100x

Biotin 10 mg·L⁻¹, folic acid 100 mg·L⁻¹, riboflavin 100 mg·L⁻¹, niacinamide 100 mg·L⁻¹, thiamin*HCl 100 mg·L⁻¹, Ca-Pantothenate 100 mg·L⁻¹, pyridoxal*HCl 200 mg·L⁻¹

15.3.5 Buffer solutions

15.3.5.1 Britton-Robinson buffer (0.12 M)

pH 2-9: H₃BO₃ 2.47 g·L⁻¹, 85% H₃PO₄ 3.92 g·L⁻¹, 2.4 CH₃COOH g·L⁻¹, adjusted to desired pH with 0.2 M NaOH

15.3.5.2 KPP buffer (0.1 M)pH 6.0: K_2HPO_4 2.35 g·L⁻¹, KH_2PO_4 11.81 g·L⁻¹pH 7.0: K_2HPO_4 10.96 g·L⁻¹, KH_2PO_4 5.24 g·L⁻¹**15.3.5.3 NaPP buffer (0.1 M)**pH 6.0: Na_2HPO_4 1.75 g·L⁻¹, $\text{NaH}_2\text{PO}_4 \cdot \text{H}_2\text{O}$ 12.1 g·L⁻¹pH 7.0: Na_2HPO_4 8.66 g·L⁻¹, $\text{NaH}_2\text{PO}_4 \cdot \text{H}_2\text{O}$ 5.38 g·L⁻¹**15.3.5.4 MOPS buffer (0.1M)**pH 6.5-8: 3-(N-morpholino) propanesulfonic acid 8.37 g·L⁻¹, sodium acetate 0.8 g·L⁻¹,
Na-EDTA*2H₂O 0.37 g·L⁻¹, adjusted with 0.2 M NaOH**15.4 Cultivation parameter****15.4.1 Production of xylanase from *A.niger* D15 (xyn2)**

Flask cultures	
Shaking flasks	3x 300 mL non-baffled
Medium	60 mL sterile filtrated 2xMM (pH 6.4)
Incubation	30°C, 200 rpm (orbital shaker)
Biostat A+	
Reactor	3 L total capacity Sartorius Biostat A plus
Impeller	2x Rushton
Medium	1.8 L sterile filtrated 2xMM (pH 6.4)
Antifoam	0.2 mL·L ⁻¹ Goldschmidt TEGO Antifoam KS911
Cultivation	30 °C, no pH control, 400 rpm
Aeration	1.8 L·min ⁻¹
Biostat C	
Reactor	15 L total capacity B.Braun Biostat C
Impeller	3x Rushton
Medium	10 L sterile filtrated 2xMM (pH 6.4)
Antifoam	0.2 mL·L ⁻¹ Goldschmidt TEGO Antifoam KS911
Cultivation	30 °C, no pH control, 400 rpm
Aeration	10 L·min ⁻¹

Quorus GLS	
Reactor	Quorus GLS 2.05 L (50 membranes & 100 membranes)
Medium	sterile filtrated 2xMM (pH 6.4)
Cultivation	30 °C, ECS pressure = 0.3 bar, flux rate = 50 mL·h ⁻¹
Aeration	2 L

15.4.2 Production of actinorhodin from *S.coelicolor* A3(2)

Flask cultures	
Shaking flasks	3x 500 mL Schott, 2 baffles
Medium	100 mL sterile filtrated ISP2 (pH 7.2)
Incubation	30°C, 200 rpm (orbital shaker)

Biostat A+	
Reactor	3 L total capacity Sartorius Biostat A plus
Impeller	2x Rushton
Medium	1.8 L sterile filtrated ISP2 (pH 7.2)
Antifoam	0.2 mL·L ⁻¹ Goldschmidt TEGO Antifoam KS911
Cultivation	30 °C, no pH control, pO ₂ set-point = 40% (adjusted by 200-350 rpm)
Aeration	1.8 L·min ⁻¹

Biostat C	
Reactor	15 L total capacity B.Braun Biostat C
Impeller	3x Rushton
Medium	10 L sterile filtrated ISP2 (pH 7.2)
Antifoam	0.2 mL·L ⁻¹ Goldschmidt TEGO Antifoam KS911
Cultivation	30 °C, no pH control, pO ₂ set-point = 40% (adjusted by 200-350 rpm)
Aeration	10 L·min ⁻¹

Quorus GLS	
Reactor	Quorus GLS 2.05 L (50 membranes & 100 membranes)
Medium	sterile filtrated ISP2 (pH 7.2)
Cultivation	30 °C, ECS pressure = 0.3 bar, flux rate = 20 mL·h ⁻¹
Aeration	2 L

15.4.3 Production of β -lactamase from *L.lactis* PRA290

Static flask cultures	
Shaking flasks	3x 300 mL non-baffled Schott
Medium	60 mL sterile filtrated LM5-V100-G75 (pH = 7,6)
Incubation	30°C, 0 rpm

Flask cultures	
Shaking flasks	3x 500 mL Schott, 2 baffles
Medium	80 mL sterile filtrated LM5-V100-G75 (pH = 7,6)
Incubation	30°C, 50 rpm (orbital shaker)

Biostat A+	
Reactor	3 L total capacity Sartorius Biostat A plus
Impeller	2x Rushton
Medium	1.8 L sterile filtrated LM5-V100-G75 (pH = 7,6)
pH-correction	2 M KOH
Cultivation	30 °C, pH set-point = 6 (kick-in @ 6.0), 300 rpm
Aeration	0 L·min ⁻¹

Biostat C	
Reactor	15 L total capacity Sartorius Biostat C
Impeller	3x Rushton
Medium	10 L sterile filtrated LM5-V100-G75 (pH = 7,6)
pH-correction	2 M KOH
Cultivation	30 °C, pH set-point = 6 (kick-in @ 6.0), 300 rpm
Aeration	0 L·min ⁻¹

Quorus LS	
Reactor	Quorus LS 0.22 L (37 membranes)
Medium	sterile filtrated ISP2 (pH 7.2)
Cultivation	30 °C, flux rate = pH dependent, pH setpoint = 6.0

15.5 Product analysis

15.5.1 Actinorhodin

Crude actinorhodin levels (the total amount of blue pigment) can be determined spectrophotometrically. 1 mL samples are centrifuged (1000 g) for 2 min. 500 μ L of the

supernatant are diluted with 500 μL sterile ISP2 broth. After addition of 500 μL 2M NaOH the solution is vigorously mixed for 10 s. 1 mL mixed sample is transferred to a 1 mL cuvette or 200 μL are aliquoted into a 96 well plate. The absorbance is measured at 640 nm and recorded. Actinorhodin concentration can be calculated with $E1\% = 355$ from Eq. 20.

$$\text{mg} \cdot \text{L}^{-1} = \frac{\text{Absorbance} \times \text{dilution}}{E1\% \times \text{Pathlength}} \times 10^5 \quad \text{Eq. 20}$$

15.5.2 Xylanase activity

This assay procedure is specific for *endo*-1,4- β -D-xylanase activity. On incubation of Azo-Xylan (birchwood) with *endo*-xylanase, the substrate is depolymerized to produce low-molecular weight dyed fragments which remain in solution on addition of ethanol to the reaction mixture. High-molecular weight material is removed by centrifugation, and the color of the supernatant is measured. *endo*-Xylanase in the sample solution is determined by reference to a standard curve. Before use, the substrate, Birchwood xylan is first purified (to remove starch) and then it is dyed with Remazolbrilliant Blue R to an extent of approximately one dye molecule per 30 sugar residues.

15.5.2.1 Substrate preparation

1 g of powdered substrate is added to 80 mL of boiling and vigorously stirring water. Stirring is continued for at least 20 min until the polysaccharide is completely dissolved. The volume is adjusted to 100 mL and 0.02 g sodium azide is added and dissolved. This solution is stored at 4 $^{\circ}\text{C}$ between use.

15.5.2.2 Assay procedure

200 μL substrate is aliquoted in 1.5 mL microfuge tubes and pre-incubated at 55 $^{\circ}\text{C}$ for 10 min before the assay is started. Process samples are diluted 100x with 0.1 M NaPP buffer (pH = 6.0) to ensure results remain within the xylanase standard curve range.

200 μL of the diluted process samples (or 200 μL buffer to define the standard) are added to the pre-incubated substrate aliquots, vortexed for 20 s and incubated for exactly 10 min at 55 $^{\circ}\text{C}$. 1 mL 95 % ethanol is added to stop the reaction and the mixture

is vortexed again for 20 s. The solution is left standing for 5 min at room temperature and subsequently centrifuged at maximum speed for 5 min. 300 μ L of the supernatants are aliquoted in 96 well plates and absorbance is determined at 590 nm.

Enzyme activities are calculated using the Megacalc spreadsheet provided by Megazyme (<http://secure.megazyme.com/downloads/en/calc/S-AXBL.xls>) using the *Trichoderma* xylanase template.

15.5.3 β -lactamase activity

Nitrocefin is the chromogenic cephalosporin developed by Glaxo Research Limited. This compound exhibits a rapid distinctive color change from yellow (max at pH 7.0 = 390nm) to red (max. at pH 7.0 = 486 nm) as the amide bond in the β -lactam ring is hydrolysed by a β -lactamase (E.C 3.5.2.6). It is sensitive to hydrolysis by all known lactamases produced by Gram-positive and Gram-negative bacteria.

15.5.3.1 Substrate preparation

One vial of 1 mg lyophilized Nitrocefin SR0112 is added the entire contents (2 ml) of one vial of rehydration fluid SR0112A yielding a working Nitrocefin solution of 500 mg/ml. For β -lactamase microtiter plate assay, the working solution of Nitrocefin (500 mg·ml⁻¹) is diluted tenfold in 0.1 M NaPP (1mM EDTA, pH = 7) buffer.

15.5.3.2 Assay procedure

The spectrophotometric assay for β -lactamase is carried out measuring changes in wavelength at 486nm.

The molar extinction coefficient of Nitrocefin at this wavelength is 20,500. Test samples are diluted 100 - 1000 fold with 0.1 M NaPP (1mM EDTA, pH = 7) to obtain a linear kinetic curve. 50 μ l test sample are aliquoted into separate wells in a 96 well microtitre plate. 50 μ l 0.1 M NaPP is used as the standard. 100 μ l Nitrocefin solution is added, the plate subsequently mixed for 20 s at 150 rpm. Measurement of the kinetic curves is started immediately and carried out for 3 – 5 min.

Volumetric activities are calculated from the slope of the kinetic curves using Eq. 21.

$$U \cdot mL^{-1} = \frac{(\text{Slope}[\text{min}^{-1}] \times RD \times d) \times 10^6 [mL]}{Ex \times \text{pathlength} [cm]} \quad \text{Eq. 21}$$

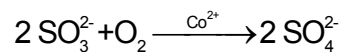
RD = reaction dilution (typically = 3); d = sample dilution; Ex = Extinction coefficient = $20500 \mu M \cdot \text{min}^{-1}$

15.6 Reactor characterization

15.6.1 Determination of $k_L a$ values using the sulfite method

The $k_L a$ value (oxygen transfer coefficient per unit volume) is a specific parameter for the modeling and design of aerobic fermentation processes. It is dependent on the geometric and procedural environment of the used fermentation system. Different methods for the determination of $k_L a$ values have been proposed in the literature. These methods can basically be divided into two separate fields: static and dynamic measurements. While dynamic measurements rely e.g. on the supply or uptake of variable oxygen concentrations, static methods rely on constant aeration and oxygen uptake. All $k_L a$ determinations in this work have been performed using the static sulfite method.

This method relies on the Co^{2+} catalyzed oxidation of sulfite ions to sulfate ions. Oxygen is chemically consumed and DO concentration remains 0 % until all sulfite ions are oxidized. The amount of consumed oxygen in a certain time frame is directly proportional to the concentration of the sulfite ions.



The procedure is as follows: a 0.5 % (w/v) sulfite solution ($5 \text{ g} \cdot \text{L}^{-1} \text{Na}_2\text{SO}_3$, $2 \text{ g} \cdot \text{L}^{-1} \text{K}_2\text{HPO}_4$) is adjusted to pH 8 using 38 % (v/v) sulfuric acid. A defined volume of this solution is placed into the reactor vessel and DO measurement is started immediately after injection of a catalytic amount of an aqueous $\text{Co}(\text{NO}_3)_2$ solution (final concentration in the reactor vessel: $1 \cdot 10^{-5} \text{ M}$) and subsequent starting of a defined aeration rate. The $k_L a$ value can finally be calculated from the time frame where the DO concentration remains at 0 %.

15.6.2 Determination of residence time distributions

Based on the determination of the residence time distribution the mixing quality of a studied reactor system can be compared to the conditions in ideal mixed reactors.

The hydrodynamic residence time τ_h is calculated from the ratio of reactor volume V_R to volumetric flow \dot{V} in a CSTR and describes the average amount of time a molecule resides within the observed reactor system Eq. 22.

$$\tau_h = \frac{V_R}{\dot{V}} \quad \text{Eq. 22}$$

To characterize the residence time of a CSTR, a tracer (electrolyte or dye) is injected into the reactor system at a specific point in time ($t=0$) and its concentration is recorded at the reactor output as a function of time. The addition of the tracer can either be performed as a pulse (Dirac pulse) or constantly (heavy-side function) (**Fig. 78**).

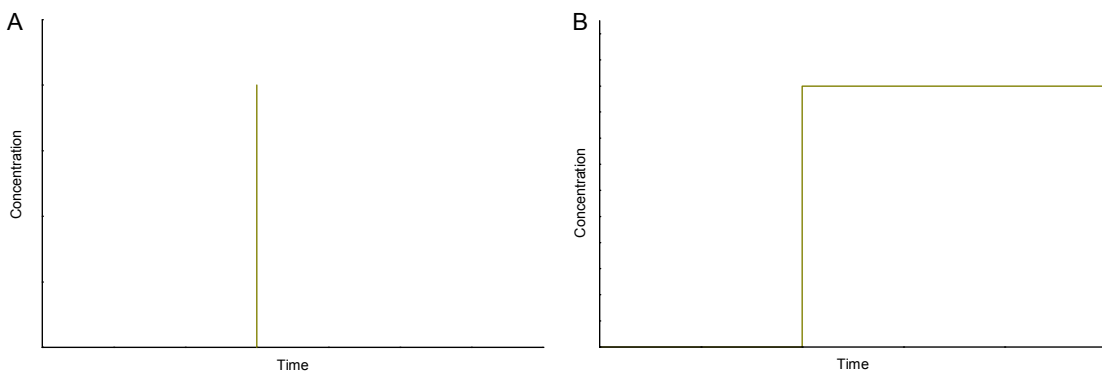


Fig. 78: Possible tracer input signals for the determination a residence time distributions. **A:** pulsed experiment. **B:** step experiment.

The corresponding response functions can be divided into real and ideal distributions. The residence time is quoted as theta (θ) (Eq. 23) and is calculated from the quotient of the time t and the hydrodynamic residence time τ_h .

$$\theta = \frac{t}{\tau_h} \quad \text{Eq. 23}$$

Exit age distributions $E(\theta)$ are the response functions of pulse experiments. $E(\theta)$ describes how many tracer molecules are distributed onto the different residence times (Fig. 79A).

The cumulative residence time distributions $F(\theta)$ define, how many tracer molecules have exited the reactor system at a certain residence time. $F(\theta)$ are the response of step experiments (Fig. 79B).

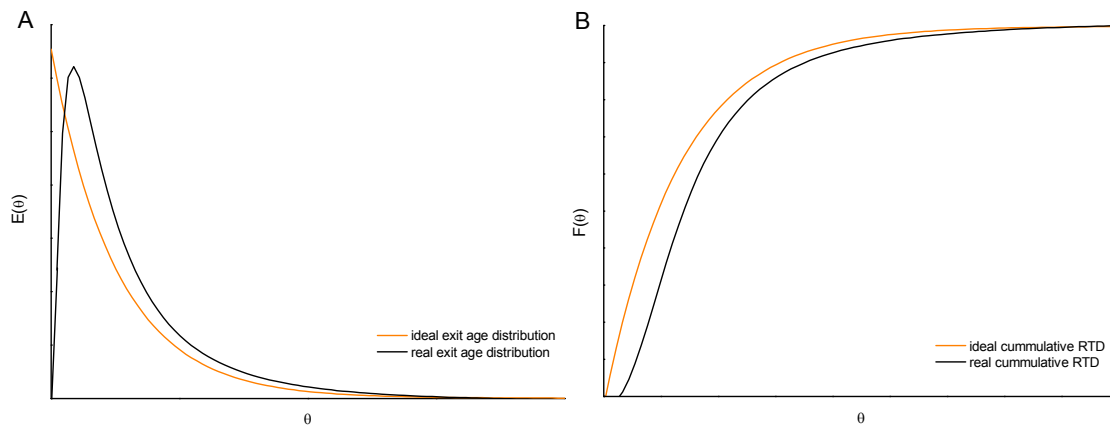


Fig. 79: A: Ideal (orange) and real (black) exit age distributions $E(\theta)$. B: Ideal (orange) and real (black) cumulative residence time distributions $F(\theta)$.

Residence time distributions recorded in this work were performed on the basis of the spectroscopic tracer detection with water-soluble methylenblue as the tracer component.

The reactor system is operated as a CSTR by constantly supplying ddH₂O into the reactor chamber at a feed rate of 0.68 mL·min⁻¹. 0.01 % (v/v) of a 0.67 mg·mL⁻¹ methylenblue solution are quickly injected into the reactor vessel. The resulting mixtures are removed from the reactor system at the same rate as ddH₂O is supplied. The tracer concentration is recorded at the reactor exit by measuring the absorption as a function of time at 664 nm. The resulting function correlated directly with the exit age distribution.

15.7 Wiring diagram of the mini-STR bioreactor hardware environment

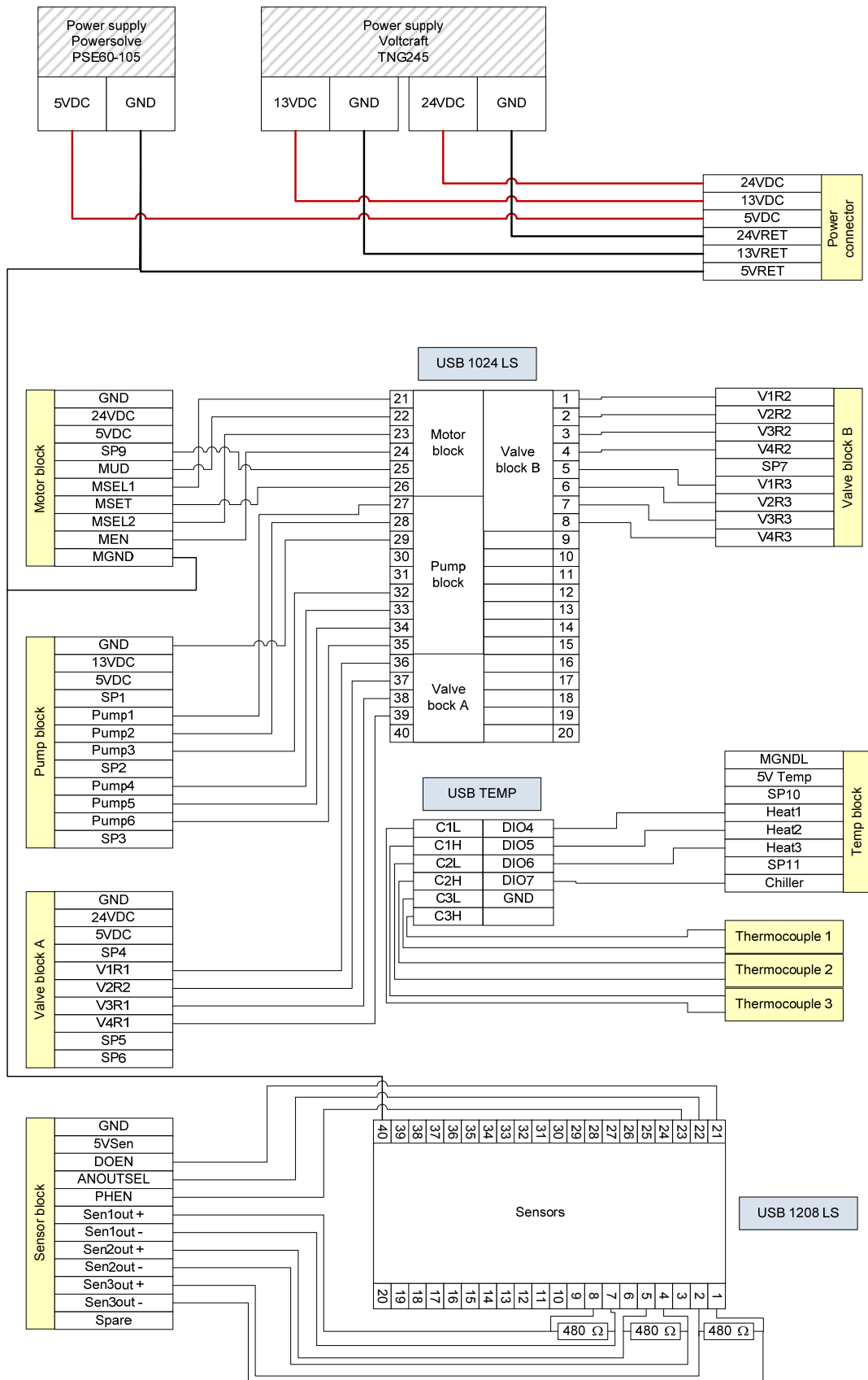


Fig. 80: Wiring diagram of the multi I/O measurement boxes (blue) and the pinouts (yellow) of the Tristation.

15.8 Calibration parameters

15.8.1 pH optoelectronics

Table 14: pH optoelectronic offset voltages

		Station 1	Station 2	Station 3
Offset voltage blue LED [V]	V_{off}^{bl}	0.02259	0.00485	-0.01014
Offset voltage UV LED [V]	V_{off}^{uv}	0.02098	0.01339	-0.00994

Table 15: Calibration parameters for SSB pH sensor patches

	Station 1	Station 2	Station 3
A_1	0.007	0.021	0.018
A_2	0.909	1.003	0.985
x_0	8.307	7.992	8.115
dx	0.653	0.536	0.602

15.8.2 DO optoelectronics

Table 16: DO optoelectronic offset voltages and phase offsets.

		Station 1	Station 2	Station 3
Offset	O_{ip} [V]	0.0100	-0.0086	-0.0099
	O_{qd} [V]	0.0118	-0.0094	-0.0096
Short lived fluorophore offset	V_{ips} [V]	0.0267	0.0078	-0.0097
	V_{qds} [V]	0.0234	0.0041	-0.0096
Phase offset	O_{ps} [°]	55.34	50.66	52.33

Table 17: Calibration parameters for SSB DO sensor patches

	Station 1	Station 2	Station 3
A_1	720.59	758.35	744.61
t_1	13.79	13.01	13.21
y_0	-7.83	-4.70	-6.44

Curriculum Vitae

Christian Endres

Persönliche Daten

Geb. am 2. August 1975 in Hannover
Adresse: Sattelhof 9
30851 Langenhagen

Schulbildung und Zivildienst

08/1993 – 07/1994 Franklin Community High School, Franklin, Indiana, USA
11.6.1997 Abitur am Gymnasium Langenhagen
08/1997 – 09/1998 Zivildienst, Altenzentrum Eichenpark des Klinikums Hannover

Studium

10/1998 – 08/2006 Chemiestudium an der Universität Hannover
Studienschwerpunkte: Technische Chemie, Physikalische Chemie
09/2006 – 04/2007 Diplomarbeit: Aufarbeitung von Polysialinsäure aus *Escherichia coli* K1 Kulturen
19.4.2007 Studienabschluss: Diplom-Chemiker

Promotionsstudium

Seit 05/2007 Promotionsstudium an der Gottfried Wilhelm Leibniz Universität Hannover, Institut für Technische Chemie
Thema der Dissertation: Evaluation, Characterization and Development of Innovative Reactor Systems in Biotechnology
01/2009 – 03/2009 Forschungsaufenthalt, Synexa Life Sciences Ltd., Kapstadt, Südafrika

Berufliche Erfahrungen

Seit 04/2010 - Sartorius Stedim Biotech GmbH, Göttingen
Wissenschaftlicher Mitarbeiter Systemgeräte-Entwicklung

Weiterbildungen

09/2007 Qualitätsmanagement für Medizinproduktehersteller nach DIN EN ISO 13485
09/2008 Gene Technology, Biosafety and Biosecurity for Project Leaders and Biosafety Officers (anerkannt gemäß § 15 GenTSV)
03/2009 Verfahrenstechnische und betriebswirtschaftliche Grundlagen biotechnologischer Prozesse

Publikationsliste

Veröffentlichungen

- Lindner P., Endres C., Bluma A., Höpfner T., Glindkamp A., Haake C., et al. (2010)
Disposable Sensor Systems. *Single-Use Technology in Biopharmaceutical Manufacture* (Eibl, R. and Eibl, D., eds), John Wiley & Sons, Wiley-VCH, Weinheim [in press]
- Endres C., Haake C., Landgrebe D., Beutel S., Stahl F., Hitzmann B., et al. (2009)
Moderne Bioprozessanalytik – eine kurze Übersicht. *Biospektrum* 2009(6), 662-665
- Khaydarov R.R., Khaydarov R.A., Estrin Y., Evgrafova S., Scheper T., Endres C., et al. (2009)
Silver Nanoparticles. *Nanomaterials: Risks and Benefits*, 287-297 (Linkov I. and Steevens J., eds)
- Rode B., Endres C., Chen R., Stahl F., Beutel S., Kasper C., et al. (2008)
Large-scale production and homogenous purification of long chain polysialic acids from *E. coli* K1.
Journal of Biotechnology 135, 202-209

Vorträge

- Endres C., Beutel S., Fraser S.J., Edwards W., and Scheper T. (2009)
Produktivitätsanalyse eines neuartigen, nicht begasten keramischen Hohlfaserreaktors. *Chemie Ingenieur Technik* 81, 1240-1241 (Dechema Jahrestagung der Biotechnologen, Mannheim)

Poster

- Endres C., Beutel S., Fraser S.J., Edwards W., Kocourek A., and Scheper T. (2008)
Evaluation of a novel scaleable and disposable membrane bioreactor for enhanced secondary metabolite and recombinant protein production in filamentous microorganisms.
International Congress on Biocatalysis, Hamburg, Germany (Poster)
- Endres C., Beutel S., Fraser S.J., Edwards W., and Scheper T. (2008)
Investigation of the productivity of a novel ceramic membrane bioreactor system for steady-state fermentations. *Bioperspectives, Hannover, Germany (Poster)*
- Endres C., Chen R., Beutel S., Fraser S.J., Edwards W., and Scheper T. (2008)
Comparison of a novel continuously operated ceramic membrane bioreactor for the cultivation of shear stress-sensitive organisms to stirred tank reactor systems
The 13th International Biotechnology Symposium, Dalian, China (Poster)
- Endres C., Rode B., Kasper C., Beutel S., Gerardy-Schahn R., and Scheper T. (2008)
Downstreaming of Bacterial Polysialic Acid *Bioperspectives, Hannover, Germany (Poster)*
- Kress S., Endres C., Riechers D., Baumfalk R., Beutel S., and Scheper T. (2009)
Optimierung und Evaluierung von Steuerungsparametern für ein Screening-Bioreaktorsystem.
27. Jahrestagung der Biotechnologen, Mannheim, Germany (Poster)